2008

Evidence for symplectic symmetry in ab initio no-core shell model results

Tomas Dytrych
Louisiana State University and Agricultural and Mechanical College, tdytrych@gmail.com

EVIDENCE FOR SYMPLECTIC SYMMETRY IN AB INITIO NO-CORE SHELL MODEL RESULTS

A Dissertation

Submitted to the Graduate Faculty of the
Louisiana State University and
Agricultural and Mechanical College
in partial fulfillment of the
requirements for the degree of
Doctor of Philosophy

in

The Department of Physics and Astronomy

by
Tomáš Dytrych
M.S., Czech Technical University in Prague, 2001
December, 2008

Dedication

To my parents Josef and Marie

To the memory of my brother Martin

Acknowledgments

First of all, I would like to thank my advisor, Professor Jerry P. Draayer, for providing guidance and expertise during all stages of this research project. It was through his support that appropriate computational resources were always available for my calculations. His enthusiasm and "can do" attitude were contagious and gave me the confidence to tackle problems that seemed overwhelming at the time. Also, I would like to thank him and his wife, Lois, for showing me the true meaning of "southern hospitality".

A great deal of credit goes to my collaborators, Drs. Kristina D. Launey and Chairul Bahri, who contributed significantly to the success of this research project. I am very grateful to Professor James P. Vary of Iowa State University for providing me with the no-core shell model results. This project would not have been possible without his enthusiastic support. I also acknowledge discussions with Dr. Petr Navrátil in the early stage of this project.

I am indebted to my high school teacher Bohumil Bureš, who initially sparked my interest in physics and mathematics, to Professor Jiří Limpouch, my former advisor at the Czech Technical University in Prague, and to Dr. Pavel Trávníček, who was very supportive of my desire to pursue a doctoral degree abroad.

I would like to extend my thanks to all my friends in the Czech Republic, far too many to list, but particularly Martin and Ondřej Doubek, Lubomír Puš, Michal Pajr, Jiří Berger, Pavel Šubrt, Viktor Votruba, Jan Páral, and Jaroslav Runčík, have been my close friends for many years and they will remain my friends no matter what the circumstances are.

During my graduate studies in Louisiana, I also have had the benefit of great friends. I wish to thank Mark Sauerwein and Mary Jane, Veronika and Deon Wills, Greg and Bára Favret, and Zuzka Bočková, for their unflagging and loyal friendship. A special thanks go to Justin Richards and Robert Schwing for introducing me to rock climbing and for sharing great times during rock climbing trips. I am also grateful to Olivier Harel and Pablo Velez for helping me out during my first days in Baton Rouge and for being great roommates.

I owe a great amount of gratitude to Valerie Cipparone for her admirable amount of patience, love, support during my work on this dissertation and for being a great hiking and backpacking companion.

Last, but not least, I would like to thank my parents for their care, unconditional love, and invaluable support throughout my entire life.

Table of Contents

Acknowledgments iii

List of Tables vii

List of Figures x

Abstract xi

Chapter

1 Introduction 1

2 Nuclear Shell Models 4
2.1 Independent Particle Model 4
2.1.1 Many-Nucleon Configurations 5
2.1.2 Validity of the Independent Particle Model 6
2.2 Interacting Shell Model 6
2.2.1 Many-Body Basis 7
2.2.2 Occupation Number Representation 10
2.2.3 Lanczos Algorithm 12

3 Ab Initio No-Core Shell Model 15
3.1 Realistic Interactions 16
3.1.1 Phenomenological Meson-Exchange Potentials 16
3.1.2 Chiral Perturbation Potentials 17
3.1.3 JISP Potentials 18
3.2 No-Core Shell Model Framework 18
3.3 Lee-Suzuki Similarity Transformation Method 21
3.3.1 Non-Hermitian Formalism 21
3.3.2 Hermitian Formalism 23
3.4 Cluster Approximation to an Effective Interaction 25
3.4.1 a-Body Cluster Approximation 25
3.4.2 Two-Body Cluster Approximation 26
3.5 Applications 27
3.6 Scale Explosion Problem 31

4 Symplectic Shell Model . . . 33
4.1 Elliott SU(3) Model of Nuclear Rotations . . . 33
4.1.1 U(3) and SU(3) Symmetry Groups . . . 34
4.1.2 Labeling Scheme . . . 35
4.1.3 SU(3) model Hamiltonians . . . 37
4.1.4 Geometrical Interpretation of SU(3) States . . . 38
4.2 Symplectic Shell Model . . . 40
4.2.1 Collective Model Chain . . . 41
4.2.2 Shell Model Chain . . . 43
4.2.3 Translationally Invariant Form of Symplectic Generators . . . 45
4.2.4 Symplectic Basis States . . . 47
4.2.5 Relation Between α-Cluster and Symplectic States . . . 48

5 Expansion of Symplectic States in M-Scheme Basis . . . 51
5.1 Construction of Symplectic Bandheads . . . 51
5.1.1 Expansion of SU(3) Irrep in M-Scheme Basis . . . 52
5.1.2 Center of Mass Spuriosity Removal . . . 53
5.2 Symplectic Basis Construction Formula in Second Quantized Form . . . 55
5.2.1 Recursive Symplectic Construction Formula . . . 56
5.2.2 Parallel Algorithm . . . 58
5.2.3 $\mathrm{Sp}(3,\mathbb{R})$ Generators in Second-Quantized Form . . . 58
5.2.4 Tests . . . 63

6 Evidence for Symplectic Symmetry in Light Nuclei . . . 64
6.1 Structure of the Lowest-Lying States of ^{12}C and ^{16}O Nuclei . . . 64
6.2 Dominant Role of 0p-0h Symplectic Irreps . . . 67
6.2.1 Ground-State Rotational Band in ^{12}C Nucleus . . . 68
6.2.2 Ground State in ^{16}O Nucleus . . . 71
6.2.3 Relevance of Elliott SU(3) Model . . . 72
6.3 Multiple-Particle-Multiple-Hole Symplectic Irreps . . . 73
6.3.1 Ground-State Rotational Band in ^{12}C Nucleus . . . 74
6.3.2 Ground State in ^{16}O Nucleus . . . 76
6.3.3 First Excited 0^+ State in ^{16}O Nucleus . . . 78
6.4 Symplectic Invariance within the Spin Parts of Realistic Eigenstates . . . 80
6.4.1 Spin Decomposition . . . 80
6.4.2 Analysis of Spin Components . . . 82
6.5 Dimension of Symplectic Model Space . . . 83

7 Conclusions . . . 86

Bibliography . . . 89

Appendix
A Lie Groups and Lie Algebras: Basic Concepts . . . 98

B Tensor Operators and Wigner-Eckart Theorem . . . 104

C SU(3) Calculus 106

Vita 109

List of Tables

2.1 Dimensions of the pf-shell nuclei valence space for the m-scheme and the J-coupled basis. 9

4.1 Overlaps of stretched symplectic basis states $(\lambda_\sigma + n\,\mu_\sigma)$, $n = 0, 2, \ldots, 12$ built over different ^{16}O $(\lambda_\sigma\,\mu_\sigma)$ bandheads to the α+^{12}C cluster basis states. 50

6.1 Comparison of the experimental data of ^{12}C with the results obtained by the NCSM calculation. 66

6.2 0p-0h Sp$(3,\mathbb{R})$ irreps in ^{12}C, $N_\sigma = 24.5$. 68

6.3 Probability distribution of NCSM eigenstates for ^{12}C across the dominant 3 0p-0h Sp$(3,\mathbb{R})$ irreps, $\hbar\Omega$=12 MeV. 69

6.4 Probability distribution of NCSM eigenstates for ^{12}C across the dominant 3 0p-0h Sp$(3,\mathbb{R})$ irreps, $\hbar\Omega$=15 MeV. 70

6.5 Probability distribution of the NCSM ground state in ^{16}O obtained with (a) $\hbar\Omega$=12 MeV and (b) $\hbar\Omega$=15 MeV, respectively, across the 0p-0h Sp$(3,\mathbb{R})$ irrep. 72

6.6 Projection of the ground 0^+_{gs} and the first excited (not fully converged) 0^+_2 NCSM states for ^{16}O unto the dominant $2\hbar\Omega$ 2p-2h symplectic bandheads for $\hbar\Omega$=12 MeV. 79

6.7 Model space dimensions for different maximum allowed $\hbar\Omega$ excitations, $N_{\max}$, for the NCSM and the 3 most significant 0p-0h Sp$(3,\mathbb{R})$ irreps. . . 84

6.8 Model spaces dimension for different maximum allowed $\hbar\Omega$ excitations, N_{max}, for the NCSM and the single 0p-0h Sp$(3,\mathbb{R})$ irrep limited to $J = 0$ states in ^{16}O. 84

List of Figures

2.1 Schematic illustration of the interacting shell model. 8

2.2 Examples of $0\hbar\Omega$, $2\hbar\Omega$, and $4\hbar\Omega$ configurations in ^{6}Li. 10

3.1 Schematic illustration of the properties of the effective Hamiltonian. . . . 20

3.2 The structure of transformed Hamiltonian $\mathcal{H} = e^{-S} H e^{S}$. 24

3.3 The scale explosion in the NCSM. 32

4.1 A traditional $(\beta\gamma)$ plot, where β ($\beta \geq 0$) is the radius vector. 39

4.2 The symplectic group $\mathrm{Sp}(3,\mathbb{R})$ contains two physically important subgroup chains. 42

4.3 The schematic plot illustrating decomposition of the shell model space as direct sum of the symplectic $\mathrm{Sp}(3,\mathbb{R})$ irreps. 44

4.4 Action of the translationally invariant symplectic raising operator $A^{(20)}_{\mathcal{L}M}$. 47

5.1 The result of the action of the projecting operator $\hat{P}(n_{\max} = 1)$ on $1\hbar\Omega$ 1p-1h $\mathrm{SU(3)}\otimes\mathrm{SU_S(2)}$ irrep in ^{4}He nucleus. 54

5.2 Schematic plot illustrating parallel scheme of $A^{(20)}_{\mathcal{L}M}\,|\sigma S_\sigma; JM_J\rangle_{\mathcal{L}M}$ calculation. 59

6.1 Experimental and calculated low-lying spectra of ^{12}C for increasing size of the model space. 65

6.2 NCSM (blue, right) and 0p-0h Sp(3, $\mathbb{R}$) (red, left) probability distribution over $0\hbar\Omega$ to $N_{\max}$ $\hbar\Omega$ subspaces for the 0^+_{gs} of ^{12}C for different model spaces, $N_{\max}$, with $\hbar\Omega = 15$MeV. 68

6.3 NCSM and Sp(3, $\mathbb{R}$) $B(E2 : 2^+_1 \rightarrow 0^+_{gs})$ transition rate in e^2fm^4 for ^{12}C as a function of the $\hbar\Omega$ oscillator strength in MeV, N_{max}=6. 71

6.4 Probability distribution for the (a) 0^+_{gs}, (b) 2^+_1 and (c) 4^+_1 states in ^{12}C and (d) 0^+_{gs} in ^{16}O over $0\hbar\Omega$ (blue, lowest) to $6\hbar\Omega$ (green, highest) subspaces. 73

6.5 Projection of NCSM wave functions for ^{12}C onto the dominant 0p-0h (orange) and $2\hbar\Omega$ 2p-2h (purple) Sp(3, $\mathbb{R}$) irreps for: a) 0^+_{gs}, (b) 2^+_1, and c) 4^+_1 as a function of the $\hbar\Omega$ oscillator strength. Results are also shown for the bare interaction. 74

6.6 Probability distribution for the (a) 0^+_{gs}, (b) 2^+_1 and (c) 4^+_1 states in ^{12}C over $0\hbar\Omega$ (blue, lowest) to $6\hbar\Omega$ (green, highest) subspaces for the most dominant 0p-0h + $2\hbar\Omega$ 2p-2h Sp(3, $\mathbb{R}$) irrep case (left) and NCSM (right) together with the leading (0 4) irrep contribution (black diamonds) as a function of the $\hbar\Omega$ oscillator strength in MeV for $N_{\max} = 6$. 75

6.7 Probabilities (specified by the area of the circles) for the symplectic states which make up the most important 0p-0h (blue) and $2\hbar\Omega$ 2p-2h (red) symplectic irreps, within the NCSM ground state in ^{12}C, $\hbar\Omega = 15$ MeV. . 76

6.8 Probability distribution for the 0^+_{gs} state in ^{16}O over $0\hbar\Omega$ (blue, lowest) to $6\hbar\Omega$ (green, highest) subspaces for the most dominant 0p-0h + $2\hbar\Omega$ 2p-2h Sp(3, $\mathbb{R}$) irrep case (left) and NCSM (right) together with the leading (0 0) irrep contribution (black diamonds) as a function of the $\hbar\Omega$ oscillator strength in MeV for $N_{\max} = 6$. 77

6.9 Probabilities (specified by the area of the circles) for the symplectic states, which make up the most dominant 0p-0h (blue) and $2\hbar\Omega$ 2p-2h (red) symplectic irreps, within (a) the 0^+ ground state and (b) the first excited 0^+_2 state in ^{16}O calculated by NCSM, $\hbar\Omega = 15$ MeV. The Sp(3, $\mathbb{R}$) states are grouped according to their $(\lambda_\omega\, \mu_\omega)$ SU(3) symmetry, which is mapped onto the $(\beta\, \gamma)$ shape variables of the collective model. 78

6.10 Projection of (a) the ground state 0^+_{gs} and (b) the first excited (not fully converged) 0^+_2 NCSM states for ^{16}O as a function of the $\hbar\Omega$ oscillator strength onto the 0p-0h (orange) Sp(3, $\mathbb{R}$) irrep and the dominant $2\hbar\Omega$ 2p-2h (purple) Sp(3, $\mathbb{R}$) irreps. Results are also shown for the bare interaction at $\hbar\Omega = 15$ MeV. 80

6.11 Probabilities for the $S = 0$ (blue, left), $S = 1$ (red, middle), and $S = 2$ (yellow, right) components of the NCSM eigenstates for (a) 0^+_{gs}, (b) 2^+_1, and (c) 4^+_1 in ^{12}C and (d) 0^+_{gs} in ^{16}O, $N_{\max} = 6$. 81

6.12 Projection of the $S_\sigma = 0$ (blue, left) and $S_\sigma = 1$ (red, right) $\mathrm{Sp}(3,\mathbb{R})$ irreps onto the corresponding significant spin components of the NSCM wave functions for (a) 0^+_{gs}, (b) 2^+_1, and (c) 4^+_1 in ^{12}C and (d) 0^+_{gs} in ^{16}O, for effective interaction for different $\hbar\Omega$ oscillator strengths and bare interaction. 82

6.13 NCSM space dimension as a function of the maximum $\hbar\Omega$ excitations, $N_{\max}$, compared to that of the $\mathrm{Sp}(3,\mathbb{R})$ subspace: (a) $J = 0, 2$, and 4 for ^{12}C, and (b) $J = 0$ for ^{16}O. 85

Abstract

Advances in the construction of realistic internucleon interactions together with the advent of massively parallel computers have resulted in a successful utilization of the *ab initio* approaches to the investigation of properties of light nuclei. The no-core shell model is a prominent *ab initio* method that yields a good description of the low-lying states in few-nucleon systems as well as in more complex p-shell nuclei. Nevertheless, its applicability is limited by the rapid growth of the many-body basis with larger model spaces and increasing number of nucleons.

To extend the scope of the *ab initio* no-core shell model to heavier nuclei and larger model spaces, we analyze the possibility of augmenting the spherical harmonic oscillator basis with symplectic $\mathrm{Sp}(3,\mathbb{R})$ symmetry-adapted configurations of the symplectic shell model which describe naturally the monopole-quadrupole vibrational and rotational modes, and also partially incorporate α-cluster correlations. In our study we project low-lying states of ^{12}C and ^{16}O determined by the no-core shell model with the JISP16 realistic interaction onto $\mathrm{Sp}(3,\mathbb{R})$-symmetric model space that is free of spurious center-of-mass excitations. The eigenstates under investigation are found to project at the 85-90% level onto a few of the most deformed symplectic basis states that span only a small fraction ($\approx 0.001\%$) of the full model space. The results are nearly independent of whether the bare or renormalized effective interactions are used in the analysis.

The outcome of this study points to the relevance of the symplectic extension of the *ab initio* no-core shell model. Further, it serves to reaffirm the Elliott SU(3) model upon which the symplectic scheme is built. While extensions of this work are clearly going to be required if the theory is to become a model of choice for nuclear structure calculations, these early results seem to suggest that there may be simplicity within the complexity of nuclear structure that has heretofore not been fully appreciated. As follow-on work to what is reported in this thesis, we expect to develop a stand alone shell-model code that builds upon the underlying symmetries of the symplectic model.

Chapter 1

Introduction

The long-standing goal of theoretical nuclear physics is to describe properties of nuclei starting from the elementary interactions among the constituent nucleons. A solution to this problem represents a formidable challenge due to the intricate nature of the strong force that precludes perturbative treatments, and due to the complexities of the strongly interacting quantum many-particle systems that exhibit single-particle as well as collective and clustering correlations. Nevertheless, the last decade has witnessed remarkable progress toward this arduous goal. Recently developed realistic interactions, such as J-matrix inverse scattering potentials [1, 2] and modern two- and three-nucleon potentials derived from meson exchange theory [3, 4, 5, 6] or by using chiral effective field theory [7, 8], succeed in modeling the essence of the strong interaction. At the same time, a dramatic increase in performance achieved by highly parallel computing systems has enabled the performance of large-scale *ab initio* nuclear structure calculations for light nuclei.

The *ab initio* methods such as no-core shell model [9], Green's function Monte Carlo [10, 11], and coupled cluster method [12], integrate the modern realistic interactions with cutting-edge numerical algorithms to reproduce characteristic features of light nuclei. Besides bridging the gap between quantum chromodynamics (QCD) and measured properties of light nuclei, the *ab initio* approaches hold promise to have a tremendous impact on advancing the present frontiers in multiple branches of physics. Realistic nuclear wave functions are crucial for gaining an understanding of astrophysical processes involving exotic and unstable nuclei, the study of electromagnetic, weak, and particle decay modes, as well as for testing fundamental symmetries in nature and probing physics beyond the standard model.

While the applicability of the coupled cluster method is limited to closed-shell nuclei and the Green's function Monte Carlo method is capable of solving the nuclear many-body problem with realistic interactions for systems with $A \leq 12$ nucleons, the no-core shell model (NCSM) can obtain bound-state solution to the problem of $A \leq 16$ interacting nucleons with no limitations on the nature of the nucleon-nucleon or three-nucleon interaction. The NCSM has achieved a good description of the low-lying states in few-nucleon systems [13, 14] as well as in more complex p-shell nuclei [9, 15, 16, 17, 18]. The main limitation of this method is inherently coupled with the use of a many-body basis constructed from spherical

harmonic oscillator single-particle states, whose size, and hence the computational complexity and associated storage requirements, grows combinatorially with the number of nucleons and with the number of allowed single-particle states. The NCSM is therefore currently not capable of modeling *sd*-shell nuclei, and often falls short of accurately reproducing characteristic features and physical observables in *p*-shell nuclei, as, for example, enhanced B(E2) transitions strengths or states dominated by multiple-particle-multiple-hole configurations.

With the goal of providing a unified description of phenomena ranging from single-particle effects to monopole-quadrupole vibrational and rotational modes, as well as clustering correlations, we consider the possibility of extending the many-body basis of the NCSM beyond its current limits through symplectic $\mathrm{Sp}(3,\mathbb{R})$ symmetry-adapted basis of the symplectic shell model [19, 20, 21]. This approach is based on recognition that the choice of coordinates is often crucial in quantum mechanical calculations, and that in order to reduce the size of a model space, an appropriate choice of basis should reflect symmetries inherent the system under study. The symplectic extension of the no-core shell-model (Sp-NCSM) [22, 23, 24, 25] with realistic interactions and with basis spanning multiple $\mathrm{Sp}(3,\mathbb{R})$ irreducible representations (irreps) will allow one to account for nuclear collective correlations beyond the current computational limits, which are required to realize experimentally measured B(E2) values without an effective charge and to accommodate highly deformed spatial configurations. The objective of this dissertation is to perform a proof-of-principle study of the Sp-NCSM approach by analyzing realistic wave functions obtained by the *ab initio* NCSM with a modern realistic internucleon interaction for the presence of an underlying symplectic $\mathrm{Sp}(3,\mathbb{R}) \supset \mathrm{SU}(3) \supset \mathrm{SO}(3)$ symmetry, which is not *a priori* imposed on the internucleon interaction.

In Chapter 2, we give a short review of the independent particle model and the interacting shell model as these two models constitute pillars underlying the NCSM. In particular, we introduce the three very important components that the interacting shell model provides to the NCSM framework: the spherical harmonic oscillator (m-scheme) basis, powerful techniques based on the formalism of the second quantization, and the Lanczos algorithm. Chapter 3 gives an outline of the *ab initio* NCSM method. We first review the modern two- and three-nucleon realistic interactions. Next we describe the construction of an effective interaction from a bare realistic potential by means of non-unitary and unitary similarity transformations. The cluster approximation to an effective interaction is also discussed. We conclude this chapter by a brief discussion of applications of microscopic nuclear wave functions, which can be obtained by the NCSM, in various fields of physics. In Chapter 4 we summarize the symplectic shell model, its underlying symmetries, and relations to various microscopic models of the nuclear collective motion. In particular, the Elliott SU(3) model of nuclear rotations is reviewed and a classification scheme for many-particle states using SU(3) quantum numbers is introduced. Next we describe construction of a translationally invariant basis of a $\mathrm{Sp}(3,\mathbb{R})$ irrep. The chapter is concluded by a short discussion of relationships between symplectic and cluster model wave functions. In order to facilitate symmetry identification in NCSM wave functions, we need to expand symplectic basis states in m-scheme basis.

Chapter 5 describes methods utilized to accomplish this task, including the parallel implementation of the algorithm. The final Chapter 6 summarizes our findings.

Chapter 2

Nuclear Shell Models

The nucleus does not appear to be a system for which the concept of a shell model, which has proven to be so successful in the atoms, could be of much relevance. A system of strongly interacting protons and neutrons, with no preferential central point other than the center-of-mass, intuitively lacks a dominating mean field analogous to the Coulomb field of the positively charged nucleus, which suffices to explain many features of atoms without recourse to the effects of the electron-electron interaction. Other descriptions of the nucleus, e.g. charged liquid drop, appear to be more natural. Nevertheless, despite early considerations to the contrary, shell structure clearly manifests itself in nuclei through regularities in various nuclear properties, especially those associated with specific number of protons and neutrons, the so-called "magic numbers".

The experimental evidence for the shell structure initiated development of nuclear models based on the mean field assumption. In this chapter we follow the development of these models from the independent particle model through the interacting shell model, as these simple models are underpinning the more advanced *ab initio* approaches to nuclear structure such as the symplectic no-core shell model (Sp-NCSM) that is the focus of this work.

2.1 Independent Particle Model

The "magic numbers" were explained by Mayer [26] and by Axel, Jensen, and Suess [27] utilizing the independent particle model (IPM) framework. The IPM assumes that, to first order, each nucleon is moving in an independent way in the average potential field produced by the forces of the remaining nucleons. In this approximation a system of strongly interacting fermions becomes a system of non-interacting fermions exposed to an external field. The IPM Hamiltonian is thus a sum of the single-particle Hamiltonian operators

$$H_0 = \sum_{i=1}^{A} \left[T_i + U(r_i) \right] = \sum_{i=1}^{A} h_0 \left(i \right), \tag{2.1}$$

where T_i denotes kinetic energy of the ith nucleon. The solution to the corresponding eigenvalue problem is noticeably simple. Each eigenstate of the Hamiltonian (2.1) is a product of the single-particle wave functions, $\varphi_\alpha(\mathbf{x})$, obtained by solving one-nucleon Schrödinger equation

$$h_0\varphi_\alpha(\mathbf{x}) = \epsilon_\alpha\varphi_\alpha(\mathbf{x}). \tag{2.2}$$

Here, α denotes a set of quantum numbers describing the single-particle state, $\mathbf{x}$ signifies the spatial coordinates and the spin degree of freedom. The mean field $U(r)$ that reproduces the nuclear magic numbers consist of a spherical harmonic oscillator term, a significant spin-orbit term and a term proportional to l^2: [1]

$$U(r) = \tfrac{1}{2}\hbar\omega r^2 - Cl\cdot s - Dl^2, \tag{2.3}$$

where the constant C (D) characterizes the strength of the spin-orbit (orbit-orbit) interaction. The single-particle wave functions

$$\varphi_{\eta ljm}(\mathbf{x}) = \langle r,\theta,\phi|\,\eta ljm\rangle = R_{\eta l}(r)\left[Y_l(\theta,\phi)\times\chi_{\frac{1}{2}}\right]^j_m \tag{2.4}$$

constitute a complete solution of the corresponding single-nucleon Schrödinger equation. Here, $R_{\eta l}(r)$ denotes the radial wave function, the spherical harmonics $Y_{lm_l}(\theta,\phi)$ and the eigenspinor $\chi_{\frac{1}{2}\sigma}$ are coupled to the total angular momentum j and its projection $m = m_l + \sigma$. The quantum numbers describing the single-particle state are as follows:

- The major harmonic oscillator shell number, $\eta = 0, 1, 2, 3, \ldots$, called s, p, sd, pf ... respectively, denotes the number of the harmonic oscillator quanta carried by a given single-particle state.
- $l = \eta, \eta-2, \ldots, 1$ or 0 is the orbital angular momentum quantum number,
- $j = l \pm 1/2$ is the total angular momentum,
- $m = j, j-1, \ldots, -j$ is the third projection of the total angular momentum j.

2.1.1 Many-Nucleon Configurations

The single-particle wave functions $\varphi_{\eta ljm}(\mathbf{x})$ form an orthonormal and complete basis of the single-particle Hilbert space. The A-nucleon states are constructed as products of the individual nucleon wave functions such that the former are anti-symmetric under the interchange of any pair of protons or neutrons in order to satisfy the Fermi-Dirac statistic of identical fermions. It is convenient to express

[1] For the sake of simplicity we will generally refrain from using a caret above a symbol to denote an operator. We will only use the caret to distinguish an operator from its associated eigenvalue in situations where the two might otherwise be confused with each other, as, for example, $\hat{L}$ and L.

a many-fermion wave function as a Slater determinant, which assures the proper antisymmetrization on the outset, e.g. a Z-proton wave function becomes,

$$\Phi_Z(\mathbf{x}_1,\ldots,\mathbf{x}_Z) = \frac{1}{\sqrt{Z!}}\begin{vmatrix} \varphi_{\pi_1}(\mathbf{x}_1) & \varphi_{\pi_1}(\mathbf{x}_2) & \ldots & \varphi_{\pi_1}(\mathbf{x}_Z) \\ \varphi_{\pi_2}(\mathbf{x}_1) & \varphi_{\pi_2}(\mathbf{x}_2) & \ldots & \varphi_{\pi_2}(\mathbf{x}_Z) \\ \vdots & \vdots & \ddots & \vdots \\ \varphi_{\pi_Z}(\mathbf{x}_1) & \varphi_{\pi_Z}(\mathbf{x}_2) & \ldots & \varphi_{\pi_z}(\mathbf{x}_Z) \end{vmatrix}, \tag{2.5}$$

where π_i and $\mathbf{x}_i$ denote quantum numbers and the spatial coordinates of the ith proton, respectively. The A-nucleon wave functions is the product of one Slater determinant for protons and another one for neutrons

$$\Psi_A(\mathbf{x}_1,\ldots,\mathbf{x}_Z,\mathbf{y}_1,\ldots,\mathbf{y}_N) = \Phi_Z(\mathbf{x}_1,\ldots,\mathbf{x}_Z)\Phi_N(\mathbf{y}_1,\ldots,\mathbf{y}_N). \tag{2.6}$$

An alternative to this representation, without any difference in physical content, is the isospin formalism in which protons and neutrons are considered to form two isospin states of a generic fermionic nuclear particle, the nucleon. As a consequence, the A-nucleon wave function must be antisymmetric under the interchange of any two nucleons, and hence the wave function is written as a single Slater determinant.

2.1.2 Validity of the Independent Particle Model

The eigenstates of the Hamiltonian (2.1) are simplistic. Being the wave functions of the form (2.6), they cannot describe realistic nuclear states which are superpositions of rather large number of the many-body configurations. For instance, the nuclear ground state, obtained in the IPM framework, is constructed directly by filling the lowest lying single-particle orbitals. This turns out to be a reasonable approximation for closed-shell nuclei, where all nucleons are coupled to zero total angular momentum, and also for the "closed-shell $\pm$ 1 nucleon" nuclei, where the single-particle effects predominate. As the number of the protons and the neutrons depart from the magic numbers, it becomes necessary to include the internucleon residual interaction to lift degeneracies inherent to the filling orbits beyond a last closed shell with more than one nucleon. As a consequence, one has to abandon the independent particle picture in order to move beyond the mean field toward a more complex framework, the interacting shell model, that enables the modeling of a system of mutually interacting nucleons.

2.2 Interacting Shell Model

The ultimate ambition of the nuclear structure physics is to find exact solution to the problem of A strongly interacting point-like non-relativistic nucleons. The general translationally invariant Hamiltonian for this problem, if one considers two-body nucleon-nucleon interactions only, can be written as

$$H = \frac{1}{A}\sum_{i<j=1}^{A}\frac{(\mathbf{p}_i-\mathbf{p}_j)^2}{2m} + \frac{1}{2}\sum_{i,j=1}^{A}V_{ij}, \tag{2.7}$$

where the first term is the relative kinetic energy operator, and V_{ij} is the nucleon-nucleon interaction. It is important to note, however, that the realistic internucleon interaction is known to have three- and even four-body terms [28, 29, 30, 31]. We will not, for the purposes of this work, address the fundamental problem of finding an appropriate realistic internucleon interaction, but rather simply assume that a realistic interaction is given.

It is impossible to find the exact solution to the given many-body Schrödinger equation in the full infinite Hilbert space. The interacting shell model (SM) [32, 33] reduces the full problem into a tractable one by splitting nucleons into two groups, as schematically depicted in Fig. 2.1. The valence nucleons interacting via a two-body force are restricted to occupy only the valence orbitals, while the inactive nucleons in the closed shells constitute an inert code. This choice of the model space reflects a basic physical fact: the most significant components of the low-lying nuclear states can be accounted for by many-body states involving the excitations of particles in a few orbitals around the Fermi level [34]. Another simplification follows from the fact that the valence space is free of center-of-mass spurious excitations [35]. On the other hand, the valence space can describe only a limited number of low-lying states of the same parity. Particularly, it can not account for states with a multi-particle-multi-hole structure occurring at low energies, as, for example, states with a pronounced α-cluster structure. Furthermore, due to the restricted number of active nucleons and small model space, one has to introduce "effective" electric and magnetic charges to obtain experimental electromagnetic transition rates.

Similarly, one has to transform the "bare" Hamiltonian (2.7) into an effective one that takes into account effects of excluded configurations and inactive nucleons,

$$H_{\mathrm{SM}} = \sum_{i\in \text{ valence particles}} h_0(i) + \frac{1}{2} \sum_{i,j\in \text{ valence particles}} V_{ij}^{\mathrm{res}}, \tag{2.8}$$

where $h_0(i) = p_i^2/2m + \frac{1}{2}m\omega r_i^2$ is spherical harmonic oscillator, and V_{ij}^{res} is a residual effective interaction. At least in principle then, the remaining problem becomes trivial, and all that is left is to select a convenient many-body basis and diagonalize the effective Hamiltonian, H_{SM}.

2.2.1 Many-Body Basis

A many-body basis represents one of the pillars of the SM. If chosen properly, it can greatly facilitate evaluation of the Hamiltonian matrix elements, and also provide means to select a model space small enough to be tractable yet incorporating configurations relevant for the description of the low-lying nuclear states. The properties of the Hamiltonian with respect to certain symmetry groups play a particularly important role in the selection of a convenient many-body basis. Here we describe the two schemes that are commonly used in the standard SM calculations: the m-scheme basis and the J-coupled basis.

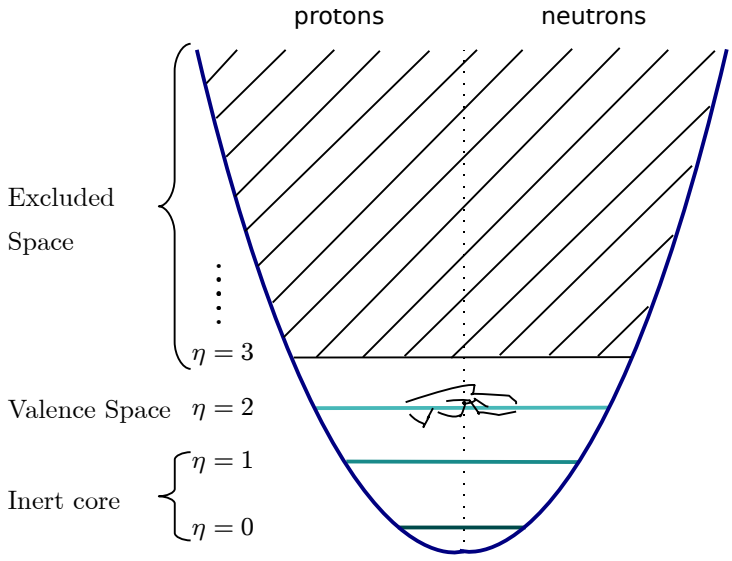

Figure 2.1: Schematic illustration of the interacting shell model. Nucleons moving in the mean field of the spherical harmonic oscillator are split into two distinct groups: active nucleons in the valence single-particle states that interact with one another through two-body effective forces; and inactive nucleons in the closed shells that compose the inert core.

M-Scheme Basis

The simplest many-body basis is provided by the IPM model: the many-body wave functions (2.6), constructed from the single-particle wave functions (2.4), compose a complete and orthogonal basis, known as the m-scheme basis.

The m-scheme states are generally not eigenstates of the $\hat{J}^2$ operator and hence do not carry the total angular momentum J as a good quantum number. As a consequence, all possible values of J are contained in the basis which imply that the dimensions of the Hamiltonian matrices are maximal.

The complete m-scheme basis is obtained by distributing N neutrons and Z protons in all possible ways allowed by the Pauli principle over available proton and neutron single-particle states. This means that the size of the m-scheme basis is given as

$$d = \begin{pmatrix} D_n \\ N \end{pmatrix} \cdot \begin{pmatrix} D_p \\ Z \end{pmatrix}, \tag{2.9}$$

where D_n and D_p denotes the number of available proton and neutron single-particle states, respectively.

By making use of symmetries of the Hamiltonian, however, this number can be reduced. Unlike J, the m-scheme states have $M_J = \sum_{i=1}^{A} m_i$ as a good quantum number. The Hamiltonian is rotationally invariant, and hence one can without loss of generality consider states with $M_J = 0$ only. Nevertheless, this reduction does

Table 2.1: Dimensions of the pf-shell nuclei valence space for the m-scheme and the J-coupled basis.

#valence nucleons	4	8	12	16	20
m-scheme: $M_J = 0$	4000	2×10^6	1.10×10^8	1.09×10^9	2.29×10^9
J-coupled: $J = 0$	156	41355	1.78×10^6	1.54×10^7	3.13×10^7

not cure the combinatorial growth of the basis size for the increasing number of valence nucleons (see Table 2.1).

The steady and rapid increase in computer storage capacity and compute power has compensated, at least in part, for this drawback. The great advantage of the m-scheme basis is its simplicity which enables a full utilization of the occupation number representation (see section 2.2.2) as pioneered by the SM code developed by the Glasgow group [36]. This code represents each Slater determinant in the computer memory by an integer word (or concatenation of integer words). Each bit of the word is associated to a given individual single-particle state $|\eta ljm\rangle$. Each bit carries the value 1 or 0 depending on whether the state is occupied or empty, and the evaluation of the matrix elements is performed by the bit operations which are computationally inexpensive. This approach proved to be highly efficient, and has been adopted by most modern SM codes [37, 38, 39].

J-Coupled Basis

Since Hamiltonian is a rotationally invariant operator, its eigenstates are characterized by the total angular momentum J. Naturally, as an alternative choice to the m-scheme, one can construct a basis composed of states carrying J as a good quantum number, the so-called J-coupled basis. The reduction in dimensionality as compared to the m-scheme basis is significant, especially if the basis is composed of $J = 0$ states only (see Table 2.1). The evaluation of the Hamiltonian matrix elements in the J-coupled scheme is, however, much more elaborate. It typically involves products of coefficients of the fractional parentage and coupling ($3J$), recoupling ($6j$) and $9j$ coefficients. Furthermore, the basis size reduction decreases with increasing value of J[34]. For example, in case of the ^{56}Ni valence space, the ratio $\dim(M = J)/\dim(J)$ is 70 for $J = 0$ but only 5.7 for $J = 6$. These disadvantages meant that whereas the earliest SM codes were of this type, they yielded to m-scheme codes as computer resources became more robust. The SM codes implementing the J-coupled scheme are, for example, the Rochester- Oak Ridge Multi-Shell code [40] and NATHAN [37].

Classification of Many-Body States in Nuclear Shell Model Framework

Many-body states are conventionally classified according to the number of the harmonic oscillator quanta they carry. The valence space, which is composed of the

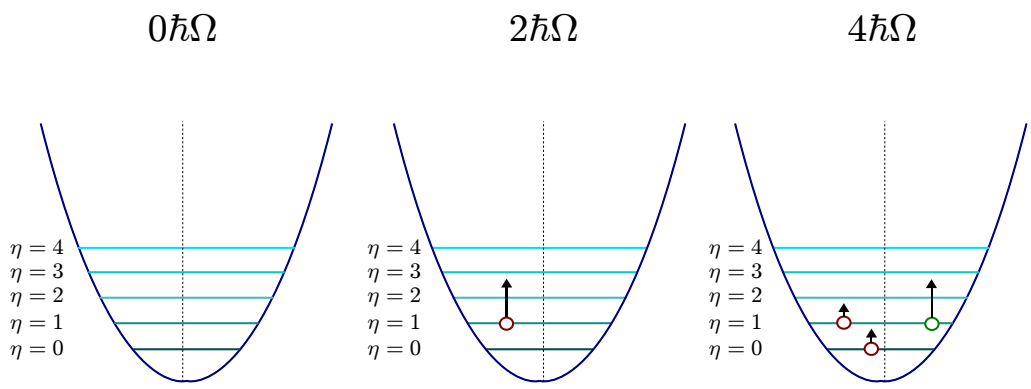

Figure 2.2: Examples of $0\hbar\Omega$, $2\hbar\Omega$, and $4\hbar\Omega$ configurations in ^{6}Li.

many-body configurations with the minimum energy of the harmonic oscillator, is in this classification denoted as the $0\hbar\Omega$ space. Many-body states carrying N more oscillator quanta than those in the $0\hbar\Omega$ space constitute the $N\hbar\Omega$ space. It is important to note that states spanning a given $N\hbar\Omega$ space have the same parity. In this way an infinite dimensional Hilbert space is partitioned into an infinite number of the finite dimensional subspaces. The examples of $0\hbar\Omega$, $2\hbar\Omega$, and $4\hbar\Omega$ many-body configurations of ^{6}Li are schematically depicted in Fig. 2.2.

2.2.2 Occupation Number Representation

The evaluation of the matrix elements in the coordinate representation of the m-scheme states is an extremely tedious process even for a system of few nucleons, and it quickly becomes unmanageable as the number of nucleons increases. The manipulation with the m-scheme states can be greatly simplified in the occupation number representation. This approach is also known as the second quantization formalism since it utilizes the method of the quantum field theory, particularly creation and annihilation operators acting in the Fock space.

A fermion in a quantum state described by a single-particle wave function $\varphi_\alpha(\mathbf{x})$ is created by action of the fermion creation operator $a^\dagger_\alpha$ on the vacuum state $|0\rangle$:

$$a^\dagger_\alpha |0\rangle = |\alpha\rangle \,, \tag{2.10}$$

where α stands for a set of single-particle quantum labels, e.g. ηljm in case of the SM framework.

The vacuum state is a reference state, and thus it can have a different meaning. In case of the traditional SM calculations, it corresponds to the inert closed-shell core. Whereas for a quantum system where all particles are active, it signifies a state with no nucleons.

The annihilation operator a_α, which is the Hermitian conjugate of the creation operator $a_\alpha^\dagger$, annihilates a fermion in the state $|\alpha\rangle$,

$$a_\alpha |\alpha\rangle = a_\alpha a_\alpha^\dagger |0\rangle = |0\rangle . \tag{2.11}$$

A Slater determinant is formed by the successive action of multiple creation operators acting in a given order,

$$|\alpha_A, \alpha_{A-1}, \ldots, \alpha_1\rangle = \prod_{i=1}^{A} a_{\alpha_i}^\dagger |0\rangle . \tag{2.12}$$

The Fermi-Dirac statistic of a many-fermion state (2.12) is built-in automatically through the anticommutation relations for the fermionic creation and annihilation operators,

$$\{a_\alpha^\dagger, a_\beta^\dagger\} = 0, \quad \{a_\alpha, a_\beta\} = 0, \tag{2.13}$$

$$\{a_\alpha^\dagger, a_\beta\} = \delta_{\alpha\beta}. \tag{2.14}$$

These relations are valid only between the creation and annihilation operators of the same kind of fermions. In case of the proton-neutron formalism both proton and neutron creation operators must be employed to construct the m-scheme states as a product of the two Slater determinants

$$|\pi_Z, \pi_{Z-1}, \ldots, \pi_1, \nu_N, \nu_{N-1}, \ldots, \nu_1\rangle = \prod_{i=1}^{Z} a_{\pi_i}^\dagger \prod_{j=1}^{N} a_{\nu_j}^\dagger |0\rangle . \tag{2.15}$$

Since the antisymmetrization between protons and neutrons is not required, proton and neutron creation and annihilation operators commute

$$\left[a_\pi^\dagger, a_\nu^\dagger\right] = 0, \quad [a_\pi, a_\nu] = 0, \quad \left[a_\pi^\dagger, a_\nu\right] = 0. \tag{2.16}$$

Operators In Occupation Number Representation

A key advantage of the occupation number representation is the simplicity of calculation of matrix elements between many-fermion Slater determinants. The simplicity becomes apparent once the many-body operators are written in the occupation number representation.

A general one-body operator for a system of K fermions reads

$$\hat{O} = \sum_{i=1}^{K} O(\mathbf{x}_i) , \tag{2.17}$$

where $\mathbf{x}_i$ represents coordinates and spin of the ith fermion. It can be shown that in the occupation number representation $\hat{O}$ becomes

$$\hat{O} = \sum_{\alpha,\beta} \langle\alpha| \hat{O} |\beta\rangle \, a_\alpha^\dagger a_\beta, \tag{2.18}$$

where the summation runs over all available single-particle states, and $\langle\alpha|\,\hat{O}\,|\beta\rangle$ denotes a one-body matrix element between single-particle states $\varphi_\alpha(\mathbf{x})$ and $\varphi_\beta(\mathbf{x})$,

$$\langle\alpha|\,\hat{O}\,|\beta\rangle = \int \varphi^*_\alpha(\mathbf{x}) O(\mathbf{x}) \varphi_\beta(\mathbf{x}) d\mathbf{x}. \tag{2.19}$$

For a general two-body operators acting on a system of K identical fermions, we have in coordinate space

$$\hat{O} = \sum_{i<j=1}^{K} O\left(\mathbf{x}_i, \mathbf{x}_j\right), \tag{2.20}$$

which in the occupation number representation becomes

$$\hat{O} = \frac{1}{4} \sum_{\alpha\beta\gamma\delta} \langle\alpha\beta|\,\hat{O}\,|\gamma\delta\rangle_{\mathbb{NAS}}\, a^\dagger_\alpha a^\dagger_\beta a_\delta a_\gamma. \tag{2.21}$$

Here, the indices α, β, γ, and δ iterate over all available single-particle states, and the subscript $\mathbb{NAS}$ indicates that the two-body matrix elements are evaluated between properly normalized and antisymmetrized two-fermion wave functions. It can be shown that

$$\langle\alpha\beta|\,\hat{O}\,|\gamma\delta\rangle_{\mathbb{NAS}} = \langle\alpha\beta|\,\hat{O}\,|\gamma\delta\rangle - \langle\alpha\beta|\,\hat{O}\,|\delta\gamma\rangle\,, \tag{2.22}$$

where

$$\langle\alpha\beta|\,\hat{O}\,|\delta\gamma\rangle = \int d\boldsymbol{x}_1 \int d\boldsymbol{x}_2\, \psi^*_\alpha(\boldsymbol{x}_1)\psi^*_\beta(\boldsymbol{x}_2) O(\boldsymbol{x}_1, \boldsymbol{x}_2) \psi_\delta(\boldsymbol{x}_1)\psi_\gamma(\boldsymbol{x}_2). \tag{2.23}$$

In our approach we treat protons and neutrons as distinguishable particles and hence the expression (2.21) must be recast into a form compatible with the proton-neutron formalism. This is done by splitting the two-body operator into three terms

$$\begin{aligned}\hat{O} = {} & \frac{1}{4} \sum_{\pi_\alpha\pi_\beta\pi_\gamma\pi_\delta} \langle\pi_\alpha\pi_\beta|\,\hat{O}\,|\pi_\gamma\pi_\delta\rangle_{\mathbb{NAS}}\, a^\dagger_{\pi_\alpha} a^\dagger_{\pi_\beta} a_{\pi_\delta} a_{\pi_\gamma} + \frac{1}{4} \sum_{\nu_\alpha\nu_\beta\nu_\gamma\nu_\delta} \langle\nu_\alpha\nu_\beta|\,\hat{O}\,|\nu_\gamma\nu_\delta\rangle_{\mathbb{NAS}}\, a^\dagger_{\nu_\alpha} a^\dagger_{\nu_\beta} a_{\nu_\delta} a_{\nu_\gamma} \\ & + \sum_{\pi_\alpha\nu_\beta\pi_\gamma\nu_\delta} \langle\pi_\alpha\nu_\beta|\,\hat{O}\,|\pi_\gamma\nu_\delta\rangle\, a^\dagger_{\pi_\alpha} a_{\pi_\gamma} a^\dagger_{\nu_\beta} a_{\nu_\delta},\end{aligned} \tag{2.24}$$

with π and ν denoting proton and neutron single-particle states respectively. Notice that the order of creation and annihilation operators in the last term has been changed utilizing the commutation relations (2.16). Also notice that in the last term we evaluate the two-body matrix elements between one-proton-one-neutron wave functions, and hence no antisymmetrization is required.

2.2.3 Lanczos Algorithm

Any review of the SM framework would not be complete without description of the Lanczos algorithm [41, 42, 43]. Its notable features, namely, O(n^2) time complexity

for sparse matrices, low memory requirements, straightforward implementation as a highly scalable parallel algorithm [44], enables large scale calculations involving nuclear Hamiltonian matrices with dimensions as high as 1.1×10^9 [45]. In contrast, the regular methods for solving complete eigenvalue problem require $\mathrm{O}(n^3)$ time, and hence they are not suitable for the large scale SM calculations where dimensions of symmetric sparse matrices are huge and only several lowest-lying eigenstates are needed.

The Lanczos iterative algorithm builds up an orthogonal "Lanczos" basis, which transforms a Hermitian matrix H into a real symmetric tridiagonal matrix T_k,

$$T_k = \begin{pmatrix} \alpha_1 & \beta_2 & 0 & 0 & \dots & 0 & 0 \\ \beta_2 & \alpha_2 & \beta_3 & 0 & \dots & 0 & 0 \\ 0 & \beta_3 & \alpha_3 & \beta_4 & \dots & 0 & 0 \\ \vdots & \vdots & \vdots & \vdots & \vdots & \vdots & \vdots \\ 0 & 0 & 0 & 0 & \dots & \alpha_{k-1} & \beta_k \\ 0 & 0 & 0 & 0 & \dots & \beta_k & \alpha_k \end{pmatrix}. \tag{2.25}$$

The subscript k signifies that T_k is obtained during kth step. Solving the eigenvalue problem for T_k is computationally simple due to the nature of a tridiagonal matrix. It can be shown that the eigenvalues of T_k converge to the eigenvalues of the original matrix. The corresponding eigenvectors, $|\psi\rangle$, are calculated as $|\psi\rangle = Q_k |\tau\rangle$, where $|\tau\rangle$ is an eigenstate of T_k and $Q_k = (|q_1\rangle \dots |q_k\rangle)$ is an orthonormal matrix whose columns are Lanczos basis vectors.

The algorithm starts with a properly chosen normalized vector $|q_1\rangle$. The first diagonal matrix element has necessarily the form $\alpha_1 = \langle q_1| H |q_1\rangle$, the second Lanczos vector, orthogonal to $|q_1\rangle$, is obtained as $|q_2\rangle = H |q_1\rangle - \alpha_1 |q_1\rangle$. Its norm yields the non-diagonal matrix element $\beta_2 = \sqrt{\langle q_2| q_2\rangle}$. Finally, $|q_2\rangle$ is normalized and added to the Lanczos basis. At step k, we have

$$\begin{aligned} \alpha_k &= \langle q_k| H |q_k\rangle & (2.26) \\ |q_{k+1}\rangle &= H |q_k\rangle - \beta_k |q_{k-1}\rangle - \alpha_k |q_k\rangle & (2.27) \\ \beta_{k+1} &= \sqrt{\langle q_{k+1}| q_{k+1}\rangle} & (2.28) \\ |q_{k+1}\rangle &= \frac{|q_{k+1}\rangle}{\beta_{k+1}}. & (2.29) \end{aligned}$$

The iteration continues until all the required eigenvalues are converged. Notice that at the end of step k we may throw away vector $|q_{k-1}\rangle$, which further reduces the memory requirements.

The computational effort at each step is dominated by only one matrix-vector multiplication $H |q_k\rangle$ which greatly facilitates the large scale SM calculations. The nuclear Hamiltonian matrices are sparse in the m-scheme basis representation. The number of non-zero matrix elements, therefore, increases linearly instead of quadratically. As a consequence, the computational complexity of the matrix-vector multiplication is almost linear.

In an exact arithmetic limit, the Lanczos algorithm builds an orthogonal basis, with the eigenvalues and eigenvectors converged to those of the original matrix. However, due to the limited arithmetic precision of computers, this is not strictly true. To solve this problem it is necessary to orthogonalize each new Lanczos vector with respect to all the preceding ones. More details on finite precision version of the Lanczos algorithm can be found in Ref. [42, 43].

Chapter 3

Ab Initio No-Core Shell Model

Our understanding of nuclear properties have experienced substantial progress over the last decade. This accomplishment was triggered by theoretical advances in the construction of realistic nuclear potential models, and, at the same time, by a dramatic increase of performance of highly parallel computing systems that allows the implementation of efficient scalable algorithms to solve the nuclear many-body problem. This development resulted in an extensive utilization of *ab initio* approaches to the nuclear many-body problem for light nuclei. The three successful *ab initio* methods: no-core shell model (NCSM) [9], Green's function Monte Carlo [10, 11], and coupled cluster expansion method [12], which integrate modern realistic interactions with cutting-edge numerical algorithms, represent an important milestone in our efforts to achieve the ultimate objective of the nuclear structure theory as stated by Maria G. Mayer [46] several decades ago: *If forces are known, one should in principle be able to calculate deductively the properties of individual complex nuclei. Only after this has been accomplished can one say that one completely understands nuclear structures.*

The NCSM has become a prominent tool for studying the microscopic aspects of the structure of light nuclei. It has achieved a good description of the nuclear spectra and observables for few-nucleon systems [13] up through more complex nuclei such as ^{12}C [9, 47] utilizing modern two- and three-nucleon interactions. Furthermore, the NCSM is currently the only *ab initio* technique capable to solve the Schrödinger equation with non-local interactions [48, 49], e.g. those derived within the chiral perturbation theory.

In this chapter, we will first briefly discuss the modern realistic two- and three-nucleon potentials. We will then review the NCSM framework including the unitary transformation approach to derive the effective Hamiltonian from the underlying realistic interactions, and will discuss the importance of the NCSM results to the other fields of physics such as probing the physics beyond the standard model, neutrino experiments, or astrophysical applications. Finally, we will discuss the bottleneck of the NCSM approach: the scale explosion, that is, the combinatorial growth of m-scheme basis size for heavier nuclei and larger model spaces.

3.1 Realistic Interactions

The unprecedented success of the *ab initio* methods in the nuclear structure physics would not be possible without improvement in the construction of realistic internucleon interactions. An internucleon interaction is considered realistic if it describes the nucleon-nucleon scattering Nijmegen dataset [50] with a χ^2 per datum very close to one, and, at the same time, reproduces the properties of the deuteron perfectly. Such a condition is not rigorous [51], e.g. it does not guarantee agreement with experimental data for $A \geq 3$ nuclear system. There presently exist, however, a "zoo" of modern realistic nuclear potentials models that reproduce a wide range of physical observables in more complex nuclei containing up to $A = 16$ nucleons. They can be divided into three main types: phenomenological meson-exchange potentials, potentials derived at a fundamental level from the low-energy regime of the quantum chromodynamics (QCD), and nucleon-nucleon potentials that use unitary transformations to partially absorb effects of multi-nucleon forces.

3.1.1 Phenomenological Meson-Exchange Potentials

The family of phenomenological meson-exchange nuclear interactions includes the Nijmegen potentials [3], the Argonne V18 potential [4], and the CD-Bonn potential [5, 6]. All of these potentials are charge dependent and use about 45 parameters to describe the nucleon-nucleon scattering at energies up to 350 MeV with an unprecedented precision. Their common theoretical background is based upon the meson-exchange model augmented by the electromagnetic interaction and a (more or less) phenomenological short-range interaction. The long-range part of the interaction is generally the one-pion-exchange potential, which in the local approximation takes form [52]

$$\begin{aligned} V_{1\pi}(\mathbf{r}) &= \frac{g_\pi^2}{12\pi}\left(\frac{m_\pi}{2M}\right)^2\left[\left(\frac{e^{-m_\pi r}}{r} - \frac{4\pi}{m_\pi^2}\delta^{(3)}(\mathbf{r})\right)\sigma_{\mathbf{1}}\cdot\sigma_{\mathbf{2}}\right. \\ &\quad \left. + \left(1 + \frac{3}{m_\pi r} + \frac{3}{(m_\pi r)^2}\right)\frac{e^{-m_\pi r}}{r}\mathbf{S_{12}}\right], \end{aligned} \tag{3.1}$$

where M and m_π denote the nucleon and pion mass, respectively, g_π is the pion-nucleon coupling constant, and $\mathbf{S_{12}}$ denotes the usual tensor-force operator

$$\mathbf{S_{12}} = \frac{3(\sigma_1\cdot\mathbf{r})(\sigma_2\cdot\mathbf{r})}{r^2} - \sigma_{\mathbf{1}}\cdot\sigma_{\mathbf{2}}. \tag{3.2}$$

The CD-Bonn potential uses the full, original, nonlocal Feynman amplitude for one-pion-exchange [6], while all other potentials apply local approximations. In spite of some seemingly significant differences, all of these phenomenological meson-exchange potential models are about equally successful in reproducing the properties of the deuteron.

On the other hand, calculations of the binding energies of $A \geq 3$ nuclei yield values that are consistently less than the corresponding experimental values by

about 5-10% [53]. The phenomenological nucleon-nucleon interaction models also fail to describe the nucleon-deuteron elastic scattering data, especially at higher energies [54]. These drawbacks are traditionally overcome by the inclusion of three-nucleon forces whose presence is a direct consequence of the quark substructure of the nucleons. The three-nucleon phenomenological interactions are constructed primarily as two-pion-exchange potentials. The best known of these models are the Tucson-Melbourne [55, 56] and the Brazil [57] potentials. Other three-nucleon interaction models are the Illinois potential [58], incorporating three-pion-exchange term, and the Urbana potential [59], based on mechanism of two-pion-exchange with the excitation of intermediate Δ resonance. The parameters of three-nucleon potentials are determined by fitting to the three-nucleon scattering data[1] as well as experimental binding energies and the first excited states of $A \geq 3$ nuclei.

The process of finding a consistent combination of phenomenological two- and three-nucleon potentials, accomplished through the fitting to various properties of $A \geq 3$ nuclear system, lacks a solid theoretical foundation. There exist several parameterizations for each three-nucleon force model depending on the nucleon-nucleon potential chosen. The resulting nuclear potentials do not take the chiral symmetry and its breaking pattern systematically into account. Furthermore, even if the particular combination of forces predicts the ^{3}H and ^{4}He binding energies precisely, it may fail for p-shell nuclei [58]. Clearly, there is a need for a systematic theory of nuclear interactions that would treat two- and many-body force on an equal footing, and at the same time would be consistent with the symmetries of the low-energy QCD.

3.1.2 Chiral Perturbation Potentials

The fundamental theory of strong interactions, QCD, is non-perturbative in the low-energy regime characteristic of nuclear physics and hence derivation of the nuclear forces from the fundamental theory of strongly coupled quarks and gluons is an incredibly complicated task. A promising advance in the theory of nuclear forces emerged when the concept of an effective field theory [28] was applied to low-energy QCD giving rise to chiral perturbation theory [30, 29]. This approach represents a best up-to-date bridge between QCD and nuclear structure. It is based on the recognition that at energies below 1 GeV, the appropriate degrees of freedom are not quarks and gluons, but pions and nucleons interacting via a force governed by spontaneously broken approximate chiral symmetry. Broken chiral symmetry [60] is a crucial constraint that generates and controls low-energy dynamics of QCD and allows the relevant dynamical features of QCD to be properly incorporated into the nuclear force problem.

The explicit and spontaneous breaking of chiral symmetry facilitates a derivation of internucleon interaction from an effective chiral Lagrangian using a perturbation expansion in powers of (Q/Λ_χ), where Q denotes a momentum or pion mass,

[1] Three-nucleon scattering experiments provide data in the total isospin $T = 1/2$ states only, and thus can not determine structure of the three-nucleon force in $T = 3/2$ channel.

and Λ_χ is the chiral symmetry breaking scale of the order of 1 GeV. The resulting power series generate two-, three- and four-nucleon forces on an equal footing, and furthermore, naturally explain the empirically known hierarchy of nuclear forces, i.e. $V_{2N} \gg V_{3N} \gg V_{4N}$.

The nucleon-nucleon interaction based on the chiral perturbation theory was constructed including all the terms appearing in the chiral perturbation expansion up to order Q^4 [7]. The accuracy of the resulting potential is comparable with the high-precision nucleon-nucleon phenomenological potentials. The leading three-nucleon interaction that appears at order Q^3 was also constructed [8]. The first calculations with the two- and three-nucleon chiral potentials have been performed in the NCSM framework for the p-shell nuclei [49, 48].

3.1.3 JISP Potentials

The computational complexity induced by the inclusion of a three-nucleon potential in the many-body quantum problem has triggered development of the nucleon-nucleon potential models that minimize the role of the three-nucleon interaction. The key principle underlying this approach is provided by the seminal work of Polyzou and Glöckle [51] who demonstrated that the three-body force effect can be, to a certain extend, reproduced by the phase-equivalent unitary non-local transformation of the two-body interaction. The nuclear potentials exploiting the residual freedoms of a realistic nucleon-nucleon interaction are the inside-nonlocal-outside-Yukawa (INOY) interaction [61], the similarity renormalization group (SRG) transformed interactions [62, 63, 64], the unitary correlation operator method (UCOM) interaction [65, 66], and the J-matrix inverse scattering potential (JISP) [1, 2]. An interaction based on the JISP potential was used to generate the NCSM results presented in this study.

The JISP potentials are constructed in two steps. The nucleon-nucleon interaction is first derived from the J-matrix inverse scattering approach [67], and consequently altered by a unitary phase-equivalent transformation in order to give an improved description of deuteron quadrupole moment, and to obtain excellent fits to the spectra of stable p-shell nuclei. The resulting interaction, JISP6 [1], yields a very good description of the spectra of $A < 10$ nuclei while providing a rapid convergence of the NCSM calculations. Results are competitive with the ones obtained with nucleon-nucleon and three-nucleon forces. Nevertheless, the JISP6 interaction overbinds nuclei with $A \geq 10$. The newer JISP16 [2] potential, obtained from JISP6 by fitting to the excitation energies of ^{6}Li and binding energies of ^{6}Li and ^{16}O, eliminates this deficiency.

3.2 No-Core Shell Model Framework

The NCSM framework can be regarded as an extension of the conventional SM. Albeit both methods share two important components, the m-scheme basis and the Lanczos algorithm, the NCSM framework goes well beyond conventional SM

approximations. While the conventional SM approach treats a nucleus as a system composed of an inert closed-shell core and interacting valence nucleons whose many-body configurations are restricted upon the $0\hbar\Omega$ subspace, the NCSM approach treats all nucleons as active particles. The model space is composed of many-body states with up to $N_{\max}$ excitations above the valence space configurations.

The *ab initio* NCSM targets solving the Schrödinger equation for a system of A point-like non-relativistic strongly interacting nucleons. The general translationally invariant Hamiltonian for this problem reads

$$H_A = \left[\sum_{i=1}^{A} \frac{\mathbf{p}_i^2}{2m} - \frac{\mathbf{P}^2}{2mA}\right] + \sum_{i<j=1}^{A} V_{ij} = \frac{1}{A}\sum_{i<j=1}^{A} \frac{(\mathbf{p}_i - \mathbf{p}_j)^2}{2m} + \sum_{i<j=1}^{A} V_{ij}, \tag{3.3}$$

where $\mathbf{P} = \sum_{i=1}^{A} \mathbf{p}_i$ is the total momentum. The first term is the relative kinetic energy operator obtained by subtracting the contribution due to the kinetic energy of the center-of-mass (c.m.) motion, and V_{ij} denotes a realistic nucleon-nucleon interaction.

In principle, three- and even four-body interactions should be included in a realistic nuclear Hamiltonian. As noted in Section 3.1, these higher-order many-body forces are a direct consequence of the quark substructure of the nucleons. They appear naturally in nuclear potentials that are derived from the low-energy limit of the QCD using the chiral perturbation theory [28, 29, 30] or the quark-meson coupling model [31]. However, for the purpose of this chapter, that is, the description of the elementary principles and techniques of the NCSM approach, we can without loss of generality limit the discussion to just two-body interactions.

In order to facilitate the use of the m-scheme basis, the Hamiltonian (3.3) is modified by adding the c.m. harmonic oscillator Hamiltonian

$$H_{\text{c.m.}} = \frac{\mathbf{P}^2}{2mA} + \frac{1}{2}Am\Omega^2\mathbf{R}^2, \tag{3.4}$$

where Ω is the harmonic oscillator frequency, $\mathbf{R} = 1/A\sum_{i=1}^{A}\mathbf{r}_i$. Using the relation,

$$\sum_{i=1}^{A}\frac{1}{2}m\Omega^2\mathbf{r}_i^2 = \frac{1}{2}mA\Omega^2\mathbf{R}^2 + \frac{m\Omega^2}{2A}\sum_{i<j=1}^{A}(\mathbf{r}_i - \mathbf{r}_j)^2, \tag{3.5}$$

the modified Hamiltonian can then be recast as

$$H_A^{\Omega} = \sum_{i=1}^{A}\left[\frac{\mathbf{p}_i^2}{2m} + \frac{1}{2}m\Omega^2\mathbf{r}_i^2\right] + \sum_{i<j=1}^{A}\left[V_{ij} - \frac{m\Omega^2}{2A}(\mathbf{r}_i - \mathbf{r}_j)^2\right], \tag{3.6}$$

where the first term is just a sum of one-particle harmonic oscillators that is diagonal in the m-scheme basis. The Hamiltonian H_A^{Ω} can be schematically written as

$$H_A^{\Omega} = \sum_{i=1}^{A} h_i + \sum_{i<j=1}^{A} V_{ij}^{A,\Omega}. \tag{3.7}$$

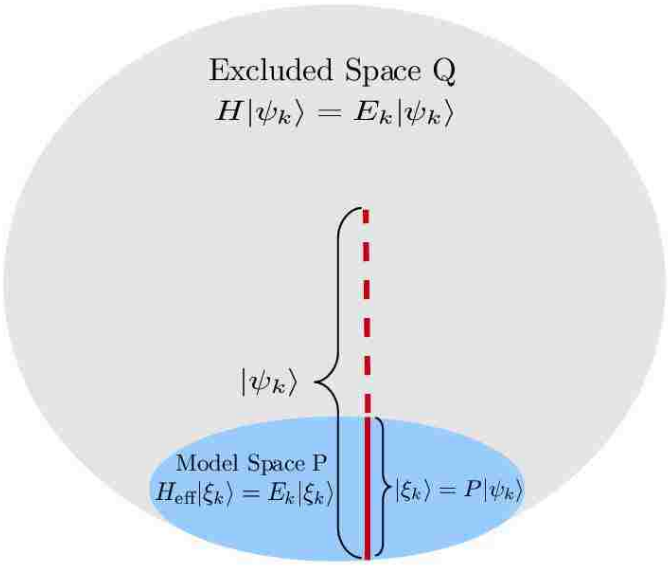

Figure 3.1: Schematic illustration of the properties of the effective Hamiltonian $H_{\rm eff}$; each eigenstate $|\xi_k\rangle$ of $H_{\rm eff}$ is a model space component of a bare Hamiltonian eigenstate $|\psi_k\rangle$ which has the same eigenvalue E_k.

Although the addition of $H_{\rm c.m.}$ introduces a pseudo-dependence upon the harmonic oscillator frequency Ω, it does not affect the final results. This can be readily seen from the fact that the intrinsic eigenstates of the Hamiltonian H_A, which are Ω-independent, are simultaneously eigenstates of the Hamiltonian H_A^Ω. The addition of the $H_{\rm c.m.}$ merely increases the energy of the intrinsic eigenstates by an overall constant $\frac{3}{2}\hbar\Omega$ which is subtracted in the final stage of the NCSM calculation.

The Hamiltonian H_A^Ω is not translationally invariant, and hence it yields spurious eigenstates with excited c.m. motion. It is necessary to choose from among the eigenstates of H_A^Ω only intrinsic ones, that is, those with the c.m. in its ground state. This is done by projecting spurious eigenstates upwards in the energy spectrum by addition of the Lawson projection term

$$\lambda \left(H_{\rm c.m.} - \frac{3}{2}\hbar\Omega \right), \tag{3.8}$$

into the Hamiltonian H_A^Ω. The Lawson projection term shifts eigenstates with excited c.m. motion up to high energies for sufficiently large value of λ, while leaving the energies of the intrinsic states unaltered.

To obtain numerical solutions of the A-body Schrödinger equation, it is necessary to truncate the full infinite Hilbert space to a finite and computationally tractable model space. The model space is comprised of all many-body states with up to $N_{\rm max}\hbar\Omega$ harmonic oscillator excitations above the valence space configurations. The bare Hamiltonian H_A^Ω would yield unreasonable results in a finite model

space unless the effect of the excluded configurations is taken into account. As a consequence, H_A^Ω must be replaced by a model space dependent effective Hamiltonian $H_{\rm eff}$ that reproduces the low-lying spectrum of the bare Hamiltonian, and whose eigenstates are the model space components of the true eigenstates of H_A^Ω, as illustrated in Fig. 3.1. Similarly, operators associated with physical observables, such as electromagnetic transitions, should also be replaced by the effective operators tailored to the given model space.

3.3 Lee-Suzuki Similarity Transformation Method

The effective operators are constructed by means of the Lee-Suzuki similarity transformation method [68, 69]. One can use either its non-Hermitian form [68], or employ its unitary generalization [69] to produce Hermitian effective operators. In this section, we will describe in detail both versions of the Lee-Suzuki method.

The Lee-Suzuki method considers a bare Hamiltonian of form $H = H_0 + V$, where H_0 is the unperturbed Hamiltonian and V is a potential. In case of the bare nuclear Hamiltonian H_A^Ω (3.7), we have $H_0 = \sum_{i=1}^A h_i$, and $V = \sum_{i<j=1}^A V_{ij}^{A,\Omega}$. We will denote the eigenstates of the bare Hamiltonian by $|\psi_k\rangle$ and the corresponding eigenvalues by E_k,

$$H\,|\psi_k\rangle = E_k\,|\psi_k\rangle \quad k = 1, \ldots, +\infty. \tag{3.9}$$

The first step is to divide the full Hilbert space into a finite-dimensional model space which is referred to as the P space, and whose dimension is denoted d_P. Complementary to the model space is the space of excluded configurations, the Q space. The basis states of the P and Q spaces are denoted as $|\alpha_P\rangle$ and $|\alpha_Q\rangle$, respectively. Associated with the model space and the excluded space are the projection operators P and Q which are given as

$$P = \sum_{|\alpha_P\rangle} |\alpha_P\rangle\,\langle\alpha_P| \tag{3.10}$$

$$Q = \sum_{|\alpha_Q\rangle} |\alpha_Q\rangle\,\langle\alpha_Q|\,. \tag{3.11}$$

In addition to the standard properties, e.g. $PQ = QP = 0$, $P^2 = P$, $P^\dagger = P$, the operators P and Q are eigenprojectors of H_0, that is

$$\begin{aligned} [H_0, P] &= [H_0, Q] = 0 \\ QH_0P &= PH_0Q = 0. \end{aligned} \tag{3.12}$$

3.3.1 Non-Hermitian Formalism

The non-Hermitian form of the Lee-Suzuki method introduces a similarity transformation induced by a transformation operator ω:

$$H \longrightarrow e^{-\omega} H e^{\omega} \equiv \mathcal{H} \tag{3.13}$$

$$|\psi\rangle \longrightarrow e^{-\omega}\,|\psi\rangle \equiv |\xi\rangle\,. \tag{3.14}$$

The transformed Hamiltonian $\mathcal{H}$ is not Hermitian ($\mathcal{H}^\dagger = e^{\omega^\dagger} H e^{-\omega^\dagger} \neq \mathcal{H}$), but has an eigenspectrum identical to that of the bare Hamiltonian H. This can be seen from the fact that if $|\psi_k\rangle$ is an eigenstate of H with eigenvalue E_k, then $e^{-\omega} H e^{\omega} e^{-\omega} |\psi_k\rangle = E_k e^{-\omega} |\psi_k\rangle$. We require that the transformation operator ω satisfies

$$\omega = Q\omega P, \tag{3.15}$$

which implies that $P\omega P = Q\omega Q = P\omega Q = 0$, and $\omega^n = 0$ for $n \geq 2$. This greatly simplifies evaluation of the similarity transformation as

$$e^{\pm\omega} = 1 \pm Q\omega P. \tag{3.16}$$

In addition to condition (3.15), we also demand that the transformation operator ω is such that $\mathcal{H}$ satisfies the decoupling condition

$$Q\mathcal{H}P = 0. \tag{3.17}$$

This provides the necessary and sufficient condition for determination of the effective Hamiltonian

$$H_{\text{eff}} = P\mathcal{H}P. \tag{3.18}$$

The rigorous proof of this statement can be found in Ref. [70]. Note that if ω satisfies (3.17), then for any state $|\xi\rangle \in P$ we have

$$\mathcal{H} |\xi\rangle = (P\mathcal{H}P + Q\mathcal{H}Q + P\mathcal{H}Q + Q\mathcal{H}P) |\xi\rangle = P\mathcal{H}P |\xi\rangle = H_{\text{eff}} |\xi\rangle . \tag{3.19}$$

This means that if $|\xi_k\rangle \in P$ is the eigenstate of H_{eff} with the eigenvalue E_k, then it is simultaneously also the eigenstate of $\mathcal{H}$ with the same eigenvalue E_k. The similarity transformation preserves the eigenspectrum, and hence there must exist an eigenstate $|\psi_k\rangle$ of the bare Hamiltonian H, such that $H |\psi_k\rangle = E_k |\psi_k\rangle$. We want to show that $|\xi_k\rangle$ is the P-space component of $|\psi_k\rangle$, that is, $P |\psi_k\rangle = |\xi_k\rangle$. Utilizing (3.14) and (3.16) we get:

$$|\psi_k\rangle = (1 + Q\omega P) |\xi_k\rangle = \underbrace{|\xi_k\rangle}_{\in P} + \underbrace{Q\omega P |\xi_k\rangle}_{\in Q} . \tag{3.20}$$

This relation implies that $|\xi_k\rangle$ is indeed equal to the P-space component of the bare eigenstate of H, and the Q-space component is obtained as $Q\omega |\xi_k\rangle$. Clearly, if the transformation operator ω satisfies requirements (3.17) and (3.15), then the operator

$$H_{\text{eff}} = P e^{\omega} H e^{-\omega} P = P H_0 P + P V P + P V Q \omega P = P H_0 P + V_{\text{eff}} \tag{3.21}$$

has the properties required for the effective Hamiltonian. The term V_{eff} denotes the effective interaction.

The matrix elements of the transformation operator ω are needed for evaluation of the effective Hamiltonian. From (3.15), it immediately follows that

$$\langle \alpha_P | \omega | \alpha_P \rangle = \langle \alpha_Q | \omega | \alpha_Q \rangle = \langle \alpha_P | \omega | \alpha_Q \rangle = 0. \tag{3.22}$$

Let $\mathcal{K}$ denotes a set of eigenstates of H projecting on the eigenstates of the effective Hamiltonian H_{eff}. Then for each $|\psi_k\rangle \in \mathcal{K}$ we have

$$0 = Qe^{-\omega} |\psi_k\rangle = Q(1 - Q\omega P) |\psi_k\rangle , \tag{3.23}$$

which implies

$$Q |\psi_k\rangle = Q\omega P |\psi_k\rangle . \tag{3.24}$$

As a consequence,

$$\langle \alpha_Q | \psi_k\rangle = \langle \alpha_Q | Q |\psi_k\rangle = \langle \alpha_Q | Q\omega P |\psi_k\rangle = \sum_{|\alpha_P\rangle} \langle \alpha_Q | \omega |\alpha_P\rangle \langle \alpha_P | \psi_k\rangle. \tag{3.25}$$

Since H_{eff} is not Hermitian, the eigenstates $|\xi_k\rangle$ are not orthogonal. If the $d_P \times d_P$ overlap matrix $\langle \alpha_P | \xi_k\rangle = \langle \alpha_P | \psi_k\rangle$ is invertible, then the matrix elements of ω are given as,

$$\langle \alpha_Q | \omega |\alpha_P\rangle = \sum_{|\psi_k\rangle \in \mathcal{K}} \langle \alpha_Q | \psi_k\rangle \langle \tilde{\psi}_k | \alpha_P\rangle. \tag{3.26}$$

where the tilde denotes the matrix element of the inverse overlap matrix $\langle \alpha_P | \psi_k\rangle$, that is, $\sum_{\alpha_p} \langle \tilde{\psi}_k | \alpha_P\rangle \langle \alpha_P | \psi_{k'}\rangle = \delta_{kk'}$ and $\sum_{\psi_k \in \mathcal{K}} \langle \alpha'_P | \tilde{\psi}_k\rangle \langle \psi_k | \alpha_P\rangle = \delta_{\alpha_P \alpha'_P}$. The biorthogonal states $\langle \tilde{\psi}_i|$ satisfy $\langle \tilde{\psi}_i | \psi_j\rangle = \delta_{ij}$.

In order to solve for ω one needs to find a set of d_P eigenstates $|\psi_k\rangle \in \mathcal{K}$ of the bare Hamiltonian H. That is, however, equivalent to solving the eigenproblem in the full Hilbert space. One therefore resorts to the cluster approximation and finds ω for a system of two- or three-nucleons and utilizes it to calculate two- and three-body matrix elements of the effective interaction. We will describe this procedure in detail in section 3.4.

3.3.2 Hermitian Formalism

As noted before, the similarity transformation (3.14) produces a non-Hermitian effective Hamiltonian. The Hermitian effective Hamiltonian is constructed through the unitary similarity transformation

$$H_{\text{eff}} = \left(Pe^{\omega^\dagger} e^{\omega} P\right)^{-\frac{1}{2}} Pe^{\omega^\dagger} H e^{\omega} P \left(Pe^{\omega^\dagger} e^{\omega} P\right)^{-\frac{1}{2}} , \tag{3.27}$$

where ω is the transformation operator introduced in previous section, and $\omega^\dagger$ denotes its hermitian conjugate. Since the above transformation is unitary, it can be rewritten as

$$H_{\text{eff}} = Pe^{-S} H e^{S} P, \tag{3.28}$$

where the transformation operator S is anti-Hermitian, $S^\dagger = -S$. It was shown in Ref. [69] that S can be expressed in terms of ω and $\omega^\dagger$ as

$$S = \operatorname{arctanh}(\omega - \omega^\dagger). \tag{3.29}$$

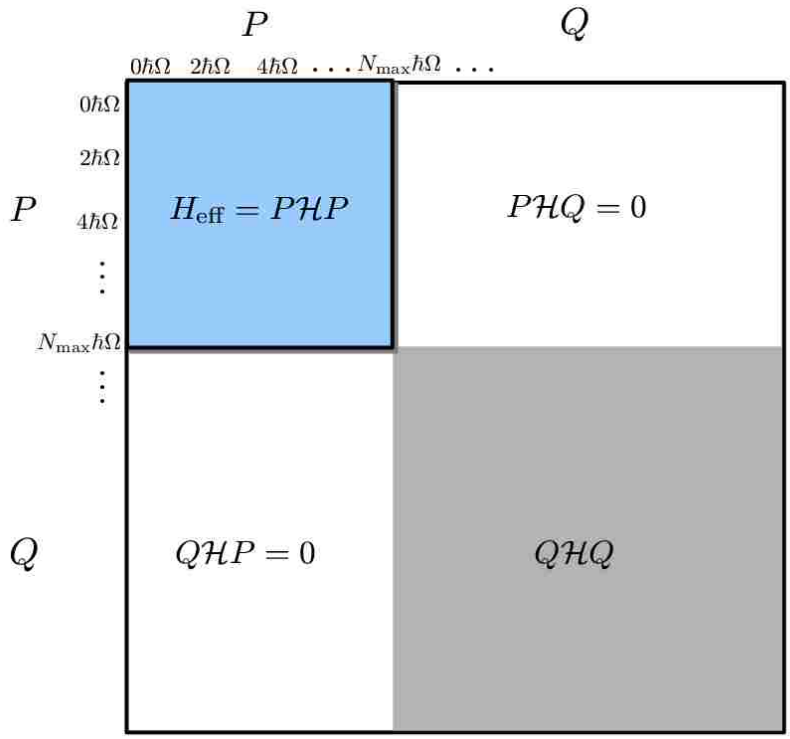

Figure 3.2: The structure of transformed Hamiltonian $\mathcal{H} = e^{-S}He^{S}$.

The operator S also satisfies the decoupling condition $Qe^{-S}He^{S}P = Pe^{-S}He^{S}Q = 0$ and the restrictive condition $PSP = QSQ = 0$ [69]. The effective interaction V_{eff} is obtained by subtraction of PH_0P term,

$$V_{\text{eff}} = H_{\text{eff}} - PH_0P. \tag{3.30}$$

A compact expression for the matrix elements of the effective Hamiltonian, derived with the help of the solution for ω (3.26), reads [14]

$$\begin{aligned}\langle\alpha_P|\, H_{\text{eff}}\, |\alpha'_P\rangle \;&=\; \sum_{|\psi_k\rangle\in\mathcal{K}} \sum_{|\alpha''_P\rangle} \sum_{|\alpha'''_P\rangle} \langle\alpha_P|\,(1+\omega^\dagger\omega)^{-\frac{1}{2}}\,|\alpha''_P\rangle\,\langle\alpha''_P|\tilde{\psi}_k\rangle E_k \langle\tilde{\psi}_k|\alpha'''_P\rangle \\ &\quad\times \langle\alpha'''_P|\,(1+\omega^\dagger\omega)^{-\frac{1}{2}}\,|\alpha'_P\rangle \end{aligned} \tag{3.31}$$

The computation of $\langle\alpha_P|\,(1+\omega^\dagger\omega)^{-1/2}\,|\alpha'_P\rangle$ is facilitated by the relation [14]

$$\langle\alpha_P|\,(1+\omega^\dagger\omega)\,|\alpha'_P\rangle = \sum_{|\psi_k\rangle\in\mathcal{K}} \langle\alpha_P|\tilde{\psi}_k\rangle\langle\tilde{\psi}_k|\alpha'_P\rangle. \tag{3.32}$$

In principle, the relation (3.31) can be utilized to find an effective interaction for a given model space P such that the lowest-lying eigenspectrum of the effective Hamiltonian H_{eff} reproduces exactly the lowest-lying eigenspectrum of the bare

Hamiltonian. The eigenstates $|\xi_k\rangle$ of H_{eff} are related to the eigenstates of the bare Hamiltonian as

$$|\psi_k\rangle = (1+\omega)[P(1+\omega^\dagger\omega)P]^{-\frac{1}{2}}\,|\xi_k\rangle\,, \tag{3.33}$$

which is the hermitian analog of relation (3.20).

Notice that until now, no approximations have been employed. In practice, however, an effective Hamiltonian is an A-body operator whose construction requires finding a set $\mathcal{K}$ of d_P lowest-lying eigenstates of a bare Hamiltonian. This makes the straightforward application of the Lee-Suzuki method for $A \geq 4$ nuclei impractical unless one resorts to an approximation.

3.4 Cluster Approximation to an Effective Interaction

An effective interaction is an A-body operator even if a bare potential consists of two-nucleon interactions only. To construct such an effective interaction is equal to finding the eigensolution of a full-space bare Hamiltonian. For this reason the Lee-Suzuki method is performed at an a-body level for which it is feasible to calculate the accurate eigensolution to the full problem. The resultant a-body effective interaction is used as an approximation to the exact, that is, A-body, effective interaction. This method, known as the cluster approximation method [71, 72, 15, 47], does not yield the effective Hamiltonian reproducing exactly a subset of the eigenspectrum of the bare Hamiltonian. The eigensolution, nevertheless, possesses a very important feature: it converges rapidly to the exact solution with increasing model space size or increasing level of clustering.

3.4.1 a-Body Cluster Approximation

In the cluster approximation, an A-body effective interaction V_{eff} is replaced by a superposition of a-body effective interactions

$$V_{\text{eff}} \simeq \frac{\begin{pmatrix} A \\ 2 \end{pmatrix}}{\begin{pmatrix} A \\ a \end{pmatrix}\begin{pmatrix} a \\ 2 \end{pmatrix}} \sum_{i_1<i_2<\cdots<i_a=1}^{A} V^{A,\Omega}_{i_1\ldots i_a\,\text{eff}}\ . \tag{3.34}$$

The a-body effective interaction is constructed through the Lee-Suzuki transformation method as

$$V^{A,\Omega}_{1\ldots a\,\text{eff}} = P_a\left(e^{-S^{(a)}}H^{\Omega}_a e^{S^{(a)}}\right)P_a - P_a\left(\sum_{i=1}^{a} h_i\right)P_a, \tag{3.35}$$

where $S^{(a)}$ is an a-body transformation operator, P_a is an a-body model space projection operator, and the a-nucleon bare Hamiltonian H^{Ω}_a is given as

$$H^{\Omega}_a = \sum_{i=1}^{a} h_i + \sum_{i<j=1}^{a} V^{A,\Omega}_{ij}. \tag{3.36}$$

Once the matrix elements of the a-particle effective interaction $V^{A,\Omega}_{1\ldots a\,\mathrm{eff}}$ are calculated, the resultant effective Hamiltonian

$$H^{(a)}_{\mathrm{eff}} = \sum_{i=1}^{A} h_i + \frac{\binom{A}{2}}{\binom{A}{a}\binom{a}{2}} \sum_{i_1<i_2<\cdots<i_a=1}^{A} V^{A,\Omega}_{i_1\ldots i_a\,\mathrm{eff}} \tag{3.37}$$

can be utilized in the NCSM calculations. Note that in order to obtain the matrix elements of the a-body effective interaction $V^{A,\Omega}_{1\ldots a\,\mathrm{eff}}$ through (3.31), one first needs to find the full space solution to the a-body Schrödinger equation (3.36). Such a task is computationally very involved even for the $a = 2$ case. In practice, therefore, one performs the Lee-Suzuki method at the two- and three-body level only.

Because of the cluster approximation, the relation (3.33) between the effective and the bare eigenstates no longer holds. However, it has been shown that even the simplest, i.e. $a = 2$, cluster approximation is a very good approximation to the exact effective Hamiltonian in the large model space limit, and that the eigenstates of the Hamiltonian $H^{(a=2)}_{\mathrm{eff}}$ are good approximations to the model space components of the bare Hamiltonian eigenstates [73].

The cluster approximation introduces a real dependence of the results upon the value of the harmonic oscillator strength Ω and the model space size $N_{\max}$. This dependence, however, decreases as the size of the model space is increased.

It can be readily seen from the equation (3.35) that if $a \to A$, the approximation becomes exact. Therefore, an improved convergence can be achieved by performing the Lee-Suzuki unitary transformation at a higher-cluster level. The convergence properties of effective interactions were investigated in case of the $A = 4$ system considering realistic two-nucleon forces. It was demonstrated that the inclusion of three-body effective interactions significantly improves the overall convergence of the results [74]. The addition of three-body effective interactions becomes imperative when genuine three-nucleon forces are included in a bare Hamiltonian. Such state-of-the-art calculations have been performed for p-shell nuclei [47, 18, 49].

3.4.2 Two-Body Cluster Approximation

Due to the computational burden, most NCSM calculations utilize the effective interactions obtained through the two-body cluster approximation. In this simplest approximation, V_{eff} is replaced by a sum of two-body effective interactions $V^{A,\Omega}_{ij\,\mathrm{eff}}$,

$$V_{\mathrm{eff}} \simeq \sum_{i<j=1}^{A} V^{A,\Omega}_{ij\,\mathrm{eff}}. \tag{3.38}$$

The two-body matrix elements of $V^{A,\Omega}_{ij\,\mathrm{eff}}$ are derived from the bare two-body Hamiltonian

$$H^{\Omega}_{2} = h_1 + h_2 + V^{A,\Omega}_{12} \tag{3.39}$$

in the following manner:

1. The two-body problem (3.39) is solved with high-precision in the relative harmonic oscillator basis for a maximal computationally tractable space [75], so that the resultant eigenstates and eigenvalues can be regarded as the eigensolution to the full two-body problem.

2. A set of d_p lowest-lying eigenstates and corresponding eigenvalues is then utilized to calculate the matrix elements of $V^{A,\Omega}_{ij\,\mathrm{eff}}$ through the prescription (3.31), where the size of the two-body model space P_2 is determined from the size of the given A-particle model space P.

The resulting effective Hamiltonian reads

$$\tilde{H}^{(a=2)}_{\mathrm{eff}} = \sum_{i=1}^{A} h_i + \sum_{i<j=1}^{A} V^{A,\Omega}_{ij\,\mathrm{eff}}, \tag{3.40}$$

and can be utilized in the NCSM calculations for the given model space P.

The important property of the two-body cluster approximation is that the two-body interaction $V^{A,\Omega}_{ij\,\mathrm{eff}}$ approaches the bare interaction $V^{A,\Omega}_{ij}$ when $P_2 \to 1$. It readily follows from the fact that the transforming operator $\omega \to 0$ with $P_2 \to 1$. As a consequence, $\tilde{H}^{(a=2)}_{\mathrm{eff}} \to H^{\Omega}_{A}$ when $N_{\max} \to \infty$, which is the essential property required for the effective Hamiltonian. As a result, the deviations of the two-body cluster approximation from the exact effective interaction can be minimized by increasing the size of the model space as much as possible. Furthermore, it has been shown that the short-range operators are renormalized well in the two-body cluster approximation [76, 77], whereas the long-range operators, such as the quadrupole transition operator, are renormalized only weakly. This implies that within the two-body cluster approximation, the short-range components of the bare interaction will be renormalized strongly as compared to the long-range correlations.

3.5 Applications

The question one may ask when facing the numerical burden of the *ab initio* NCSM approach, and generally all other *ab initio* methods, is whether a prospective outcome justifies the immense effort taken to develop and perform such complex calculations. In order to persuade the reader that this is indeed the case, we will demonstrate the importance of an accurate microscopic description of *p*- and *sd*-shell nuclei not only for a better understanding of the nuclear structures, but also for various fields of physics where the nuclear structure input is needed, and in many cases is key to achieving better predictive capability. Microscopic nuclear wave functions are important for investigations probing fundamental symmetries and physics beyond the standard model, the study of electroweak physics including neutrino experiments, and understanding the astrophysical processes that involve exotic and unstable nuclei which are not experimentally accessible.

Testing Nuclear Potential Models

The NCSM calculations with modern realistic two- and three-nucleon interactions have achieved good convergence for the lowest-lying states in p-shell nuclei, and hence serve as a stringent test of the nuclear interaction models. One of the most important problems in the theory of nuclear interactions is the structure of the three-nucleon force that has not yet been fully elucidated despite numerous experimental and theoretical investigations. The exact solutions to three- and four-nucleon problems obtained through the Faddeev-Yakubovski equations [78, 79] have been traditionally used to determine unknown parameters of the various three-nucleon interaction models. Such an approach achieves only limited success as the correct description of the $A \leq 4$ nuclei does not guarantee agreement with experiment for p-shell nuclei.

The study of the ^{10}B performed within the NCSM reveals that the Argonne and CD-Bonn realistic nucleon-nucleon potentials predict the $1^+, T = 0$ state as the ground state for this nuclei [80]. This is, however, in disagreement with experimental observation of $3^+, T = 0$ ground state. The inclusion of the Tucson-Melbourne three-nucleon interaction results in the correct level ordering as well as a level-spacing improvement in comparison to experiment [18, 47]. This study proves that the spectra of the p-shell nuclei are sensitive to the three-nucleon force. At the same time, it also manifests the ability of the *ab initio* NCSM to provide indispensable information on the structure of the three-nucleon force. This ability has been recently demonstrated by a study which succeeded to constraint values of the two low-energy constants that parametrize the short-range part of the three-nucleon interaction derived within the chiral perturbation theory [49].

The accuracy of the NCSM also facilitates construction of the nuclear potential models. For example, the JISP potentials have been derived using the NCSM calculations of stable $A = 6$ and $A = 16$ nuclei [1, 2] (see section 3.1.3).

Parity-Violating Elastic Electron Scattering

Two primary motivations underlie the high-precision measurements of parity-violating scattering of longitudinally polarized electrons from even-even, N=Z light nuclei. These types of experiments serve as a test for a new physical phenomena beyond the standard model. It also offers a window into the quark content of the nucleon; namely, providing information on the strange quark contributions to the distribution of charge and magnetization of the nucleon [81, 82]. The accuracy of recent state-of-the-art measurements enabled placing tight constraints on the size of possible contributions from physics beyond the standard model [83], and for the first time, the strange electric form factor of the nucleon was isolated [84].

The parity-violating electron scattering experiments measure the parity-violating asymmetry

$$\mathcal{A} = \frac{d\sigma_+ - d\sigma_-}{d\sigma_+ + d\sigma_-}, \tag{3.41}$$

where $d\sigma_{+(-)}$ is the cross section for right (left) handed electrons. The parity-violating asymmetry $\mathcal{A}$ for scattering of polarized electrons from a $0^+, T = 0$ nuclear targets can be derived from the low-energy electroweak interaction between electron and quarks. Assuming the existence of a non-negligible strangeness content of the nucleon, the parity violating asymmetry is given as

$$\mathcal{A} = -\frac{Gq^2}{4\pi\alpha\sqrt{2}} \left(\frac{\tilde{F}_C(q)}{F_C(q)} + \frac{F_C^{(s)}(q)}{F_C(q)} \right), \tag{3.42}$$

where G is the Fermi constant, α is the fine structure constant, and q is the magnitude of the three-momentum transfer. The asymmetry $\mathcal{A}$ depends on the nuclear structure through the electromagnetic form factor $F_C(q)$, as well as on subnucleonic structure described by the neutral current form factor $\tilde{F}_C(q)$, and the strangeness form factor $F_C^{(s)}(q)$.

For an isospin invariant system the ratio $\tilde{F}_C(q)/F_C(q)$ is independent of nuclear structure being equal to $-4\sin^2\theta_W$. However, mostly because of the Coulomb interaction, isospin symmetry is violated and the ratio must be modified by the isospin-mixing correction term Γ [85, 9]

$$\frac{\tilde{F}_C(q)}{F_C(q)} = -4\sin^2\theta_W\,(1+\Gamma)\,. \tag{3.43}$$

The accurate evaluation of the isospin-mixing correction term Γ is important for design of parity-violating electron scattering experiments and analysis of the resulting experimental data. In practice, one should aim to minimize the nuclear structure effects and perform experiment for the momentum transfer q such that Γ is below the experimental precision.

The theoretical estimates of Γ based on realistic nuclear structure considerations were evaluated in Ref. [85]. Specifically, the Hartree-Fock and interacting shell model methods were utilized to compute Γ for ^{4}He, ^{12}C, ^{16}O, and ^{28}Si, yielding estimates reliable to $\pm 20\%$. The more accurate evaluation of the isospin-mixing corrections was performed by the NCSM for ^{12}C [9] with the CD-Bonn nucleon-nucleon interaction. This investigation identified the kinetic regions for which $\Gamma < 1\%$, and hence provided results relevant for the design of the prospective parity-violating electron scattering experiments on ^{12}C target nuclei. In the same study, the electromagnetic and strangeness charge form factors were computed, and the ratio $F_C^{(s)}(q)/F_C(q)$ was analyzed with respect to the dependence on the strangeness radius and magnetic moments. This study clearly demonstrates the predictive capability of the *ab initio* NCSM approach. Nevertheless, the accurate estimation of isospin-mixing corrections for ^{28}Si still remains to be done as the region of *sd*-shell nuclei is not accessible for the NCSM.

Gamow-Teller Transitions In the A=14 Multiplet

Numerous theoretical attempts were made to explain anomalously slow β decay from the $0^+, T = 1$ ground states of ^{14}C and ^{14}O nuclei to the $1^+, T = 0$ ground

state of stable ^{14}N nucleus. While all the quantum numbers are suggesting that β decay can proceed through the Gamow-Teller (GT) transition, the experimental decay rate indicates that the transition matrix elements are very close to zero. This anomaly results in long lifetime of ^{14}C and thus facilitates dating techniques.

The theoretical investigations of this anomaly were typically performed within the shell-model framework with $0\hbar\Omega$ [86, 87, 88] or $0\hbar\Omega + 2\hbar\Omega$ model space [89]. It was shown that the tensor force induces a configuration mixing that may leads to nearly vanishing transition matrix elements.

The allowed GT transitions from the ground state of ^{14}N to the lowest-lying states of ^{14}C were studied within the NCSM framework [90] using the Argonne interaction and a $6\hbar\Omega$ model space. Results show that the ground-state-to-ground-state GT matrix element is rapidly decreasing with increasing size of the model space. The NCSM calculations also predict a strong summed GT strength for the 2^+ states versus a weak value for the 1^+ states. However, neither an accurate reproduction of the experimental strengths, nor a detailed description of fragmentation over three 2^+ final states has been achieved [91].

This result is interpreted as an indication that the NCSM is affected by the incapability of the computationally manageable model spaces to describe α-clustering nature of the lowest-lying states of ^{14}C [92].

Neutrino Studies

Neutrino studies represent another field of physics where the microscopic wave function resulting from the NCSM calculations are of great importance. Neutrino scattering analysis are largely influenced by nuclear corrections related to ^{12}C as an ingredient of liquid scintillators and ^{16}O as the main component of the water Čerenkov detectors. Presently available shell model approaches with input to ν-nucleus scattering are typically restricted in regard to both the interactions and model spaces used [93, 94]. The cross section of neutrino-^{12}C exclusive scattering has been investigated using the wave functions obtained in the NCSM [95]. The theoretical prediction obtained for CD-Bonn two-nucleon interaction and the $6\hbar\Omega$ model space is smaller by factor of 2.4 as compared to the experimental cross section. When realistic three-nucleon Tucson-Melbourne interaction is included, the predicted cross section is about 30% lower then experiment in the $4\hbar\Omega$ model space. Qualitatively similar results were obtained for a different electroweak reaction, namely, the muon capture on ^{12}C. Improvements comparing to experiment are expected when higher-$\hbar\Omega$ configurations are taken into account.

Test of Standard Model and Detection of Dark Matter

Probing isospin symmetry breaking based on superallowed $0^+ \rightarrow 0^+$ Fermi β decays is of special current interest as it provides the most precise test for the unitarity of the Cabibbo-Kobayashi-Masakawa (CKM) quark-mixing matrix and for the conserved vector current hypothesis in the standard model. Any deviation from the CKM unitarity, or evidence for nonidentical corrected ft values for the super-

allowed decays, points to new physics beyond the standard model. However, the present theoretical prediction of the nuclear-structure dependent correction [96, 97] introduces systematic deviation that outweighs the experimental uncertainties. A novel *ab initio* approach is needed to decrease theoretical uncertainties when applied to the superallowed β emitters as ^{14}O and ^{26}Al together with the recently accessed ^{18}Ne [98] and ^{22}Mg [99, 100], as the *sd*-shell region is currently out of reach by the NCSM calculations due to the computationally intractable model space sizes.

Nuclear corrections for *sd*-shell nuclei are also significant in data analysis related to a possible detection of dark matter, which presumably is an essential cosmic building block. Present dark matter detectors rely on identification of weakly interacting massive particles (WIMP) in elastic scattering from the detector nuclei, such as ^{29}Si in the Cryogenic Dark Matter Search experiment. Other nuclei involved in the WIMP-nucleus scattering include ^{19}F, ^{23}Na, and ^{27}Al.

Astrophysics

Modeling of astrophysical processes and calculating reaction rates require accurate nuclear masses, proton and neutron separation energies, level energies, transition rates and spectroscopic factors. For nuclei where experimental data might not be available or hold large uncertainties, *ab initio* calculations [101, 102] hold promise to provide accurate nuclear structure data for the light nuclei.

For example, ^{18}F and ^{19}Ne with unknown structure data near the ^{18}F+p threshold [103] are of key interest for understanding the synthesis of heavier nuclei in the extreme temperatures and densities of X-ray bursts. They are also important for modeling of nova explosions. The radioactive decay of ^{18}F is the strongest source of γ-ray emission during the first hours after the explosion and the observations of γ-rays from nova ejecta provide a direct test of the explosion models [104].

In addition, better reaction rate predictions, as, for example, proton capture on ^{14,15}O and ^{17}F [105], are important for determining the isotopes synthesized and energy generated in explosive hydrogen burning in, e.g., novae, X-ray bursts, X-ray pulsars, supernovae, and possibly in accretion disks around black holes [104]. Another example of a recent interest is ^{22}Mg with its nuclear structure essential for both reaction rates in oxygen-neon nova outburst and for precision tests related to isospin symmetry breaking [100].

3.6 Scale Explosion Problem

The applicability of the *ab initio* NCSM approach is severally limited due to the scale explosion problem. The term scale explosion describes the fact that the dimensionality of the m-scheme basis, and the computational complexity and associated storage requirements therefore, grow combinatorially with increasing nucleon number and increasing cutoff $N_{\max}$ (as can be seen in Fig. 3.3). Hence even with the most powerful supercomputers available, the *ab initio* NCSM is neither able to model *sd*-shell

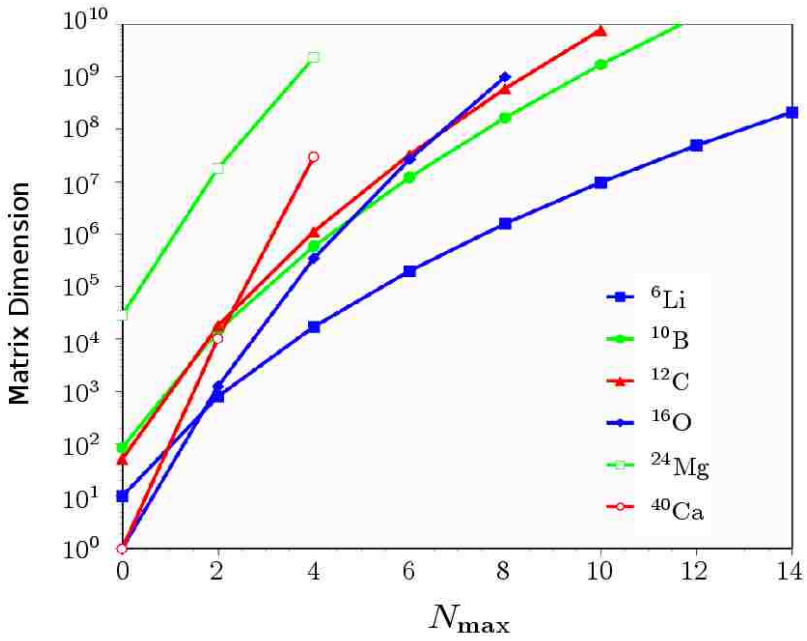

Figure 3.3: The scale explosion in the NCSM. Matrix dimensions of representative nuclei showing the explosive growth with increased cutoff $N_{\max}$.

nuclei, nor properly describe various important features of p-shell nuclei, including the enhanced E2 transitions strengths or low-lying intruder α-cluster states.

Furthermore, the nuclear Hamiltonian matrices are no longer sparse once the three-nucleon force is introduced, and hence one can not use specialized algorithms and data structures that take advantage of the sparse structure of the matrix. As a result, the model space must be significantly reduced once three-nucleon interactions are included.

In order to extend the scope of the NCSM approach to heavier nuclei and larger model spaces, we propose augmenting the model space by configurations that are essential for a description of the most dominant modes of the nuclear collective dynamics. Our approach is based on the classification of nuclear many-body states according to their transformation properties with respect to physically relevant subgroups of the symplectic $\mathrm{Sp}(3,\mathbb{R})$ symmetry group which underpins a microscopic description of the nuclear collective motion. The proposed *ab initio* symplectic no-core shell model (Sp-NCSM) framework extends the NCSM concept by recognizing that the choice of coordinates is crucial and should reflect the symmetries inherent to nuclear systems.

Chapter 4

Symplectic Shell Model

The symplectic shell model is a microscopic model of the nuclear collective motion. It provides a practical mean for identifying the dominant shell model configurations required for a description of monopole and quadrupole vibrational and rotational collective dynamics. The symplectic model is based on the non-compact $\mathfrak{sp}(3,\mathbb{R})$[1] Lie algebra which encompasses subalgebras that underpin the Elliott SU(3) model [106, 107, 108], the rigid rotor model [109], and the general collective model [110, 111].

We start our discussion by reviewing the Elliott SU(3) model of nuclear rotations. This has the advantage that many of the concepts that underpins the symplectic model can be discussed in the framework of this simpler model. We will then review the symplectic shell model with an emphasis on the construction of symplectic $\mathrm{Sp}(3,\mathbb{R})$ symmetry-adapted states. We will conclude this chapter by discussing relation between symplectic and cluster model wave functions.

4.1 Elliott SU(3) Model of Nuclear Rotations

The Elliott SU(3) model of nuclear rotations [106, 107, 108, 112, 113] is an algebraic model that is fully embedded in the interacting shell model framework. It approximates the nuclear mean field by a three-dimensional many-particle harmonic oscillator and attempts to describe the nuclear rotational states in the p- and sd-shell nuclei solely in terms of valence, i.e. $0\hbar\Omega$, configurations. The highly deformed states spanning higher-$\hbar\Omega$ subspaces are neglected with the argument that the splitting between oscillators shells is large enough to make contribution of excited configurations to low-lying nuclear states negligible. The nucleons within the fully occupied shells are inactive and constitute an inert core.

The Elliott model makes use of the symmetry group SU(3) for the classification of the many particle states as well as for the construction of the effective inter-nucleon interaction. This approach simplifies calculations while providing valuable physical insight into the structure of nuclear wave functions. The nucleus is treated as a many-fermion system and hence only properly antisymmetrized SU(3) symmetry-adapted configurations are considered.

[1] We use lowercase (capital) letters for algebras (groups).

4.1.1 U(3) and SU(3) Symmetry Groups

We will first review symmetries of an isotropic three-dimensional harmonic oscillator, U(3) and SU(3) groups. A microscopic realization of nine infinitesimal generators of the group U(3) for a system of A particles can conveniently be written as

$$C_{ij} = \frac{1}{2}\sum_{n=1}^{A}\left(b^{\dagger}_{ni}b_{nj} + b_{nj}b^{\dagger}_{ni}\right), \quad i,j = \text{x,y or z}, \tag{4.1}$$

where $b^{\dagger}_{ni}$ and b_{ni} are the harmonic oscillator raising and lowering operators for the nth particle

$$b^{\dagger}_{ni} = \sqrt{\frac{m\Omega}{2\hbar}}\left(x_{ni} - \frac{i}{m\Omega}p_{ni}\right) \tag{4.2}$$

$$b_{ni} = \sqrt{\frac{m\Omega}{2\hbar}}\left(x_{ni} + \frac{i}{m\Omega}p_{ni}\right). \tag{4.3}$$

The operators C_{ij} thus shift an oscillator quanta for each particle from the jth direction to the ith direction while keeping the overall number of oscillator quanta constant. The generators of U(3) do not connect different major oscillator shells.

Utilizing the commutation relations for the harmonic oscillator ladder operators,

$$\left[b^{\dagger}{}_{ni}, b^{\dagger}{}_{mj}\right] = [b_{ni}, b_{mj}] = 0$$
$$\left[b_{ni}, b^{\dagger}{}_{mj}\right] = \delta_{nm}\delta_{ij},$$

one can show that all nine operators C_{ij} obey the commutation rules for the Lie algebra $\mathfrak{u}(3)$

$$[C_{ij}, C_{kl}] = \delta_{jk}C_{il} - \delta_{il}C_{kj}. \tag{4.4}$$

The three-dimensional harmonic oscillator Hamiltonian

$$H_0 = \frac{1}{2m}\sum_{n=1}^{A}p_n^2 + \frac{1}{2}m\Omega^2\sum_{n=1}^{A}x_n^2, \tag{4.5}$$

can be written in terms of U(3) generators as $H_0 = \sum_i C_{ii}$, and by invoking the commutation relations (4.4), it is a trivial matter to verify that $[H_0, C_{kl}] = 0$ for all generators of U(3). As a consequence, $U^{\dagger}H_0U = H_0$ for all unitary transformations $U \in$ U(3). Because of the invariance of the harmonic oscillator Hamiltonian with respect to U(3), each eigenstate of H_0 can be labeled with an irreducible representation label of U(3), and each eigenvalue has the degeneracy of the dimension of the representation.

It is convenient to transform the nine generators of U(3) into the spherical SO(3) tensors. A new set of U(3) generators consists of H_0, L_{1q}, and $\mathcal{Q}^a_{2q}$, which are SO(3) tensors of rank zero, one, and two, respectively. The subscripts $1q$ and

$2q$ denote their angular momentum character ($l = 1; q = 0, \pm 1$ and $l = 2; q = 0, \pm 1, \pm 2$). A new set of U(3) generators reads:

$$\begin{aligned} H_0 &= C_{11} + C_{22} + C_{33} && (4.6)\\ L_{10} &= -i\,(C_{12} - C_{21}) && (4.7)\\ L_{1\pm1} &= \frac{1}{\sqrt{2}}\left((C_{13} - C_{31}) \pm i(C_{23} - C_{32})\right) && (4.8)\\ \mathcal{Q}^a_{20} &= 2C_{33} - C_{11} - C_{22} && (4.9)\\ \mathcal{Q}^a_{2\pm1} &= \mp\sqrt{\frac{3}{2}}\left((C_{13} + C_{31}) \pm i(C_{23} + C_{32})\right) && (4.10)\\ \mathcal{Q}^a_{2\pm2} &= \sqrt{\frac{3}{2}}\left((C_{11} - C_{22}) \pm i(C_{21} + C_{12})\right). && (4.11) \end{aligned}$$

The operator L_{1q} is the orbital angular momentum operator

$$L_{1q} = \sum_{n=1}^{A} \left(\boldsymbol{x}_n \times \boldsymbol{p}_n\right)_{1q}. \tag{4.12}$$

The five components of the algebraic quadrupole operator $\mathcal{Q}^a_{2q}$ can be written in terms of coordinate and momentum observables as

$$\mathcal{Q}^a_{2q} = \sqrt{\frac{4\pi}{5}} \sum_{n=1}^{A} \left(\frac{x_n^2}{b^2} Y_{2q}(\hat{\boldsymbol{x}}_n) + b^2 p_n^2 Y_{2q}(\hat{\boldsymbol{p}}_n) \right), \tag{4.13}$$

where the oscillator length is given by $b = \sqrt{\hbar/m\Omega}$. The commutation relations for the spherical tensors can be deduced from (4.4) to be

$$\begin{aligned} [L_{1q}, L_{1q'}] &= -\sqrt{2}\langle 1q; 1q' \,|\, 1q + q'\rangle L_{1q+q'} && (4.14)\\ \left[\mathcal{Q}^a_{2q}, L_{1q'}\right] &= -\sqrt{6}\langle 2q; 1q' \,|\, 2q + q'\rangle \mathcal{Q}^a_{2q+q'} && (4.15)\\ \left[\mathcal{Q}^a_{2q}, \mathcal{Q}^a_{2q'}\right] &= 3\sqrt{10}\langle 2q; 2q' \,|\, 1q + q'\rangle L_{1q+q'} && (4.16) \end{aligned}$$

with H_0 commuting with all U(3)generators. The operator H_0 is associated with the group U(1). The unitary transformations $\exp(i\alpha H_0) \in$ U(1) simply introduce an overall change of phase for arbitrary real coefficient α, and hence are of no physical interest. The subset of eight operators L_{1q} ($q = 0, \pm 1$) and $\mathcal{Q}^a_{2q}$ ($q = 0, \pm 1, \pm 2$) satisfy commutations relations for the infinitesimal generators of the SU(3) group.

4.1.2 Labeling Scheme

The irreducible representations of the group U(3) are labeled by a set of three non-negative integers $f_1 \geq f_2 \geq f_3$ corresponding to the length of rows in the Young tableau. Furthermore, $\sum_{i=1}^{3} f_i = N$, where N is the total number of oscillator quanta. The group SU(3) is obtained from U(3) by removing those transformations which simply introduce an overall change of phase. As a consequence, those

representations of SU(3) which correspond to Young tableaux differing only in the number of complete columns become equivalent. We thus need only two numbers to label SU(3) irreps, $(\lambda\,\mu)$, which are defined as

$$\lambda = f_1 - f_2 \tag{4.17}$$
$$\mu = f_2 - f_3. \tag{4.18}$$

An obvious subgroup of SU(3) is the well-known rotational group SO(3), generated by the orbital angular momentum operators L_{1q}. This means that we can classify many-body configurations according to their transformation properties with respect to the physical group reduction chain SU(3) $\supset$ SO(3). The total orbital angular momentum L is therefore a good quantum number in this scheme. In addition, by coupling the orbital angular momentum L to the complementary many-particle spin degree of reedom S, one can achieve a classification scheme with good total angular momentum J:

$$\begin{array}{ccccccc} \mathrm{SU}(3) & \supset & \mathrm{SO}(3) & & & & \\ & & \otimes & \supset & \mathrm{SU}(2) & \supset & U(1) \\ & & \mathrm{SU_S}(2) & & & & \end{array} \tag{4.19}$$

$$(\lambda\mu) \quad \kappa \quad (LS) \qquad J \qquad M_J$$

The multiplicity label κ reflects the fact that that multiple occurrences of L are possible within a generic irrep $(\lambda\,\mu)$ of SU(3). Here M_J is the projection of J along the z-axis of the laboratory frame. It is important to note that one can choose an alternative, and from a mathematical point of view more natural labeling scheme that reduces SU(3) canonically; that is, with respect to its SU(2) $\otimes$ U(1) subgroup chain, SU(3) $\supset$ SU(2) $\otimes$ U(1). Nevertheless, most applications of SU(3), including the symplectic shell model, utilizes reduction with respect to its physical subgroup chain, SU(3) $\supset$ SO(3).

The labeling scheme (4.19) does not account for the fact that the nucleus is a proton-neutron system. One can introduce the isospin degree of freedom and treat protons and neutrons as different states of an isospin 1/2 doublet. The isospin formalism gives rise to wave functions

$$|(\lambda\mu)\kappa(LS)JM_J;TT_z\rangle\,, \tag{4.20}$$

which are totally antisymmetric with respect to interchange of any two nucleons and, in addition to SU(3)$\otimes$SU$_\mathrm{S}$(2) quantum numbers, carry two additional labels, the total isospin number T and its projection $T_z = Z/2 - N/2$, where N and Z denote the number of protons and neutrons. The other approach is to construct antisymmetric SU(3) irreps individually for protons and neutrons, and then couple them into a total wave function with a good SU(3) symmetry. This approach, so-called "proton-neutron formalism", gives rise to SU(3) configurations

$$|(\lambda_\pi\,\mu_\pi)S_\pi \times (\lambda_\pi\,\mu_\pi)S_\pi;(\lambda\mu)\kappa(LS)JM_J\rangle \tag{4.21}$$

which are antisymmetric only with respect to interchange of protons and neutrons, separately.

4.1.3 SU(3) model Hamiltonians

The quadrupole-quadrupole interaction, $Q^c \cdot Q^c$, is a very important ingredient of the long-range part of the inter-nucleon interaction. It plays a particularly significant role in explaining a microscopic origin of nuclear rotations. It is important to emphasize that the mass quadrupole operator

$$Q^c_{2q} = \sqrt{\frac{16\pi}{5}} \sum_{n=1}^{A} \frac{x_n^2}{b^2} Y_{2q}(\hat{\boldsymbol{x}}_n) \tag{4.22}$$

differs from $\mathcal{Q}^a_{2q}$ (4.13). Within a major oscillator shell the matrix elements of Q^c_{2q} and $\mathcal{Q}^a_{2q}$ are identical, but Q^c_{2q} couple states spanning the ηth shell with those of the η'th shell, $\eta' = \eta \pm 2$, whereas the matrix elements of $\mathcal{Q}^a_{2q}$ between states belonging to different shells vanish.

In order to show the way in which the rotational spectra arise in the shell model, Elliott considered the effective Hamiltonian

$$H = H_0 - \frac{1}{2}\chi \mathcal{Q}^a \cdot \mathcal{Q}^a, \tag{4.23}$$

where H_0 is the three-dimensional harmonic oscillator Hamiltonian. The advantage of using the algebraic quadrupole operator instead of the mass quadrupole operator lies in the fact that $\mathcal{Q}^a \cdot \mathcal{Q}^a$ can be expressed in terms of Casimir operators of $\mathfrak{su}(3)$ and $\mathfrak{so}(3)$ Lie algebras as

$$\mathcal{Q}^a \cdot \mathcal{Q}^a = 6\hat{C}_2 - 3\hat{L}^2, \tag{4.24}$$

and hence it is diagonal in a SU(3)$\supset$SO(3) symmetry-adapted basis. It is clear that, within a single SU(3) irrep, Hamiltonian (4.23) is equivalent to the quantum rotor Hamiltonian

$$H = H_0 + \frac{3}{2}\chi \hat{L}^2 + \text{const}, \tag{4.25}$$

and hence gives rise to a rotational band with excitation energies proportional to $L(L+1)$. The eigenvalues of the Hamiltonian (4.23) are given by

$$E_{(\lambda\,\mu)L} = N_0\hbar\Omega - \frac{1}{2}\chi\left[6C_2(\lambda,\mu) - 3L(L+1)\right], \tag{4.26}$$

where $N_0\hbar\Omega$ is the harmonic oscillator energy, L is the orbital angular momentum and $C_2(\lambda,\mu)$ denotes the expectation value of the second degree Casimir operator of $\mathfrak{su}(3)$ given by

$$C_2(\lambda,\mu) = \frac{2}{3}\left(\lambda^2 + 3\lambda + 3\mu + \lambda\mu + \mu^2\right). \tag{4.27}$$

If the model space incorporates multiple SU(3) irreps, then the Hamiltonian (4.23) has a spectrum which is composed out of multiple rotational bands lying at relative excitation energies determined by the factor $-3\chi C_2(\lambda,\mu)$. Each rotational band corresponds to a single SU(3) irrep. Such a structure of eigenstates does not reproduce all features of realistic low-lying rotational spectra like the K-band splitting and the inter-band $E2$ transitions. The inclusion a special

minimal set of SO(3) scalars, the so-called SU(3)→SO(3) integrity basis, allows one to reproduce these properties as well [114, 115].

In the simplest version, the Elliott model takes into account only the "leading" SU(3) irrep, that is, the irrep with the largest value $C_2(\lambda, \mu)$. Such a choice gives rise to the rotational band with the lowest energy, which is evident from (4.26). A realistic inter-nucleon interaction contains many terms that strongly mix SU(3) irreps. More sophisticated calculations allowing mixing of SU(3) configurations within a single shell were performed to study the combined effects of the quadrupole-quadrupole, pairing, and spin-orbit interactions [116, 117, 118].

Generally, spaces restricted to $0\hbar\Omega$ SU(3) irreps are inadequate for modeling the low-lying highly deformed states with a dominant multi-particle-multi-hole structure that are found in nuclei throughout the periodic table. Clearly, one needs to include SU(3) irreps that span higher-$\hbar\Omega$ subspaces and which incorporate core excited configurations. The number of possible SU(3) configurations grows combinatorially with increasing number of active oscillator shells. It is thus imperative to select only those SU(3) symmetry-adapted configurations that are relevant for the description of nuclear deformed geometry and nuclear collective dynamics. The selection scheme is underpinned by a geometric interpretation of the SU(3) states that is based on relation between SU(3) and the rigid rotor symmetry groups, and by the symplectic shell model, which enables to relate SU(3) irreps with the nuclear collective motion.

4.1.4 Geometrical Interpretation of SU(3) States

A very important property of the SU(3) model is its relation to the microscopic rigid rotor model [109] whose algebra is associated with the rotational limit of the geometric collective (Bohr-Mottelson-Frankfurt) model [119, 120, 121]. This in turn allows an interpretation of the microscopic quantum labels λ and μ in terms of the collective shape variables β and γ of the geometric collective model describing deformation of the nucleus with respect to the principal axis frame.

The relation between the rigid rotor and the Elliott SU(3) model can be derived from the relationship between their Lie algebras. The basic assumption of the rigid rotor model is that the inertia tensor in the model Hamiltonian

$$H_{\rm ROT} = \sum_{i=1}^{3} \frac{1}{2\mathcal{I}_i} \hat{L}_i^2 \tag{4.28}$$

is a function of the mass quadrupole moments Q^c_{2q}. The Lie algebra of the rigid rotor is thus spanned by the five commuting mass quadrupole moment operators and the three components of the angular momentum, $\mathfrak{rot}(3) = \left\{Q^c_{2q}, L_{1q}\right\}$, whereas the $\mathfrak{su}(3)$ is span of $\left\{\mathcal{Q}^a_{2q}, L_{1q}\right\}$. Both Lie algebras satisfy the following commutation relations:

$$[L_{1q}, L_{1q'}] = -\sqrt{2}\langle 1q; 1q' | \, 1q + q' \rangle L_{1q+q'} \tag{4.29}$$

$$[Q_{2q}, L_{1q'}] = -\sqrt{6}\langle 2q; 1q' | \, 2q + q' \rangle Q_{2q+q'}, \tag{4.30}$$

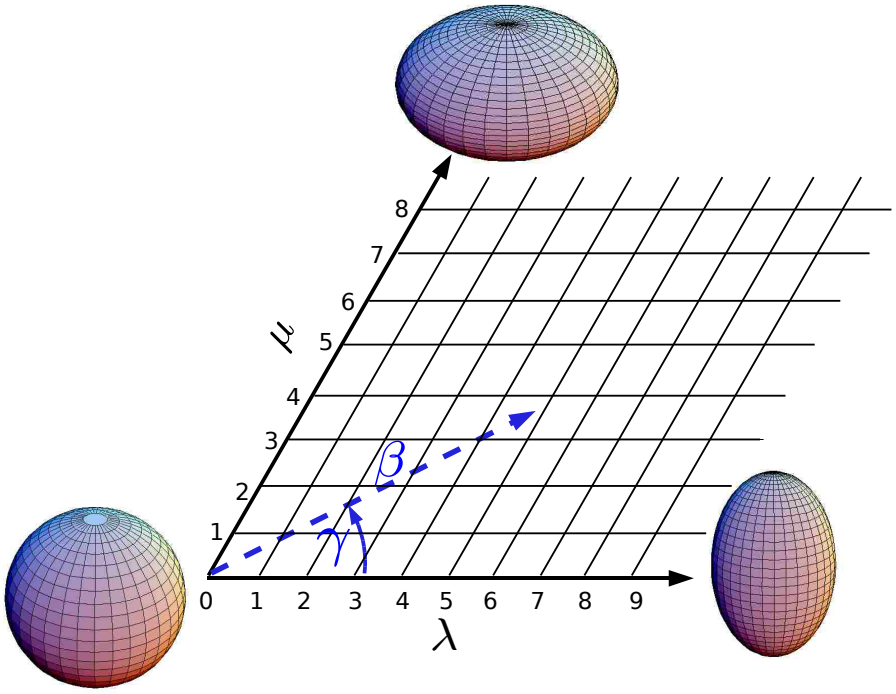

Figure 4.1: A traditional ($\beta\gamma$) plot, where β ($\beta \geq 0$) is the radius vector and γ ($0 \leq \gamma \leq \pi/3$) the azimuthal angle, demonstrates the relationship between the collective model shape variables ($\beta\gamma$) and the SU(3) irrep labels ($\lambda\,\mu$).

where Q denotes $\mathcal{Q}^a$ and Q^c in case of $\mathfrak{su}(3)$ and $\mathfrak{rot}(3)$, respectively. The difference between the two algebras lie in the commutators for their quadrupole operators:

$$[Q_{2q}, Q_{2q'}] = 3\sqrt{10}\langle 2q; 2q' |\, 1q + q'\rangle L_{1q+q'} \times \begin{cases} 0 & \text{for } \mathfrak{rot}(3) \\ +1 & \text{for } \mathfrak{su}(3) \end{cases} \tag{4.31}$$

To demonstrate the contraction $\mathfrak{su}(3) \to \mathfrak{rot}(3)$ one can introduce a rescaled quadrupole operator, $\mathcal{Q}' = \mathcal{Q}^a \hat{C}_2^{-1/2}$, where $\hat{C}_2$ is the second-order Casimir invariant of $\mathfrak{su}(3)$. The commutation relations (4.29) and (4.30) remain the same for the new set of generators, but the third one becomes

$$[\mathcal{Q}'_{2q}, \mathcal{Q}'_{2q'}] = 3\sqrt{10}\langle 2q; 2q' |\, 1q + q'\rangle \hat{C}_2^{-1/2} L_{1q+q'}. \tag{4.32}$$

This implies that $[\mathcal{Q}'_{2q}, \mathcal{Q}'_{2q'}] \approx 0$ for $L \ll C_2(\lambda, \mu)$ and thus in this contraction limit the operators $\left\{\mathcal{Q}'^a_{2q}, L_{1q}\right\}$ span the $\mathfrak{rot}(3)$ Lie algebra. This argument also unveils a difference; namely, since the $\mathfrak{su}(3)$ algebra is compact the angular momentum L is bound (by $\lambda + \mu$ in a $(\lambda\,\mu)$ irrep), whereas the non-compact rotor algebra $\mathfrak{rot}(3)$ supports unbound L values.

An alternative way of relating $\mathfrak{su}(3)$ and $\mathfrak{rot}(3)$ algebras is to explore relations between their Casimir invariants. This approach is based on the rationale that the

invariant measures of two models used to describe the same quantum phenomena must be related to each other. The relation between two invariants of the rigid rotor algebra, the traces of the square and cube of the mass quadrupole moment matrix $\mathrm{Tr}\left[(Q^c)^2\right]$ and $\mathrm{Tr}\left[(Q^c)^3\right]$, and the second- and third-order Casimir invariants of SU(3) was derived in Ref. [122] by the invoking a linear mapping between the eigenvalues of these invariant operators

$$\begin{aligned}\langle \mathrm{Tr}\left[(Q^c)^2\right]\rangle = \frac{3}{2}k^2\beta^2 \quad &\leftrightarrow \quad C_2(\lambda,\mu) = \frac{2}{3}\left(\lambda^2+3\lambda+3\mu+\lambda\mu+\mu^2\right)\\ \langle \mathrm{Tr}\left[(Q^c)^3\right]\rangle = \frac{3}{4}k^3\beta^3\cos 3\gamma \quad &\leftrightarrow \quad C_3(\lambda,\mu) = \frac{1}{9}(\lambda-\mu)(\lambda+2\mu+3)(2\lambda+\mu+3).\end{aligned}$$

Here the constant $k=\sqrt{\frac{5}{9\pi}}A\langle r^2\rangle$, where A is the number of nucleons and $\langle r^2\rangle$ is the nuclear mean square radius. The exact relation between the microscopic quantum numbers λ and μ and the shape variables β and γ reads [122]:

$$\beta^2 = \left(\frac{4\pi}{5A^2\langle r^2\rangle^2}\right)(\lambda^2+\lambda\mu+\mu^2+3\lambda+3\mu+3) \tag{4.33}$$

$$\gamma = \tan^{-1}\left[\frac{\sqrt{3}(\mu+1)}{2\lambda+\mu+3}\right]. \tag{4.34}$$

This implies that each SU(3) irrep $(\lambda\,\mu)$ corresponds to an unique shape parametrized by deformation parameters $(\beta\gamma)$. The variables β and γ can vary continuously, whereas the quantum labels $(\lambda\,\mu)$ are discrete and a set of their possible values is limited due to the fermionic nature of the nucleons, a feature that is not included in the collective model. This is illustrated in Fig. 4.1 with the help of a grid which is superposed on the $(\beta\gamma)$-plane of the geometric collective model. Note, in particular, that SU(3) irreps with $\mu = 0$ correspond to a prolate shapes, irreps with $\lambda = 0$ correspond to an oblate geometry, and irreps with $\lambda = \mu$ describe a maximally asymmetric shape. A spherical nucleus is described by the $(0\,0)$ irrep.

In short, the SU(3) classification of many-body states allows for a geometrical analysis of the eigenstates of a nuclear system via the relations (4.33) and (4.34) and hence gives insight into phenomena associated with nuclear deformation.

4.2 Symplectic Shell Model

The symplectic model [19, 20, 21] is a microscopic algebraic model of nuclear collective dynamics that includes monopole and quadrupole collective vibrations as well as vorticity degrees of freedom for a description of rotational dynamics in a continuous range from irrotational to rigid rotor flows. It can be regarded as both a microscopic realization of the successful phenomenological Bohr-Mottelson-Frankfurt collective model and a multi-$\hbar\Omega$ extension of the Elliott's SU(3) model. The symplectic model is fully embedded in the no-core shell model (NCSM), which means that it reaches beyond a single shell to embrace higher-lying states including core excited configurations. It thus allows one to realize nuclear collective states in terms of the shell model configurations.

While the NCSM divides the many-nucleon Hilbert space into "horizontal" layers of $N\hbar\Omega$ subspaces, the symplectic model divides it into "vertical" slices of collective states that carry $\mathrm{Sp}(3,\mathbb{R})$ irreducible representations, which is schematically illustrated in Fig. 4.3. The symplectic model thus allows one to restrict a model space of the NCSM to vertical slices that admit the most important modes of nuclear collective dynamics.

The symplectic model is based on the 21-dimensional algebra $\mathfrak{sp}(3,\mathbb{R})$ of generators of semi-simple non-compact symmetry group $\mathrm{Sp}(3,\mathbb{R})$. This group has a fundamental representation as a group of all linear transformations on a six-dimensional real vector space that leave matrix

$$J = \begin{pmatrix} 0 & I_3 \\ -I_3 & 0 \end{pmatrix}$$

invariant. Here, I_3 is the 3×3 identity matrix.

The symplectic model has a very rich group structure (see Fig. 4.2). In particular, there are two important subgroup chains that unveil the physical content of the symplectic model: the shell model subgroups chain associated with the Elliott SU(3) group, and the collective model chain related to the general collective motion GCM(3) group. The intersection of these chains is the group of rotations SO(3).

4.2.1 Collective Model Chain

The significance of the symplectic $\mathrm{Sp}(3,\mathbb{R})$ symmetry for a microscopic description of a quantum many-body system of interacting particles emerges from the physical relevance of its 21 infinitesimal generators. The basis of the symplectic $\mathfrak{sp}(3,\mathbb{R})$ algebra has realization in terms of well defined microscopic shell model one-body Hermitian operators. The generators of $\mathrm{Sp}(3,\mathbb{R})$ can be constructed as bilinear products of canonical coordinates:

$$Q_{ij} = \sum_n x_{ni}x_{nj} \tag{4.35}$$

$$S_{ij} = \sum_n (x_{ni}p_{nj} + p_{ni}x_{nj}) \tag{4.36}$$

$$L_{ij} = \sum_n (x_{ni}p_{nj} - x_{nj}p_{ni}) \tag{4.37}$$

$$K_{ij} = \sum_n p_{ni}p_{nj}, \tag{4.38}$$

where x_{ni} and p_{ni} denote ith Cartesian component of the position and the momentum of the nth nucleon. The commutation relations for these generators can be inferred from the elementary Heisenberg commutation relations

$$[x_{ni}, p_{mj}] = i\hbar\delta_{nm}\delta_{ij}. \tag{4.39}$$

The six monopole and quadrupole moments Q_{ij}, the six generators of monopole and quadrupole deformations S_{ij}, the three generators of rotations L_{ij}, and the six

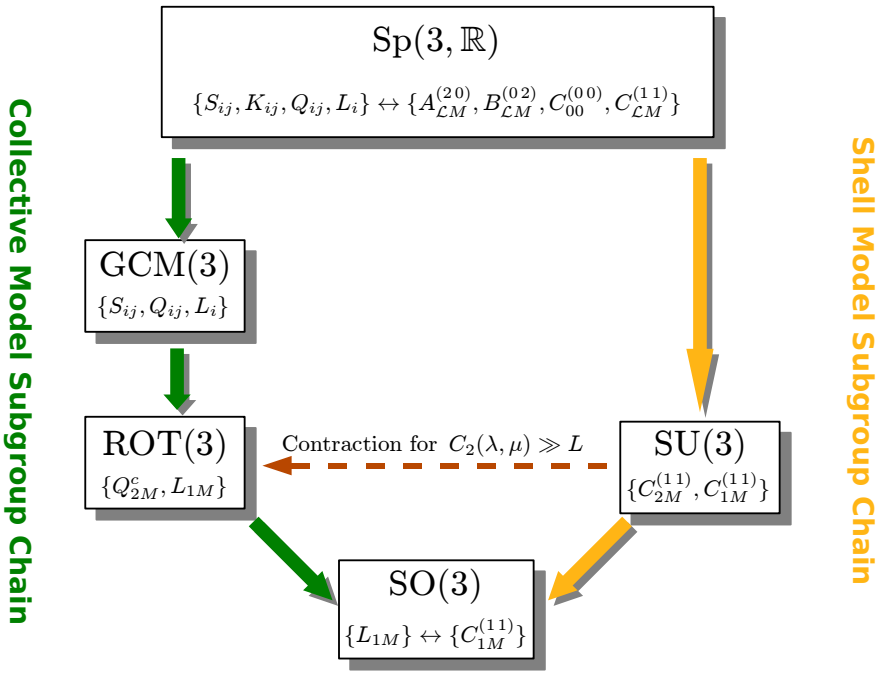

Figure 4.2: The symplectic group $\mathrm{Sp}(3,\mathbb{R})$ contains two physically important subgroup chains: the collective model chain, $\mathrm{Sp}(3,\mathbb{R}) \supset \mathrm{GCM}(3) \supset \mathrm{ROT}(3) \supset \mathrm{SO}(3)$, and the shell model chain, $\mathrm{Sp}(3,\mathbb{R}) \supset \mathrm{SU}(3) \supset \mathrm{SO}(3)$.

generators of quadrupole flow tensor K_{ij}, constitute the 21-dimensional Lie algebra $\mathfrak{sp}(3,\mathbb{R})$, which is the smallest Lie algebra that contains both the mass quadrupole moments Q^c as well as the many-nucleon kinetic energy, $\sum_n p_n^2/2m$.

The symplectic algebra $\mathfrak{sp}(3,\mathbb{R})$ contains several algebraic models of nuclear collective motion that give rise to rotational spectra. Symmetry groups associated with these models form the collective model subgroup chain:

$$\mathrm{Sp}(3,\mathbb{R}) \supset \mathrm{GCM}(3) \supset \mathrm{ROT}(3) \supset \mathrm{SO}(3).$$

The general collective motion group GCM(3) is generated by a 15-dimensional noncompact algebra spanned by the operators $\{Q_{ij}, L_{ij}, S_{ij}\}$. It is the symmetry group of the microscopic collective model [110, 111]. This model represents a fully microscopic extension of the Bohr-Mottelson-Frankfurt model. While the latter can describe monopole-quadrupole vibrations and either the rigid rotor or the irrotational flow characteristics of rotational motion, the collective dynamics embraced by the GCM(3) structure includes a vorticity degree of freedom and thus describes a continuous range of rotational dynamics from the rigid rotor to the irrotational flow. It is important to note that in the classical limit, $\mathrm{Sp}(3,\mathbb{R})$ and GCM(3) sym-

metries are important for stellar dynamics as they underpin symmetry of rotating stars and galaxies [123].

The algebra $\mathfrak{rot}(3)$ associated with a rigid rotor is also a subalgebra of $\mathfrak{sp}(3,\mathbb{R})$. States of a rigid rotor do not have square-integrable wave functions in the many-nucleon Hilbert space [124]. Therefore one cannot utilize the basis of the collective model chain in microscopic nuclear structure calculations.

Due to the presence of the quadrupole flow tensor K_{ij} among the generators of $\mathrm{Sp}(3,\mathbb{R})$, the many-body three-dimensional harmonic oscillator Hamiltonian is an element of the symplectic $\mathfrak{sp}(3,\mathbb{R})$ algebra. The symplectic model thus unifies the Bohr-Mottelson-Frankfurt model and the shell model associated with the U(3) group. This also means that we can construct a basis of the Hilbert space according to a classification scheme that reduces another alternative subgroup chain of $\mathrm{Sp}(3,\mathbb{R})$; namely, the shell model subgroup chain.

4.2.2 Shell Model Chain

The shell model subgroup chain, $\mathrm{Sp}(3,\mathbb{R}) \supset \mathrm{SU}(3) \supset \mathrm{SO}(3)$, is directly responsible for the computational tractability of the symplectic model. It transcends the Elliott SU(3) group and as a consequence bridges between the microscopic shell model and the nuclear collective dynamics. The shell structure of the $\mathrm{Sp}(3,\mathbb{R})$ generators is elucidated if the symplectic algebra is realized in terms of bilinear products in the harmonic oscillator raising and lowering operators:

$$A_{ij} = \sum_{n=1}^{A} b^{\dagger}_{ni} b^{\dagger}_{nj} \tag{4.40}$$

$$B_{ij} = \sum_{n=1}^{A} b_{ni} b_{nj} \tag{4.41}$$

$$C_{ij} = \frac{1}{2} \sum_{n=1}^{A} \left(b^{\dagger}_{ni} b_{nj} + b_{nj} b^{\dagger}_{ni} \right). \tag{4.42}$$

The nine generators C_{ij} close on the commutation relations of the $\mathfrak{u}(3)$ Lie algebra. The $\mathfrak{su}(3)$ subalgebra of $\mathfrak{u}(3)$ is spanned by the eight independent traceless operators $C_{ij} - \frac{1}{3}\delta_{ij} \sum_k C_{kk}$. The operators C_{ij} act only within a major harmonic oscillator shell, while the six operators A_{ij} are $2\hbar\Omega$ raising operators and their adjoint B_{ij} are $2\hbar\Omega$ lowering operators. The action of the symplectic generators is schematically depicted in Fig. 4.3.

The Cartesian components of the monopole and quadrupole moments operators Q_{ij} can be expressed in terms of the symplectic generators as

$$Q_{ij} = \frac{1}{2} \left(A_{ij} + C_{ij} + C_{ji} + B_{ij} \right), \tag{4.43}$$

and thus they connect not only states within a single major oscillator shell, but also states differing in oscillator energy by $\pm 2\hbar\Omega$.

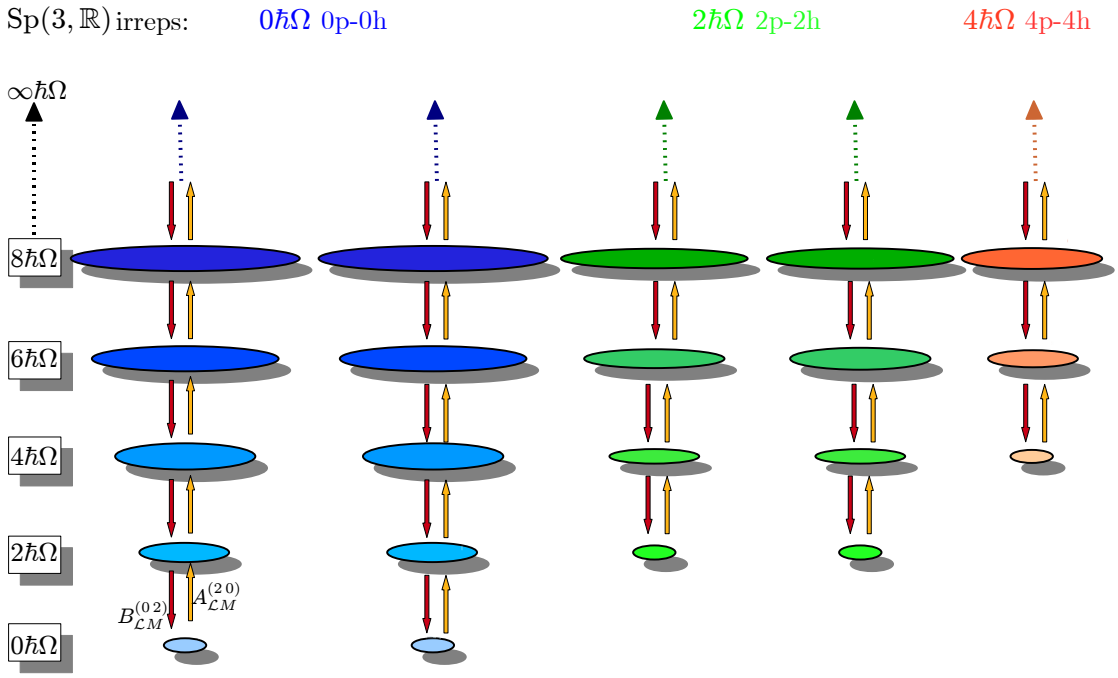

Figure 4.3: The schematic plot illustrating decomposition of the shell model space as direct sum of the symplectic $\mathrm{Sp}(3,\mathbb{R})$ irreps. Each ellipsoid in the figure corresponds to a definite deformation of the nucleus as given by the SU(3) quantum numbers $(\lambda_\omega\,\mu_\omega)$ via the relations (4.33) and (4.34). The action of the symplectic raising and lowering operators $A^{(20)}_{\mathcal{L}M}$ and $B^{(02)}_{\mathcal{L}M}$ within a $\mathrm{Sp}(3,\mathbb{R})$ irrep is also schematically depicted.

To construct $\mathrm{Sp}(3,\mathbb{R})$ irreducible representations in the basis of the shell model subgroup chain, it is advantageous to express the symplectic generators as SU(3) tensor operators. The harmonic oscillator raising and lowering operators can be written as three-dimensional SU(3) tensor operators transforming according to the $(1\,0)$ and $(0\,1)$ irreps, respectively [125]:

$$b^{\dagger(1\,0)}_{1\,\pm1} = \mp\frac{1}{\sqrt{2}}\left(b^\dagger_1 \pm i b^\dagger_2\right), \quad b^{\dagger(1\,0)}_{1\,0} = b^\dagger_3,$$

and

$$b^{(0\,1)}_{1\,\pm1} = \mp\frac{1}{\sqrt{2}}\left(b_1 \pm i b_2\right), \quad b^{(0\,1)}_{1\,0} = b_3.$$

The operators $b^{\dagger(1\,0)}_{1\,q}$ and $b^{(0\,1)}_{1\,q}$ satisfy the conjugation relation $b^{(0\,1)}_{1\,q} = (-1)^q (b^{\dagger(1\,0)}_{1\,-q})^\dagger$, and their commutator is given by $\left[b^{(0\,1)}_{1\,q}, b^{\dagger(1\,0)}_{1\,q'}\right] = (-1)^q \delta_{q(-q')}$. Since the harmonic oscillator ladder operators are SU(3) tensors, they can be coupled to form new SU(3)

tensors. In this way, the symplectic generators in form of SU(3) tensor operators are obtained:

$$A^{(2\,0)}_{\mathcal{L}M} = \frac{1}{\sqrt{2}}\sum_{n=1}^{A}\left[b^{\dagger(1\,0)}_{n}\times b^{\dagger(1\,0)}_{n}\right]^{(2\,0)}_{\mathcal{L}M} \tag{4.44}$$

$$B^{(0\,2)}_{\mathcal{L}M} = \frac{1}{\sqrt{2}}\sum_{n=1}^{A}\left[b^{(0\,1)}_{n}\times b^{(0\,1)}_{n}\right]^{(0\,2)}_{\mathcal{L}M} \tag{4.45}$$

$$C^{(1\,1)}_{\mathcal{L}M} = \sqrt{2}\sum_{n=1}^{A}\left[b^{\dagger(1\,0)}_{n}\times b^{(0\,1)}_{n}\right]^{(1\,1)}_{\mathcal{L}M} \tag{4.46}$$

$$\tag{4.47}$$

$$H^{(0\,0)}_{00} = \sqrt{3}\sum_{n=1}^{A}\left[b^{\dagger(1\,0)}_{n}\times b^{(0\,1)}_{n}\right]^{(0\,0)}_{00} + \frac{3}{2}A \tag{4.48}$$

The eight operators $C^{(1\,1)}_{\mathcal{L}M}$ generate the SU(3) subgroup of $\mathrm{Sp}(3,\mathbb{R})$ and are related to the angular momentum operator L_{1q} and the Elliott algebraic quadrupole moment tensor $\mathcal{Q}^{a}_{2q}$ as follows

$$C^{(1\,1)}_{1q} = L_{1q}, \quad q=0,\pm1 \tag{4.49}$$

$$C^{(1\,1)}_{2q} = \frac{1}{\sqrt{3}}\mathcal{Q}^{a}_{2q}, \quad q=0,\pm1,\pm2. \tag{4.50}$$

The mass quadrupole operator Q^{c}_{2q} can be expressed as a linear combination of $\mathcal{L}=2$ components of SU(3) tensors:

$$Q^{c}_{2q} = \sqrt{3}\left[A^{(2\,0)}_{2q} + B^{(0\,2)}_{2q} + C^{(1\,1)}_{2q}\right] \tag{4.51}$$

The lowering tensor $B^{(0\,2)}$ is the adjoint of $A^{(2\,0)}$ tensor and their spherical components are related as

$$B^{(0\,2)}_{\mathcal{L}M} = (-)^{\mathcal{L}-M}(A^{(2\,0)}_{\mathcal{L}-M})^{\dagger}. \tag{4.52}$$

4.2.3 Translationally Invariant Form of Symplectic Generators

The symplectic generators introduced in the preceding sections are not translationally invariant and hence give rise to irreducible representations that are contaminated with spurious center-of-mass (c.m.) excitations. One way to overcome this problem is to construct the $\mathrm{Sp}(3,\mathbb{R})$ generators in terms of intrinsic coordinates, namely, $x'_{ni} = x_{ni} - X_i$ and $p'_{ni} = p_{ni} - P_i$, defined with respect to the center-of-mass momentum $P_i = \sum_{n=1}^{A} p_{ni}$ and position $X_i = (1/A)\sum_{n=1}^{A} x_{ni}$ [126]. The translationally invariant $\mathrm{Sp}(3,\mathbb{R})$ generators can be then written in SU(3)-coupled form

as

$$A^{(2\,0)}_{\mathcal{L}M} = \frac{1}{\sqrt{2}}\sum_{n=1}^{A}\left[b^{\dagger(1\,0)}_{n}\times b^{\dagger(1\,0)}_{n}\right]^{(2\,0)}_{\mathcal{L}M} - \frac{1}{\sqrt{2}A}\sum_{s,t=1}^{A}\left[b^{\dagger(1\,0)}_{s}\times b^{\dagger(1\,0)}_{t}\right]^{(2\,0)}_{\mathcal{L}M}, \tag{4.53}$$

$$B^{(0\,2)}_{\mathcal{L}M} = \frac{1}{\sqrt{2}}\sum_{n=1}^{A}\left[b^{(0\,1)}_{n}\times b^{(0\,1)}_{n}\right]^{(0\,2)}_{\mathcal{L}M} - \frac{1}{\sqrt{2}A}\sum_{s,t=1}^{A}\left[b^{(0\,1)}_{s}\times b^{(0\,1)}_{t}\right]^{(0\,2)}_{\mathcal{L}M}, \tag{4.54}$$

$$C^{(1\,1)}_{\mathcal{L}M} = \sqrt{2}\sum_{n=1}^{A}\left[b^{\dagger(1\,0)}_{n}\times b^{(0\,1)}_{n}\right]^{(1\,1)}_{\mathcal{L}M} - \frac{\sqrt{2}}{A}\sum_{s,t=1}^{A}\left[b^{\dagger(1\,0)}_{s}\times b^{(0\,1)}_{t}\right]^{(1\,1)}_{\mathcal{L}M}, \tag{4.55}$$

$$H^{(0\,0)}_{00} = \sqrt{3}\sum_{n=1}^{A}\left[b^{\dagger(1\,0)}_{n}\times b^{(0\,1)}_{n}\right]^{(0\,0)}_{00} - \frac{\sqrt{3}}{A}\sum_{s,t=1}^{A}\left[b^{\dagger(1\,0)}_{s}\times b^{(0\,1)}_{t}\right]^{(0\,0)}_{00} + \frac{3}{2}(A-1). \tag{4.56}$$

This form of the intrinsic $\mathrm{Sp}(3,\mathbb{R})$ generators can be also obtained from the translationally non-invariant $\mathrm{Sp}(3,\mathbb{R})$ generators (4.44)-(4.48) after the subtraction of the center-of-mass realization of the $\mathfrak{sp}(3,\mathbb{R})$ algebra, which is spanned by the two-body operators:

$$\begin{aligned}
A^{(2\,0)\mathrm{cm}}_{\mathcal{L}M} &= \frac{1}{\sqrt{2}}\left[\mathfrak{B}^{\dagger}\times\mathfrak{B}^{\dagger}\right]^{(2\,0)}_{\mathcal{L}M},\\
B^{(0\,2)\mathrm{cm}}_{\mathcal{L}M} &= \frac{1}{\sqrt{2}}\left[\mathfrak{B}\times\mathfrak{B}\right]^{(0\,2)}_{\mathcal{L}M},\\
C^{(1\,1)\mathrm{cm}}_{\mathcal{L}M} &= \sqrt{2}\left[\mathfrak{B}^{\dagger}\times\mathfrak{B}\right]^{(1\,1)}_{\mathcal{L}M},\\
H^{(0\,0)\mathrm{cm}}_{00} &= \sqrt{3}\left[\mathfrak{B}^{\dagger}\times\mathfrak{B}\right]^{(0\,0)}_{00} + \frac{3}{2},
\end{aligned}$$

These operators are expressed by means of the c.m. harmonic oscillator ladder operators

$$\mathfrak{B}^{\dagger}_{i} = \frac{1}{\sqrt{A}}\sum_{n=1}^{A} b^{\dagger}_{ni}, \tag{4.57}$$

$$\mathfrak{B}_{i} = \frac{1}{\sqrt{A}}\sum_{n=1}^{A} b_{ni}. \tag{4.58}$$

The translationally invariant symplectic raising operators (4.53) are utilized to generate basis states of $\mathrm{Sp}(3,\mathbb{R})$ irreps and hence it is instructive to examine their action on A-nucleon configurations. The first term in (4.53) raises a single nucleon by two shells, that is, it induces $2\hbar\Omega$ one-particle-one-hole (1p-1h) monopole ($\mathcal{L}=0$) or quadrupole ($\mathcal{L}=2$) excitations. The second term eliminates the spurious c.m. excitations in the symplectic states by evoking small ($\sim 1/A$) $2\hbar\Omega$ two-particle-two-hole (2p-2h) corrections (two particles raised by one shell each). This is schematically illustrated in Fig. 4.4.

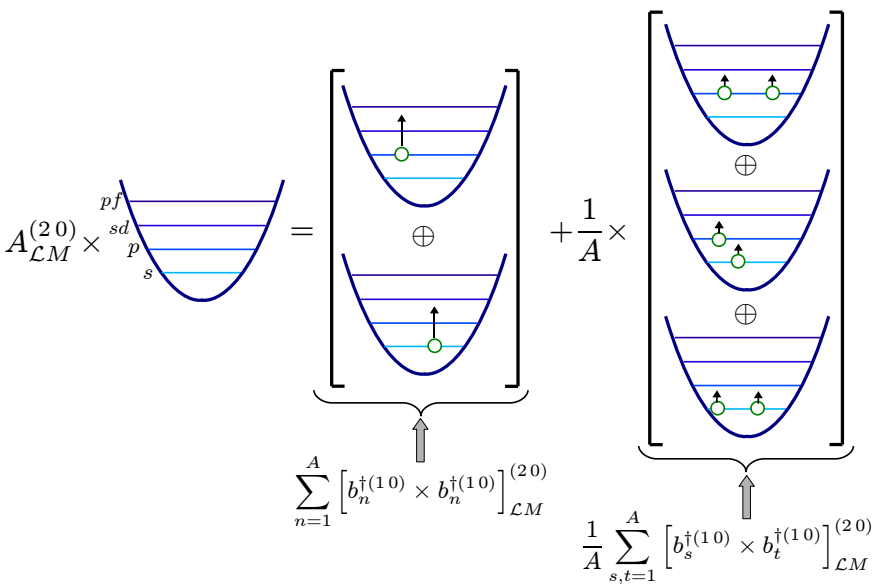

Figure 4.4: Action of the translationally invariant symplectic raising operator $A^{(20)}_{\mathcal{L}M}$.

4.2.4 Symplectic Basis States

The symplectic states are labeled (in standard notation [19, 21]) in the shell model chain as:

$$\begin{array}{ccccccccccc} \mathrm{Sp}(3,\mathbb{R}) & \supset & \mathrm{SU}(3) & \supset & \mathrm{SO}(3) & & & & & & \\ & & & & \otimes & \supset & \mathrm{SU}(2) & \supset & U(1) & & \\ & & & & \mathrm{SU_S}(2) & & & & & & \\ \sigma & & n\rho & & \omega & \kappa & (LS_\sigma) & & J & & M_J \end{array} \tag{4.59}$$

Note that the elements of the $\mathfrak{sp}(3,\mathbb{R})$ algebra act merely on nucleon spatial coordinates leaving the spin part unaffected. Each symplectic irrep thus carries a definite value of the total intrinsic spin S_σ, which can be coupled with the total orbital angular momentum L to produce the total angular momentum J and its projection M_J.

A basis of a symplectic irrep is constructed by acting with symmetrically coupled polynomials in the symplectic raising operators, $A^{(20)}$, on a set of basis states of a symplectic bandhead, $|\sigma; S_\sigma\rangle$, which is a $\mathrm{Sp}(3,\mathbb{R})$ lowest-weight state,

$$|\sigma n\rho\omega\kappa(LS_\sigma)JM_J\rangle = \left[\left[A^{(20)} \times A^{(20)} \cdots \times A^{(20)}\right]^n \times |\sigma; S_\sigma\rangle\right]^{\rho\omega}_{\kappa(LS_\sigma)JM_J}, \tag{4.60}$$

where $\sigma \equiv N_\sigma\,(\lambda_\sigma\,\mu_\sigma)$ labels $\mathrm{Sp}(3,\mathbb{R})$ irreps with $(\lambda_\sigma\,\mu_\sigma)$ denoting a SU(3) lowest-weight state, $n \equiv N_n\,(\lambda_n\,\mu_n)$, and $\omega \equiv N_\omega\,(\lambda_\omega\,\mu_\omega)$. The quantum number $N_\omega = N_\sigma + N_n$ is the total number of oscillator quanta related to the eigenvalue, $N_\omega\hbar\Omega$, of a three-dimensional harmonic oscillator Hamiltonian that excludes the c.m. spurious modes.

The quantum numbers $(\lambda_n\,\mu_n)$ specify the overall SU(3) symmetry of $N_n/2$ coupled symplectic raising operators. A multiple coupling of $(2\,0)$ irrep always produces a set of unique irreps and thus there is no need to introduce an additional multiplicity label. As the raising operators $A^{(2\,0)}_{\mathcal{L}M}$ commute, only the symmetrically coupled raising operators are non-vanishing [20]. It can be shown that all possible $(\lambda_n\,\mu_n)$ quantum numbers are enumerated by a set Ω^n defined as:

$$\Omega^n = \{(\lambda_n\,\mu_n)\,|n_1+n_2+n_3=N_n, \lambda_n=n_1-n_2, \mu_n=n_2-n_3, n_1\geq n_2\geq n_3\}\,,$$

where n_1, n_2, n_3 range over all even non-negative integers.

The $\rho\omega \equiv \rho N_\omega\,(\lambda_\omega\,\mu_\omega)$ quantum labels specify the SU(3) symmetry of the symplectic state. The symbol ρ denotes a multiplicity label which is needed to distinguish between multiple occurrences of the $(\lambda_\omega\,\mu_\omega)$ irrep within the direct product $(\lambda_\sigma\,\mu_\sigma)\times(\lambda_n\,\mu_n)$. In accordance with the mapping between the microscopic $(\lambda\,\mu)$ SU(3) labels and the shape variables of the Bohr-Mottelson collective model $(\beta\gamma)$, the symplectic basis states bring forward important information about the nuclear shapes and deformation, which is schematically depicted in Fig. 4.3.

The basis states, $|\sigma\kappa_\sigma(L_\sigma S_\sigma)J_\sigma M_{J_\sigma}\rangle$, of the symplectic bandhead σ are the starting state configurations upon which a $\mathrm{Sp}(3,\mathbb{R})$ irrep is built according to (4.60). A symplectic bandhead is a $\mathrm{Sp}(3,\mathbb{R})$ lowest-weight state and, consequently, it is annihilated upon the action of the $B^{(02)}_{\mathcal{L}M}$ symplectic lowering operators,

$$B^{(2\,0)}_{\mathcal{L}M}\,|N_\sigma\,(\lambda_\sigma\,\mu_\sigma)\,\kappa_\sigma(L_\sigma S_\sigma)J_\sigma M_{J_\sigma}\rangle = 0. \tag{4.61}$$

Trivially, all the SU(3) irreps that span the $0\hbar\Omega$ and $1\hbar\Omega$ subspaces satisfy the above condition. However, a general SU(3) irrep belonging to a higher-$\hbar\Omega$ subspace is not guaranteed to be a symplectic bandhead, and thus one has to test explicitly whether it is annihilated by the symplectic lowering operators. Note that if one were to include all possible symplectic bandheads and allowed symplectic excitations thereof, one would span the entire shell model Hilbert space.

It is important to note that the construction formula (4.60) does not produce an orthogonal basis. Specifically, the symplectic states with identical $N_\omega(\lambda_\omega\,\mu_\omega)$ labels but different ρ and n quantum numbers are generally not orthogonal. In order to find a unitary transformation that give rise to an orthonormal basis it is necessary to evaluate inner products between overlapping symplectic states. This is done by making use of the $\mathcal{K}$-matrix theory [127, 128, 129]. In our work, we are expanding symplectic states in an m-scheme basis, and hence we perform orthogonalization numerically by a modified Gram-Schmidt orthogonalization method.

4.2.5 Relation Between α-Cluster and Symplectic States

To achieve an unified description of nuclear collective dynamics, α-cluster modes, which manifest themselves most obviously in low-lying spectra of $A=4n$, $N=Z$ nuclei, should also be taken into account. In view of the pronounced α-cluster structure of many low-lying highly deformed intruder states, e.g. 0^+_2 states in ^{12}C and ^{16}O [130, 131, 132, 133], it is relevant to ask whether the clustering correlations

can be efficiently described by the $\mathrm{Sp}(3,\mathbb{R})$ symmetry-adapted basis. In an attempt to answer this question, we will now discuss the relation between the microscopic cluster model wave functions [132, 134, 135], which incorporate the physics of α-clustering, and the symplectic $\mathrm{Sp}(3,\mathbb{R})$ excitations, which describe naturally the quadrupole and monopole vibrational and rotational modes.

The translationally invariant states of the microscopic cluster model for a nucleus made up of fragments of mass number f and $A-f$ can be written in the SU(3)-coupled form as [136]:

$$|(\lambda_c\,\mu_c)\times(Q\,0);(\lambda_\omega\,\mu_\omega)\alpha_\omega\rangle = \mathcal{A}\left|[\{\varphi_f^{(\lambda_1\,\mu_1)}\times\phi_{A-f}^{(\lambda_2\,\mu_2)}\}^{(\lambda_c\,\mu_c)}\times\chi^{(Q\,0)}(\boldsymbol{R})](\lambda_\omega\,\mu_\omega)\alpha_\omega\right\rangle,$$

where $\mathcal{A}$ is the antisymmetrization operator. The properly antisymmetrized internal wave functions $\varphi_f^{(\lambda_1\,\mu_1)}$ and $\phi_{A-f}^{(\lambda_2\,\mu_2)}$ of the two fragments are assumed to be the lowest possible Pauli-allowed states with SU(3) symmetry $(\lambda_1\,\mu_1)$ and $(\lambda_2\,\mu_2)$, and they are coupled to a final SU(3) symmetry $(\lambda_c\,\mu_c)$. The relative motion wave function χ is a harmonic-oscillator function in the relative distance vector $\boldsymbol{R}$ between the two fragments. It carries Q oscillator quanta and hence it spans the SU(3) irrep $(Q\,0)$. The minimum value of Q is uniquely determined by the Pauli principle. The SU(3) symmetry of the total wave function is the resultant of the coupling $(\lambda_c\,\mu_c)\times(Q\,0)$ and denoted $(\lambda_\omega\,\mu_\omega)$ and its subgroup label α_ω.

The overlaps between a cluster wave function and a stretched symplectic wave function can be readily calculated using the recursive formula [137]:

$$\begin{aligned}&\langle\sigma(N_n{+}2\;0)(\lambda_\omega\,\mu_\omega)\alpha_\omega|\,(\lambda_c\,\mu_c)\times(Q{+}2\;0);(\lambda_\omega\,\mu_\omega)\alpha_\omega\rangle\\&\quad=\sqrt{\tfrac{1}{2}(Q+1)(Q+2)}\,U[(\lambda_c\,\mu_c)(Q\,0)(\lambda_\omega\,\mu_\omega)(2\,0);(\lambda'_\omega\,\mu'_\omega)11(Q{+}2\;0)11]\\&\qquad\times\langle\sigma(N_n\,0)(\lambda'_\omega\,\mu'_\omega)\alpha'_\omega|\,(\lambda_c\,\mu_c)\times(Q,0);(\lambda'_\omega\,\mu'_\omega)\alpha'_\omega\rangle,\end{aligned}\tag{4.62}$$

where $U[(\lambda_c\,\mu_c)(Q\,0)(\lambda_\omega\,\mu_\omega)(2\,0);(\lambda'_\omega\,\mu'_\omega)11(Q{+}2\;0)11]$ is an SU(3)-Racah coefficient. The symplectic stretched states are those states with $\mu_\omega=\mu_\sigma$ and maximum value of $\lambda_\omega=\lambda_\sigma+N_n$ for $N_n\hbar\Omega$ excitations above the symplectic bandhead, and hence in the above equation $(\lambda_\omega\,\mu_\omega)=(\lambda_\sigma{+}N_n{+}2\;\mu_\sigma)$ and $(\lambda'_\omega\,\mu'_\omega)=(\lambda_\sigma{+}N_n\;\mu_\sigma)$.

The $\alpha{+}^{12}$C cluster model of ^{16}O reproduces the isospin zero states below 15 Mev remarkably well [134, 135], including the first excited 0_2^+ state. This model describes the states of ^{16}O by exciting the relative motion degree of freedom of an α-particle and the ^{12}C nucleus. The internal wave functions of the α and ^{12}C clusters are restricted to the lowest Pauli-allowed states with SU(3) symmetry $(0\,0)$ and $(0\,4)$, respectively. The possible SU(3) symmetries $(\lambda_\omega\,\mu_\omega)$ of the cluster wave functions are

$$(0\,4)\times(Q\,0)=(Q{-}4\;0)\oplus(Q{-}3\;1)\oplus(Q{-}2\;2)\oplus(Q{-}1\;3)\oplus(Q\;4).$$

All cluster states with $Q<4$ are forbidden due to the Pauli principle. Only the $(0\,0)$ state is Pauli-allowed for $Q=4$, two states with $(1\,0)$, and $(2\,1)$ are allowed for $Q=5$, three states with $(2\,0)$, $(3\,1)$, and $(4\,2)$ for $Q=6$, four states with $(3\,0)$, $(4\,1)$, $(5\,2)$, and $(6\,3)$ for $Q=7$. For $Q\geq 8$, all five cluster wave functions are Pauli-allowed.

Table 4.1: Overlaps of stretched symplectic basis states $(\lambda_\sigma + n\,\mu_\sigma)$, $n = 0, 2, \ldots, 12$ built over different ^{16}O $(\lambda_\sigma\,\mu_\sigma)$ bandheads to the α+^{12}C cluster basis states of the same $(\lambda_\sigma + n\,\mu_\sigma)$ SU(3) symmetry according to formula (4.62) [137]. Each overlap is calculated at a given $\hbar\Omega$ level, e.g., the overlaps for the 4p-4h (8 4) symplectic irrep is given for $4\hbar\Omega$ (second column) up through $16\hbar\Omega$ (last column).

Symplectic bandhead $(\lambda_\sigma\,\mu_\sigma)$	Overlaps						
	λ_σ μ_σ	λ_σ+2 μ_σ	λ_σ+4 μ_σ	λ_σ+6 μ_σ	λ_σ+8 μ_σ	λ_σ+10 μ_σ	λ_σ+12 μ_σ
(0 0)	1.00	0.808	0.558	0.376	0.263	0.191	0.143
(2 1)	1.00	0.816	0.581	0.405	0.290	0.213	0.161
(4 2)	1.00	0.818	0.602	0.437	0.322	0.242	0.185
(6 3)	1.00	0.822	0.629	0.476	0.364	0.281	0.220
(8 4)	1.00	0.832	0.668	0.531	0.421	0.335	0.267

Furthermore, it turns out that the cluster wave functions with SU(3) symmetry (0 0), (2 1), (4 2), (6 3), and (8 4), are identical with the most deformed n-particle-n-hole (np-nh) Sp$(3,\mathbb{R})$ bandheads, with $n = 0, \ldots, 4$. The overlaps between the cluster and the stretched symplectic states spanning the leading np-nh Sp$(3,\mathbb{R})$ irreps were calculated in Ref. [137, 138] using the recursive formula (4.62). The results, which are summarized in Table 4.1, indicate that these states display a high-degree of overlap, particularly for the first few symplectic excitations above the bandheads and for irreps built over strongly deformed intrinsic bandheads. It is also evident, that the restriction of the symplectic model space to the dominant 0p-0h irreps is not sufficient to describe highly deformed states with a pronounced α-cluster structure. Qualitatively similar results were obtained for ^{20}Ne and ^{24}Mg systems [137]. In summary, certain features of the α-cluster dynamics are reflected in the symplectic Sp$(3,\mathbb{R})$ basis states with symplectic configurations beyond the dominant 0p-0h irreps being essential.

Chapter 5

Expansion of Symplectic States in M-Scheme Basis

To facilitate identification of the most important $\mathrm{Sp}(3,\mathbb{R})$ symmetry-adapted components within NCSM realistic wave functions, we needed to expand symplectic basis states in the same basis utilized within the NCSM, the m-scheme basis. Therefore, our task was to find an expansion of a translationally invariant symplectic bandhead in terms of Slater determinants formed of harmonic oscillator wave functions, upon which we apply the symplectic $\mathrm{Sp}(3,\mathbb{R})$ basis construction formula (4.60) using proton-neutron second-quantized formalism.

Methods utilized to accomplish this task are reviewed in this chapter. We first describe a procedure for generating SU(3) irreps in terms of m-scheme configurations. Next we introduce a c.m. removal operator utilized to ensure translational invariance of the generated irreps. Then we recast the symplectic construction formula into an alternative recursive form which is computationally less expensive and, at the same time, suitable for implementation in the form of a parallel algorithm. Finally, we derive analytic expressions for one-body and two-body matrix elements of $\mathrm{Sp}(3,\mathbb{R})$ generators in the basis of spherical harmonic oscillator wave functions.

5.1 Construction of Symplectic Bandheads

A symplectic bandhead is a SU(3) irrep satisfying condition (4.61). Therefore, our task was to find the expansion of a general $N\hbar\Omega$ kp-kh SU(3) irrep in terms of m-scheme configurations and then verify whether it represents a $\mathrm{Sp}(3,\mathbb{R})$ lowest-weight state. The resultant set of symmetry-adapted states must be free of spurious c.m. excitations and span a basis that is reduced with respect to physical group chain:

$$\begin{array}{ccccccc} \mathrm{SU}(3) & \supset & \mathrm{SO}(3) & & & & \\ & & \otimes & \supset & \mathrm{SU}(2) & \supset & U(1) \\ & & \mathrm{SU_S}(2) & & & & \\ & & & & & & \\ (\lambda\,\mu) & \kappa & (LS) & & J & & M_J \end{array}$$

5.1.1 Expansion of SU(3) Irrep in M-Scheme Basis

Neither of the two methods [139, 140] that have been utilized in past studies to generate SU(3) irreps in terms of harmonic oscillator Slater determinants meets all of the above requirements. The method described in Ref. [139] determines the expansion coefficients by diagonalization of the operator $\hat{C}_2 - \alpha \hat{L}^2$ in the m-scheme basis. The operator $\hat{L}^2$ is subtracted from the second Casimir invariant $\hat{C}_2$ in order to split states spanning the same SU(3) irrep but carrying different angular momenta. The applicability of this method is limited for two reasons. First, it fails to distinguish between two SU(3) irreps with different labels $(\lambda\,\mu)$ but with degenerate values of $\hat{C}_2$. Secondly, it is computationally expensive beyond the valence space due to the rapid increase in dimensions of $N\hbar\Omega$ model spaces.

The method implemented in Ref. [140, 141] uses a basis that reduces the canonical SU(3)$\supset$U(1)$\otimes$SU(2) subgroup chain, and hence it is not labeled by the orbital angular momentum L. It constructs the highest weight states of the leading proton and neutron SU(3) irreps in the cylindrical harmonic oscillator basis, and subsequently employs the elements of the $\mathfrak{su}(3)$ Lie algebra to generate the rest of the basis. The resulting irreps are coupled to a final SU(3) irrep spanning the proton-neutron Hilbert space.

Our method relies on the fact that the creation operators for fermions in the spherical harmonic oscillator basis are irreducible tensors[1] with respect to the spatial SU(3) and the intrinsic spin $\mathrm{SU_S}(2)$ symmetries with tensor characters $(\eta\,0)$ and $\frac{1}{2}$ [142, 143], respectively,

$$a^{\dagger}_{\eta(l\frac{1}{2})jm_j} \rightarrow a^{\dagger(\eta 0)}_{(l\frac{1}{2})jm_j}. \tag{5.1}$$

Here, the principal quantum number $\eta = 0, 1, 2, \ldots$ labels a harmonic oscillator shell; l, $\frac{1}{2}$, j and m_j label the orbital angular momentum, the intrinsic spin, the total angular momentum and its projection, respectively.

An SU(3) symmetry-adapted state of N fermions is thus created by acting with an SU(3)-coupled product of N fermion creation operators on the vacuum state,

$$|\mathbf{f}(\lambda\,\mu)\kappa(LS)JM_J\rangle = \left[a^{\dagger(\eta_1\,0)}_{\frac{1}{2}} \times a^{\dagger(\eta_2\,0)}_{\frac{1}{2}} \times \cdots \times a^{\dagger(\eta_N\,0)}_{\frac{1}{2}}\right]^{(\lambda\,\mu)}_{\kappa(LS)JM_J} |0\rangle\,, \tag{5.2}$$

where $\mathbf{f} = \{\eta_1, \ldots, \eta_N\}$. Now, let us consider a system of A nucleons composed by Z protons and N neutrons. A distribution of the nucleons over the harmonic oscillator shells is given by two sets of the principal quantum numbers, $\mathbf{f}_\pi = \{\eta_1, \ldots, \eta_Z\}$ for protons and $\mathbf{f}_\nu = \{\eta'_1, \ldots, \eta'_N\}$ for neutrons. Let us further suppose that proton and neutron creation operators can be coupled to tensor operators with $(\lambda_\pi\,\mu_\pi)S_\pi$ and $(\lambda_\nu\,\mu_\nu)S_\nu$ characters, respectively. The construction formula for an SU(3) basis

[1] The annihilation operator $a_{\eta ljm_j}$ is not a proper irreducible SU(3)$\otimes$SU$_\mathrm{S}$(2) tensor. One has to introduce annihilation tensor operator $\tilde{a}^{(0\,n)}_{ljm_j}$ of rank $(0\,\eta)\frac{1}{2}$ which is related to the annihilation operator as $\tilde{a}^{(0\,\eta)}_{ljm_j} = (-1)^{\eta+1-j+m_j} a_{\eta ljm_j}$.

state, $|\xi\rho_0\,(\lambda_0\,\mu_0)\,\kappa_0\,(L_0S_0)\,J_0M_{J_0}\rangle$, in the proton-neutron formalism is given as,

$$|\xi\rho_0\,(\lambda_0\,\mu_0)\,\kappa_0\,(L_0S_0)\,J_0M_{J_0}\rangle = \left[\mathcal{P}^{(\lambda_\pi\,\mu_\pi)}_{\mathbf{f}_\pi S_\pi}(a^\dagger_\pi) \times \mathcal{P}^{(\lambda_\nu\,\mu_\nu)}_{\mathbf{f}_\nu S_\nu}(a^\dagger_\nu)\right]^{\rho_0(\lambda_0\,\mu_0)}_{\kappa_0(L_0S_0)J_0M_{J_0}} |0\rangle\,. \quad (5.3)$$

The label $\xi = \{\mathbf{f}_\pi(\lambda_\pi\,\mu_\pi)S_\pi, \mathbf{f}_\nu(\lambda_\nu\,\mu_\nu)S_\nu\}$ schematically denotes additional quantum numbers included to distinguish different distributions of nucleons over the harmonic oscillator shells and different symmetry coupling of protons and neutrons, ρ_0 gives the multiplicity of $(\lambda_0\,\mu_0)$ for a given ξ set of quantum numbers, and $\mathcal{P}^{(\lambda_\pi\,\mu_\pi)}_{\mathbf{f}_\pi S_\pi}$ and $\mathcal{P}^{(\lambda_\nu\,\mu_\nu)}_{\mathbf{f}_\nu S_\nu}$ denote irreducible tensor operators constructed as coupled products of Z proton ($a^\dagger_\pi$) and N neutron ($a^\dagger_\nu$) creation operators,

$$\mathcal{P}^{(\lambda_\pi\,\mu_\pi)}_{\mathbf{f}_\pi S_\pi}(a^\dagger_\pi) = \left[a^{\dagger(\eta_1\,0)}_{\pi\frac{1}{2}} \times \cdots \times a^{\dagger(\eta_Z\,0)}_{\pi\frac{1}{2}}\right]^{(\lambda_\pi\mu_\pi)}_{S_\pi}, \quad (5.4)$$

$$\mathcal{P}^{(\lambda_\nu\,\mu_\nu)}_{\mathbf{f}_\nu S_\nu}(a^\dagger_\nu) = \left[a^{\dagger(\eta'_1\,0)}_{\nu\frac{1}{2}} \times \cdots \times a^{\dagger(\eta'_N\,0)}_{\nu\frac{1}{2}}\right]^{(\lambda_\nu\mu_\nu)}_{S_\nu}. \quad (5.5)$$

Upon a complete uncoupling of the irreducible tensors in the formulas (5.3), (5.4), and (5.5), we obtain expansion in terms of products of A creation operators. When applied on the vacuum state, each term in the expansion generates an A-nucleon m-scheme state with the probability amplitude given by the corresponding coefficient in the expansion. In order to construct properly antisymmetrized symmetry-adapted states, special care must be taken to accurately accommodate the anticommutation relation for fermion creation operators, $\{a^\dagger_i, a^\dagger_j\} = 0$. We implemented the construction formula (5.3) as a recursive algorithm, by making use of the formula for uncoupling $\mathrm{SU}(3)\supset\mathrm{SO}(3)\otimes\mathrm{SU}_S(2)$ tensor operators

$$\begin{aligned}&\left[X^{(\lambda_1\,\mu_1)}_{S_1} \times Y^{(\lambda_2\,\mu_2)}_{S_2}\right]^{\rho(\lambda\,\mu)}_{\kappa(LS)JM_J} = \\ &\sqrt{(2S+1)(2L+1)} \sum_{\kappa_1 l_1, \kappa_2 l_2} \langle(\lambda_1\,\mu_1)\kappa_1 l_1; (\lambda_2\,\mu_2)\kappa_2 l_2 \| (\lambda\,\mu)\kappa L\rangle_\rho \\ \times \sum_{\substack{m_{j_1}, m_{j_2}\\ j_1, j_2}} C^{JM_J}_{j_1 m_{j_1} j_2 m_{j_2}} &\sqrt{(2j_2+1)(2j_1+1)} \left\{ \begin{array}{ccc} l_1 & l_2 & L \\ S_1 & S_2 & S \\ j_1 & j_2 & J \end{array} \right\} X^{(\lambda_1\,\mu_1)}_{l_1 S_1 j_1 m_{j_1}} Y^{(\lambda_2\,\mu_2)}_{l_2 S_2 j_2 m_{j_2}}.\end{aligned} \quad (5.6)$$

As it would be highly inefficient to generate the whole basis of a given SU(3) irrep by means of the construction formula (5.3), we utilize this approach for finding expansion of states with the projection number $M_{J_0} = J_0$ only. The rest of states is readily obtained by the successive action of the total angular momentum lowering operator $\hat{J}_-$.

5.1.2 Center of Mass Spuriosity Removal

The symmetry-adapted states generated by the procedure described above are not translationally invariant, with the exception of those constructed within the $0\hbar\Omega$

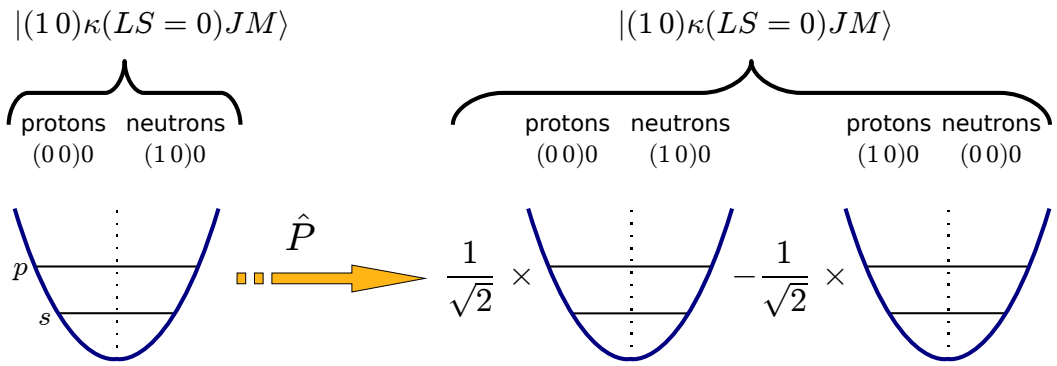

Figure 5.1: The result of the action of the projecting operator $\hat{P}(n_{\max}=1)$ on $1\hbar\Omega$ 1p-1h SU(3)⊗SU$_{\rm S}$(2) irrep in ^{4}He nucleus.

model space [35]. Therefore, the symplectic bandhead construction procedure has to be supplemented by a method eliminating the spurious c.m. excitations.

Techniques for identification and elimination of spurious c.m. excitations in the shell model configurations using the SU(3) classification scheme and the group theoretical methods were initially proposed by Verhaar [144] and Hecht [145], respectively. The method of Verhaar relays on diagonalization of the c.m. harmonic oscillator Hamiltonian, $H_{\rm cm} = \big(\mathfrak{B}^\dagger\cdot\mathfrak{B}+3/2\big)\hbar\Omega$, in a space spanned by SU(3) irreps of the same rank. The eigenstates of $H_{\rm cm}$ corresponding to an eigenvalue of $\frac{3}{2}\hbar\Omega$ do not contain any spurious c.m. excitations and hence compose the subspace of translationally invariant irreps.

We use an alternative and simpler approach based on U(3) symmetry-preserving c.m. projection operators [24]. The method was briefly outlined by Hecht in Ref.[145] but never utilized for eliminating the c.m. spuriosity from SU(3) or Sp$(3,\mathbb{R})$ symmetry-adapted configurations. The projection technique is based on the fact that a general SU(3) symmetry-adapted A-particle state of $n_{\max}\hbar\Omega$ excitations above the lowest energy configuration can be written in an SU(3)-coupled form as

$$|(\lambda\,\mu)\kappa LM\rangle = \sum_{n=0}^{n_{\max}} \sum_{(\lambda\,\mu)_{\rm intr}} c_n^{(\lambda\,\mu)_{\rm intr}}\, |(n\,0)\times(\lambda\,\mu)_{\rm intr};(\lambda\,\mu)\kappa LM\rangle\,, \tag{5.7}$$

where $c_n^{(\lambda\,\mu)_{\rm intr}}$ denotes a probability amplitude. The SU(3) quantum numbers, $(\lambda\,\mu)_{\rm intr}$, label the intrinsic wave functions of $(n_{\max}-n)\hbar\Omega$ excitations that are coupled with the c.m. SU(3) irreps $(n\,0)$ of $n\hbar\Omega$ excitations into the final SU(3) symmetry $(\lambda\,\mu)$. Note that for the non-spurious part of the state, $n=0$, the quantum numbers $(\lambda\,\mu)_{\rm intr}$ coincide with $(\lambda\,\mu)$.

In order to eliminate the c.m. spuriosity from A-particle SU(3)-symmetric states one needs to project out all the $n\geq 1$ terms on the right hand side of the expansion (5.7) as they describe excited c.m. motion. This is done by employing

the simplest U(3) Casimir invariant, namely, the c.m. number operator

$$\hat{N}^{\rm cm} = \mathfrak{B}^{\dagger} \cdot \mathfrak{B}, \tag{5.8}$$

in an U(3) symmetry-preserving projecting operator,

$$\hat{P}(n_{\rm max}) = \prod_{k_0=1}^{n_{\rm max}} \left(1 - \frac{\hat{N}^{\rm cm}}{k_0} \right). \tag{5.9}$$

The $|(n\,0) \times (\lambda\,\mu)_{\rm intr}; (\lambda\,\mu)\kappa LM\rangle$ states (5.7) are eigenstates of $\hat{N}^{\rm cm}$ with eigenvalues n. Therefore, they are also eigenstates of the $\hat{P}(n_{\rm max})$ operator with eigenvalues equal to 0 for excitations $n = 1, \ldots, n_{\rm max}$ and 1 when $n = 0$, which corresponds to a non-spurious state. Therefore, the c.m. spurious excitations vanish under the action of $\hat{P}(n_{\rm max})$, while a non-spurious state (or the spurious-free part of a state) remains unaltered. The non-spurious states, which are obtained after the projection, are properly orthonormalized and then utilized in the calculations.

The projection operator $\hat{P}(n_{\rm max})$ is a scalar with respect to SU(3) and $\mathrm{SU_S}(2)$, and hence it preserves $(\lambda_0\,\mu_0)\kappa_0(L_0S_0)J_0M_{J_0}$ quantum labels. However, it mixes the additional quantum numbers, denoted in the construction formula (5.3) as ξ, which are included to distinguish between a different construction for protons and neutrons. This is illustrated in Fig. 5.1 for the $1\hbar\Omega$ 1p-1h $(1\,0)S = 0$ irrep in the ^{4}He nucleus that has a single proton promoted to the p-shell. Upon the c.m. removal, we recover a configuration that is a superposition of two irreps, one with a single proton and the other with a single neutron promoted to the p-shell.

The projection operator (5.9) can be also used to remove the c.m. spuriosity out of symplectic $\mathrm{Sp}(3,\mathbb{R})$ states if these were constructed by means of the non-translationally invariant symplectic raising operators.

5.2 Symplectic Basis Construction Formula in Second Quantized Form

Although one is tempted to implement the construction formula (4.60) straightforwardly as the action of polynomials in the $A^{(2\,0)}_{\mathcal{L}M}$ raising operators on a symplectic bandhead, such an approach is not advisable as it becomes computationally cumbersome for higher-$\hbar\Omega$ subspaces. There are two main reasons for this. First, a kth degree polynomial in $A^{(2\,0)}_{\mathcal{L}M}$ represents a $2k$-body operator, which leads to highly complex calculations for $k > 1$. The second reason is that each symplectic state belonging to a $N\hbar\Omega$ subspace is a linear combination of nearly all $N\hbar\Omega$ m-scheme states, and hence, besides elaborate polynomial operators, we are also faced with the scale explosion problem.

An alternative approach is to transform the symplectic construction formula into a recursive relation [136, 146] that allows one to construct a symplectic state of excitation $N_\omega\hbar\Omega$ by the action of the $A^{(2\,0)}_{\mathcal{L}M}$ raising operators on a special linear combination of symplectic states of excitation $(N_\omega - 2)\hbar\Omega$. Such a recursive scheme

makes a parallel implementation rather straightforward and, at the same time, it is computationally less expensive as it enables one to utilize results obtained in the previous step.

5.2.1 Recursive Symplectic Construction Formula

Before we start deriving the recursive form of the symplectic $\mathrm{Sp}(3,\mathbb{R})$ basis construction formula, it is convenient to introduce some shorthand notation. Let SU(3) representation labels be denoted as

$$\begin{aligned} n &\equiv (\lambda_n\, \mu_n) \\ \sigma &\equiv (\lambda_\sigma\, \mu_\sigma) \\ \omega &\equiv (\lambda_\omega\, \mu_\omega)\,. \end{aligned}$$

The symbol α will signify the SU(3) basis states labels in the SU(3)$\supset$SO(3) subroup chain, e.g.,

$$\alpha_\omega \equiv \kappa_\omega L_\omega M_\omega.$$

The polynomials in the symplectic raising operators, which appear in the construction formula as a result of the coupling of $A^{(2\,0)}_{\mathcal{L}M}$ operators into an irreducible SU(3)$\supset$SO(3) tensor, will be denoted as

$$\mathcal{P}^{n'}_{\alpha'_n}(A^{(2\,0)}) \equiv \left[A^{(2\,0)}\cdots\times A^{(2\,0)}\right]^{n'}_{\alpha'_n}. \tag{5.10}$$

The derivation starts with the symplectic $\mathrm{Sp}(3,\mathbb{R})$ construction formula (4.60) written in the SU(3)-uncoupled form,

$$|\sigma n'\rho'\omega'\alpha'_\omega\rangle = \sum_{\alpha'_n\alpha_\sigma} \langle n'\alpha'_n;\sigma\alpha_\sigma|\,\omega'\alpha'_\omega\rangle_{\rho'}\mathcal{P}^{n'}_{\alpha'_n}(A^{(2\,0)})\,|\sigma\alpha_\sigma\rangle\,, \tag{5.11}$$

where $\langle n'\alpha'_n;\sigma\alpha_\sigma|\,\omega'\alpha'_\omega\rangle_{\rho'}$ denotes an SU(3) $\supset$ SO(3) Wigner coupling coefficient, and $|\sigma n'\rho'\omega'\alpha'_\omega\rangle$ is a symplectic state. Using the orthonormal property of SU(3) coupling coefficients (C.3), we can express the action of $\mathcal{P}^{n'}_{\alpha'_n}(A^{(2\,0)})$ on a symplectic bandhead state $|\sigma\alpha_\sigma\rangle$ as

$$\mathcal{P}^{n'}_{\alpha'_n}(A^{(2\,0)})\,|\sigma\alpha_\sigma\rangle = \sum_{\rho'\omega'\alpha'_\omega} \langle n'\alpha'_n;\sigma\alpha_\sigma|\,\omega'\alpha'_\omega\rangle_{\rho'}\,|\sigma n'\rho'\omega'\alpha'_\omega\rangle\,. \tag{5.12}$$

The polynomials in the symplectic raising operators can be decoupled recursively as

$$\mathcal{P}^{n}_{\alpha_n}(A^{(2\,0)}) = \sum_{n'\alpha'_n\mathcal{L}M} \langle(2\,0)\mathcal{L}M;n'\alpha'_n|\,n\alpha_n\rangle A^{(2\,0)}_{\mathcal{L}M}\mathcal{P}^{n'}_{\alpha'_n}(A^{(2\,0)}). \tag{5.13}$$

Now, we insert the expression (5.13) into (5.11) and by making use of the relation (5.12) we find the recursive form of the construction formula

$$\begin{aligned} |\sigma n\rho\omega\alpha_\omega\rangle \;=\; & \sum_{\alpha_n\alpha_\sigma} \langle n\alpha_n;\sigma\alpha_\sigma|\,\omega\alpha_\omega\rangle_{\rho} \sum_{n'\alpha'_n\mathcal{L}M} \langle(2\,0)\mathcal{L}M;n'\alpha'_n|\,n\alpha_n\rangle A^{(2\,0)}_{\mathcal{L}M} \\ & \sum_{\rho'\omega'\alpha'_\omega} \langle n'\alpha'_n;\sigma\alpha_\sigma|\,\omega'\alpha'_\omega\rangle_{\rho'}\,|\sigma n'\rho'\omega'\alpha'_\omega\rangle\,, \end{aligned} \tag{5.14}$$

which can be further simplified by invoking property (C.10) of SU(3)-Racah coefficients [147] to

$$|\sigma n\rho\omega\alpha_\omega\rangle = \sum_{\mathcal{L}M} A^{(2\,0)}_{\mathcal{L}M} \sum_{n'\rho'\omega'} U\left[(2\,0)n'\omega\sigma; n1\rho; \omega'\rho'1\right] \sum_{\alpha'_\omega} \langle (2\,0)\mathcal{L}M; \omega'\alpha'_\omega |\, \omega\alpha_\omega\rangle \, |\sigma n'\rho'\omega'\alpha'_\omega\rangle \,. \tag{5.15}$$

Here, $U\left[(2\,0)n'\omega\sigma; n1\rho; \omega'\rho'1\right]$ denotes an SU(3)-Racah coefficient. Since the coupling of the $(2\,0)$ SU(3) irrep with any other SU(3) irrep is always multiplicity free, there are two arguments in the above SU(3)-Racah coefficient that take on a value of one only. They correspond to multiplicities of SU(3) irreps resulting from $(2\,0) \times (\lambda_{n'}\, \mu_{n'})$ and $(2\,0) \times (\lambda_{\omega'}\, \mu_{\omega'})$ coupling, respectively.

Notice that up to now the spin degree of freedom has been ignored. The symplectic raising operators, and in fact all $\mathrm{Sp}(3,\mathbb{R})$ generators, act merely on the spatial part of a wave function leaving the spin part unaltered. This allowed us, without loss of generality, to neglect the spin degree of freedom. Now, in order for the total angular momentum J and its projection M_J to be good quantum numbers, we have to consider the total intrinsic spin S_σ and recast the formula (5.15) into the (LS)-coupled scheme. We obtain

$$\begin{aligned} |\sigma n\rho\omega\kappa(LS_\sigma); JM_J\rangle = & \sum_{M_L\Sigma} C^{JM_J}_{LM_LS_\sigma\Sigma} \sum_{\mathcal{L}M} A^{(2\,0)}_{\mathcal{L}M} \sum_{n'\rho'\omega'} U\left[(2\,0)n'\omega\sigma; n1\rho; \omega'\rho'1\right] \\ & \sum_{\kappa'L'M'_L} C^{LM_L}_{\mathcal{L}ML'M'_L} \langle (2\,0)\mathcal{L}; \omega'\kappa'L' \| \omega\kappa L\rangle \\ & \sum_{J'M'_J} C^{J'M'_J}_{L'M'_LS_\sigma\Sigma} \, |\sigma n'\rho'\omega'\kappa'(L'S_\sigma); J'M'_J\rangle \,. \end{aligned} \tag{5.16}$$

Here, $\langle (2\,0)\mathcal{L}M; \omega'\kappa'L' \| \omega\kappa L\rangle$ denotes a reduced SU(3) coupling coefficient [see (C.5)]. This formula can be further simplified. By invoking properties of SO(3) Clebsch-Gordan coefficients given in Ref. [148] [equation (10) on page 245 and equation (12) on page 260], we obtain

$$\begin{aligned} |\sigma n\rho\omega\kappa(LS_\sigma); JM_J\rangle = & (-1)^{S_\sigma}\sqrt{2L+1} \sum_{\mathcal{L}M} A^{(2\,0)}_{\mathcal{L}M} \\ & \sum_{n'\rho'\omega'} U\left[(2\,0)n'\omega\sigma; n1\rho; \omega'\rho'1\right] \sum_{\kappa'L'} \langle (2\,0)\mathcal{L}; \omega'\kappa'L' \| \omega\kappa L\rangle \\ & \sum_{J'} (-1)^{J'+L'}\sqrt{2J'+1} \begin{Bmatrix} L' & S_\sigma & J' \\ J & \mathcal{L} & L \end{Bmatrix} \\ & \sum_{M'_J} C^{JM_J}_{J'M'_J\mathcal{L}M} \, |\sigma n'\rho'\omega'\kappa'(L'S_\sigma)J'M'_J\rangle \,. \end{aligned} \tag{5.17}$$

This formula greatly facilitates the construction process as it utilizes results of the preceding step. The starting case is the m-scheme expansion of a symplectic bandhead, $\{|\sigma\kappa_\sigma(L_\sigma S_\sigma)J_\sigma M_{J_\sigma}\rangle\}$, upon which we apply the formula (5.17) to obtain symplectic states of excitation $(N_\sigma + 2)\hbar\Omega$. The foregoing procedure is then repeated

until all symplectic basis states of a given $\mathrm{Sp}(3,\mathbb{R})$ irrep up to excitation $N_{\max}\hbar\Omega$ are expanded.

5.2.2 Parallel Algorithm

The construction formula (5.17) can be schematically written as

$$|\sigma n\rho\omega\kappa(LS_\sigma);JM_J\rangle \;=\; (-1)^{S_\sigma}\sqrt{2L+1}\sum_{\mathcal{L}M} A^{(2\,0)}_{\mathcal{L}M}\,|\sigma S_\sigma;JM_J\rangle_{\mathcal{L}M}\,, \quad (5.18)$$

where $|\sigma S_\sigma;JM_J\rangle_{\mathcal{L}M}$ denotes a special combination of symplectic states of excitation $N_\omega\hbar\Omega$ spanning a given $\mathrm{Sp}(3,\mathbb{R})$ irrep σ and carrying the total intrinsic spin S_σ. This state is obtained as

$$|\sigma S_\sigma;JM_J\rangle_{\mathcal{L}M} = \sum_{n'\rho'\omega'} U\,[(2\,0)n'\omega\sigma;n1\rho;\omega'\rho'1]\sum_{\kappa'L'}\langle((2\,0)\mathcal{L};\omega'\kappa'L'\|\omega\kappa L\rangle$$
$$\sum_{J'}(-1)^{J'+L'}\sqrt{2J'+1}\left\{\begin{array}{ccc} L' & S_\sigma & J' \\ J & \mathcal{L} & L\end{array}\right\}\sum_{M'_J} C^{JM_J}_{J'M'_J\mathcal{L}M}\,|\sigma n'\rho'\omega'\kappa'(L'S_\sigma)J'M'_J\rangle\,. \quad (5.19)$$

The construction algorithm is notably simple. For each value of $\mathcal{L}$ and M we construct $|\sigma S_\sigma;JM_J\rangle_{\mathcal{L}M}$ according to the prescription (5.19), and then apply the symplectic raising operator $A^{(2\,0)}_{\mathcal{L}M}$. In this way we produce five states of excitation $(N_\omega+2)\hbar\Omega$ spanning the irrep σS_σ. These states are added and multiplied by the phase factor $(-1)^{S_\sigma}\sqrt{2L+1}$ yielding the resulting symplectic state $|\sigma n\rho\omega\kappa(LS_\sigma);JM_J\rangle$.

The parallel implementation of this procedure is schematically depicted in Fig. 5.2. At the beginning, each process is assigned with a particular set of $(N_\omega-2)\hbar\Omega$ m-scheme states, so that $|\sigma S_\sigma;JM_J\rangle_{\mathcal{L}M}$ is split evenly among collaborating processes. In the next step, every process applies the $A^{(2\,0)}_{\mathcal{L}M}$ operator on the part of $|\sigma S_\sigma;JM_J\rangle_{\mathcal{L}M}$ it maintains (Step 1 in Fig. 5.2), and obtains a certain linear combination of $N_\omega\hbar\Omega$ m-scheme states. Some of the resulting m-scheme configurations, as indicated in Fig. 5.2, occur simultaneously in other processes' results. In the last step, these "overlapping" m-scheme states are redistributed so that at the end each process retains a linear combination of unique configurations (Step 2 in Fig. 5.2). This represents the most time consuming part of the algorithm due to a large amount of data to be interchanged.

The parallel algorithm was implemented using the MPI library [149]. The symplectic $\mathrm{Sp}(3,\mathbb{R})$ states in ^{16}O and ^{12}C were generated successfully up to $6\hbar\Omega$ model space utilizing about 60 processes.

5.2.3 $\mathrm{Sp}(3,\mathbb{R})$ Generators in Second-Quantized Form

The most convenient way of evaluating the action of the symplectic $\mathrm{Sp}(3,\mathbb{R})$ generators upon an m-scheme configuration is to utilize the second-quantization formalism.

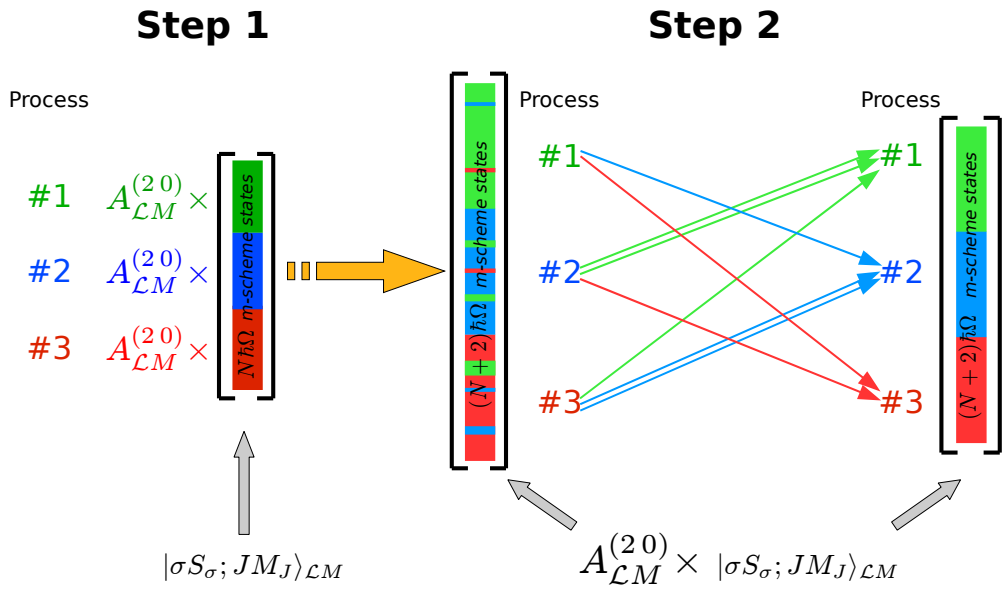

Figure 5.2: Schematic plot illustrating parallel scheme of $A^{(20)}_{\mathcal{L}M}\,|\sigma S_\sigma; JM_J\rangle_{\mathcal{L}M}$ calculation.

We thus need to derive analytic expressions for one-body and two-body matrix elements of the $\mathrm{Sp}(3,\mathbb{R})$ generators in the spherical harmonic oscillator basis. We start with the symplectic generators written in a translationally invariant form which explicitly separates one-body and two-body operator terms

$$
\begin{aligned}
A^{(20)}_{\mathcal{L}M} &= \frac{A-1}{\sqrt{2}A}\sum_{i=1}^{A}\left[b_i^{\dagger(10)}\times b_i^{\dagger(10)}\right]^{(20)}_{\mathcal{L}M} - \frac{2}{\sqrt{2}A}\sum_{t<s}^{A}\left[b_s^{\dagger(10)}\times b_t^{\dagger(10)}\right]^{(20)}_{\mathcal{L}M}\\
B^{(02)}_{\mathcal{L}M} &= \frac{A-1}{\sqrt{2}A}\sum_{i=1}^{A}\left[b_i^{(01)}\times b_i^{(01)}\right]^{(02)}_{\mathcal{L}M} - \frac{2}{\sqrt{2}A}\sum_{t<s}^{A}\left[b_s^{(01)}\times b_t^{(01)}\right]^{(02)}_{\mathcal{L}M}\\
C^{(11)}_{\mathcal{L}M} &= \sqrt{2}\frac{A-1}{A}\sum_{i=1}^{A}\left[b_i^{\dagger(10)}\times b_i^{(01)}\right]^{(11)}_{\mathcal{L}M} - \frac{\sqrt{2}}{A}\sum_{t,s=1,\,s\neq t}^{A}\left[b_s^{\dagger(10)}\times b_t^{(01)}\right]^{(11)}_{\mathcal{L}M}.
\end{aligned}
$$

Matrix Elements of $A^{(20)}_{\mathcal{L}M}$

The one-body part of the symplectic raising operator $A^{(20)}_{\mathcal{L}M}$ in the second quantization formalism takes form

$$
\frac{A-1}{\sqrt{2}A}\sum_{\{-\}}\langle\eta_f l_f j_f m_{j_f}|\left[b^{\dagger(10)}\times b^{\dagger(10)}\right]^{(20)}_{\mathcal{L}M}|\eta_i l_i j_i m_{j_i}\rangle\, a^{\dagger}_{\eta_f l_f j_f m_{j_f}} a_{\eta_i l_i j_i m_{j_i}}, \tag{5.20}
$$

with the abbreviation $\{-\} = \{\eta_f, l_f, j_f, m_{j_f}, \eta_i, l_i, j_i, m_{j_i}\}$. We thus have to determine the matrix elements of the irreducible SU(3) tensor operator

$$\left[b^{\dagger(1\,0)} \times b^{\dagger(1\,0)}\right]^{(2\,0)}_{\mathcal{L}M} \tag{5.21}$$

in the spherical harmonic oscillator basis. It is convenient to express the SU(3) tensor (5.21) in terms of SO(3) tensor operators as this allows us to make use of all relations for SO(3) tensorial calculus collected in Ref. [148]. By employing the formula for the coupling of two irreducible SU(3) tensor operators (C.8) we find that

$$\left[b^{\dagger(1\,0)} \times b^{\dagger(1\,0)}\right]^{(2\,0)}_{\mathcal{L}M} \;=\; \langle (1\,0)11;(1\,0)11\|(2\,0)1\mathcal{L}\rangle \left[b_1^{\dagger(1\,0)} \times b_1^{\dagger(1\,0)}\right]_{\mathcal{L}M}, \tag{5.22}$$

where $b_1^{\dagger(1\,0)}$ is the spherical SO(3) tensor with $l = 1$ character. The irreducible tensor operator on the right-hand side of the relation (5.22) is the SO(3) angular momentum tensor of rank $\mathcal{L}M$, and the coupling of the harmonic oscillator raising operators is thus performed in the SO(3) scheme. The reduced SU(3) coupling coefficient $\langle (1\,0)11;(1\,0)11\|(2\,0)1\mathcal{L}\rangle \;=\; (-)^{1+\mathcal{L}/2}$ and thus the equation (5.22) becomes,

$$\left[b^{\dagger(1\,0)} \times b^{\dagger(1\,0)}\right]^{(2\,0)}_{\mathcal{L}M} = (-)^{1+\mathcal{L}/2} \left[b_1^{\dagger(1\,0)} \times b_1^{\dagger(1\,0)}\right]_{\mathcal{L}M}. \tag{5.23}$$

In the next step, we make use of the relation given in Ref. [148] [equation (10) on page 476], for the matrix elements of SO(3)-coupled product of two irreducible SO(3) tensor operators. We get

$$\begin{aligned}
&\left\langle \eta_f l_f m_{l_f}; \tfrac{1}{2}\sigma_f \right| \left[b_1^{\dagger(1\,0)} \times b_1^{\dagger(1\,0)}\right]_{\mathcal{L}M} \left| \eta_i l_i m_{l_i}; \tfrac{1}{2}\sigma_i \right\rangle = \delta_{\sigma_f\sigma_i} (-)^{l_f+l_i-\mathcal{L}} \frac{\sqrt{2\mathcal{L}+1}}{\sqrt{2l_f+1}} C^{l_f m_{l_f}}_{l_i m_{l_i} \mathcal{L}M} \\
&\sum_{\eta_t l_t} \left\{ \begin{array}{ccc} 1 & 1 & \mathcal{L} \\ l_i & l_f & l_t \end{array} \right\} \langle \eta_f l_f \| b_1^{\dagger(1\,0)} \| \eta_t l_t \rangle \langle \eta_t l_t \| b_1^{\dagger(1\,0)} \| \eta_i l_i \rangle.
\end{aligned} \tag{5.24}$$

The transformation of this expression into the (LS)-coupled harmonic oscillator basis yields

$$\begin{aligned}
&\left\langle \eta_f l_f j_f m_{j_f} \right| \left[b_1^{\dagger(1\,0)} \times b_1^{\dagger(1\,0)}\right]_{\mathcal{L}M} \left| \eta_i l_i j_i m_{j_i} \right\rangle = (-)^{1-\frac{\mathcal{L}}{2}+l_f+l_i} \frac{\sqrt{2\mathcal{L}+1}}{\sqrt{2l_f+1}} \\
&\sum_{m_{l_f} m_{l_i} \sigma} C^{j_f m_{j_f}}_{l_f m_{l_f} \frac{1}{2}\sigma} C^{j_i m_{j_i}}_{l_i m_{l_i} \frac{1}{2}\sigma} C^{l_f m_{l_f}}_{l_i m_{l_i} \mathcal{L}M} \\
&\sum_{\eta_t l_t} \left\{ \begin{array}{ccc} 1 & 1 & \mathcal{L} \\ l_i & l_f & l_t \end{array} \right\} \langle \eta_f l_f \| b_1^{\dagger(1\,0)} \| \eta_t l_t \rangle \langle \eta_t l_t \| b_1^{\dagger(1\,0)} \| \eta_i l_i \rangle.
\end{aligned} \tag{5.25}$$

Finally, we simplify this formula by invoking the relation for a sum involving product of three SO(3) Clebsch-Gordan coefficients (see Ref. [148], equation (12) on page

260). The resulting expression for the one-body matrix elements of the symplectic raising operator reads

$$\langle \eta_f l_f j_f m_{j_f}| \left[b^{\dagger(1\,0)} \times b^{\dagger(1\,0)}\right]^{(2\,0)}_{\mathcal{L}M} |\eta_i l_i j_i m_{j_i}\rangle = \delta_{\eta_f \eta_i+2}(-)^{\phi}\sqrt{2\mathcal{L}+1}\sqrt{2j_i+1}$$
$$C^{j_f m_{j_f}}_{j_i m_{j_i} \mathcal{L}M} \left\{ \begin{array}{ccc} l_i & \frac{1}{2} & j_i \\ j_f & \mathcal{L} & l_f \end{array} \right\} \sum_{\eta_t l_t} \left\{ \begin{array}{ccc} 1 & 1 & l \\ l_i & l_f & l_t \end{array} \right\} \langle \eta_f\, l_f \| b^{\dagger(1\,0)} \| \eta_t\, l_t\rangle \langle \eta_t\, l_t \| b^{\dagger(1\,0)} \| \eta_i\, l_i\rangle, \tag{5.26}$$

with the phase $\phi = \frac{3}{2} + \frac{\mathcal{L}}{2} + j_i + l_i$.

In order to implement the two-body part of the $A^{(2\,0)}_{\mathcal{L}M}$ raising operator in the second quantized form, we have to find the matrix element of the SU(3) tensor

$$-\frac{\sqrt{2}}{A}\left[b^{\dagger(1\,0)}(1) \times b^{\dagger(1\,0)}(2)\right]^{(2\,0)}_{\mathcal{L}M} \tag{5.27}$$

in the two-nucleon harmonic oscillator basis, $\{|\eta_1 l_1 j_1 m_{j_1}; \eta_2 l_2 j_2 m_{j_2}\rangle\}$. Here, the SU(3) tensor operators $b^{\dagger(1\,0)}(1)$ and $b^{\dagger(1\,0)}(2)$ act on particle 1 and particle 2, respectively. We first transform (5.27) into the SO(3) tensorial form by invoking the relation (5.23):

$$\left[b^{\dagger(1\,0)}(1) \times b^{\dagger(1\,0)}(2)\right]^{(2\,0)}_{\mathcal{L}M} = (-)^{1+\frac{\mathcal{L}}{2}} \left[b^{\dagger(1\,0)}_1(1) \times b^{\dagger(1\,0)}_1(2)\right]_{\mathcal{L}M}. \tag{5.28}$$

Since the harmonic oscillator ladder operators are spin scalars, we can consider $b^{\dagger(1\,0)}_{lm}$ to be the tensor operator with either (LS)-uncoupled or (LS)-coupled tensor characters, i.e.

$$b^{\dagger(1\,0)}_{lm_l\,00} = b^{\dagger(1\,0)}_{(l0)jm_j},$$

with $j = l = 1$ and $m_j = m_l$. Similarly, the symplectic $\mathrm{Sp}(3,\mathbb{R})$ generators can be considered as either (LS)-uncoupled or (LS)-coupled tensors with $J = \mathcal{L}$ and $M_J = M$. It is more convenient to consider temporarily $[b^{\dagger(1\,0)}_1(1) \times b^{\dagger(1\,0)}_1(2)]_{\mathcal{L}M}$ as (LS)-coupled tensors and employ straightforwardly the formula given in Ref. [148] [equation (25) on page 479] for matrix elements of a product of two irreducible (LS)-coupled tensors which depend on variables of two different single-particle spaces:

$$\langle \eta_1' l_1' j_1' m_{j_1}'; \eta_2' l_2' j_2' m_{j_2}'| \left[b^{\dagger(1\,0)}_1(1) \times b^{\dagger(1\,0)}_1(2)\right]_{\mathcal{L}M} |\eta_1 l_1 j_1 m_{j_1}; \eta_2 l_2 j_2 m_{j_2}\rangle =$$
$$\frac{\langle \eta_1' l_1' j_1' \| b^{\dagger(1\,0)}_1 \| \eta_1 l_1 j_1\rangle \langle \eta_2' l_2' j_2' \| b^{\dagger(1\,0)}_1 \| \eta_2 l_2 j_2\rangle}{\sqrt{(2j_1'+1)(2j_2'+1)}} \sum_{\alpha,\beta=\pm1,0} C^{j_1' m_{j_1}'}_{j_1 m_{j_1} 1\alpha} C^{\mathcal{L}M}_{1\alpha 1\beta} C^{j_2' m_{j_2}'}_{j_2 m_{j_2} 1\beta} \tag{5.29}$$

In the next step, we have to transform reduced matrix elements of $b^{\dagger(1\,0)}_{j=1}$ from the (LS)-coupled into the (LS)-uncoupled scheme. Utilizing the relation given in Ref. [148] [equation (5) on page 484] we get

$$\langle n' l' j' \| b^{\dagger(1\,0)}_{j=1} \| n l j\rangle = (-)^{j+l'+\frac{1}{2}+1}\sqrt{2j+1}\sqrt{2j'+1} \left\{ \begin{array}{ccc} l & \frac{1}{2} & j \\ j' & 1 & l' \end{array} \right\} \langle n' l' \| b^{\dagger(1\,0)}_{l=1} \| n l\rangle \tag{5.30}$$

Substituting (5.30) into (5.29), we obtain the analytic formula for the two-body matrix elements of the symplectic raising operator:

$$\begin{aligned}
&\langle \eta_1' l_1' j_1' m_{j_1}'; \eta_2' l_2' j_2' m_{j_2}' | \left[b^{\dagger(1\,0)}(1) \times b^{\dagger(1\,0)}(2) \right]^{(2\,0)}_{\mathcal{L}M} | \eta_1 l_1 j_1 m_{j_1}; \eta_2 l_2 j_2 m_{j_2} \rangle = \\
&\delta_{\eta_1' \eta_1 + 1} \delta_{\eta_2' \eta_2 + 1} (-)^{\phi} \langle \eta_1' l_1' \| b_1^{\dagger(1\,0)} \| \eta_1 l_1 \rangle \langle \eta_2' l_2' \| b_1^{\dagger(1\,0)} \| \eta_2 l_2 \rangle \sqrt{2j_1 + 1} \sqrt{2j_2 + 1} \\
&\left\{ \begin{array}{ccc} l_1 & \frac{1}{2} & j_1 \\ j_1' & 1 & l_1' \end{array} \right\} \left\{ \begin{array}{ccc} l_2 & \frac{1}{2} & j_2 \\ j_2' & 1 & l_2' \end{array} \right\} \sum_{\alpha,\beta=\pm 1,0} C^{j_1' m_{j_1}'}_{j_1 m_{j_1} 1\alpha} C^{\mathcal{L}M}_{1\alpha 1\beta} C^{j_2' m_{j_2}'}_{j_2 m_{j_2} 1\beta}
\end{aligned} \tag{5.31}$$

with $\phi = j_1 + l_1' + j_2 + l_2' + \mathcal{L}/2$. The two-body matrix elements for two-protons and two-neutrons harmonic oscillator basis states are first evaluated by the formula (5.31) and subsequently properly antisymmetrized by invoking the relation (2.22).

Matrix Elements of $B^{(0\,2)}_{\mathcal{L}M}$ and $C^{(1\,1)}_{\mathcal{L}M}$

The matrix elements of the symplectic lowering operators $B^{(0\,2)}_{\mathcal{L}M}$ are readily obtained from the relations (5.26) and (5.31) upon replacing $b_1^{\dagger(1\,0)}$ with $b_1^{(0\,1)}$. Notice that the both phase factors $(-1)^{\phi}$ remain unaltered as

$$\langle (0\,1)11; (0\,1)11 \| (0\,2)1\mathcal{L} \rangle \;=\; \langle (1\,0)11; (1\,0)11 \| (2\,0)1\mathcal{L} \rangle .$$

The derivation of the analytic expressions for one- and two-body matrix elements of $C^{(1\,1)}_{\mathcal{L}M}$ generators is analogous to the derivation of formulas (5.26) and (5.31). We thus merely provide the resulting expressions. The one-body matrix elements can be calculated as:

$$\begin{aligned}
&\langle \eta_f l_f j_f m_{j_f} | \left[b^{\dagger(1\,0)} \times b^{(0\,1)} \right]^{(1\,1)}_{\mathcal{L}M} | \eta_i l_i j_i m_{j_i} \rangle = \delta_{\eta_f \eta_i} (-1)^{\phi} \sqrt{2\mathcal{L} + 1} \sqrt{2j_i + 1} C^{j_f m_{j_f}}_{j_i m_{j_i} \mathcal{L}M} \\
&\left\{ \begin{array}{ccc} l_i & \frac{1}{2} & j_i \\ j_f & \mathcal{L} & l_f \end{array} \right\} \sum_{\eta_t l_t} \left\{ \begin{array}{ccc} 1 & 1 & \mathcal{L} \\ l_i & l_f & l_t \end{array} \right\} \langle \eta_f\, l_f \| b_1^{\dagger(1\,0)} \| \eta_t\, l_t \rangle \langle \eta_t\, l_t \| b_1^{(0\,1)} \| \eta_i\, l_i \rangle ,
\end{aligned}$$

with $\phi = \frac{1}{2} + j_i + l_i + \mathcal{L}$. The two-body matrix elements are given as:

$$\begin{aligned}
&\langle \eta_1' l_1' j_1' m_{j_1}'; \eta_2' l_2' j_2' m_{j_2}' | \left[b^{\dagger(1\,0)}(1) \times b^{(0\,1)}(2) \right]^{(1\,1)}_{\mathcal{L}M} | \eta_1 l_1 j_1 m_{j_1}; \eta_2 l_2 j_2 m_{j_2} \rangle = \\
&\delta_{\eta_1' \eta_1 - 1} \delta_{\eta_2' \eta_2 + 1} (-)^{\phi} \langle \eta_1' l_1' \| b_1^{\dagger(1\,0)} \| \eta_1 l_1 \rangle \langle \eta_2' l_2' \| b_1^{(0\,1)} \| \eta_2 l_2 \rangle \sqrt{2j_1 + 1} \sqrt{2j_2 + 1} \\
&\left\{ \begin{array}{ccc} l_1 & \frac{1}{2} & j_1 \\ j_1' & 1 & l_1' \end{array} \right\} \left\{ \begin{array}{ccc} l_2 & \frac{1}{2} & j_2 \\ j_2' & 1 & l_2' \end{array} \right\} \sum_{\alpha,\beta=\pm 1,0} C^{j_1' m_{j_1}'}_{j_1 m_{j_1} 1\alpha} C^{\mathcal{L}M}_{1\alpha 1\beta} C^{j_2' m_{j_2}'}_{j_2 m_{j_2} 1\beta}
\end{aligned} \tag{5.32}$$

with $\phi = j_1 + l_1' + j_2 + l_2' + \mathcal{L}$.

Reduced Matrix Elements of Harmonic Oscillator Ladder Operators

The reduced matrix elements of the harmonic oscillator ladder operators, $b_1^{\dagger(1\,0)}$ and $b_1^{(0\,1)}$, with the phase convention that the radial part of the harmonic oscillator wave

functions are positive at infinity, have the form,

$$\langle \eta_f l_f \| b_1^{\dagger(1\,0)} \| \eta_i l_i \rangle = \Big(-\sqrt{l_i}\sqrt{\eta_i - l_i + 2}\ \delta_{l_f,l_i-1} + \sqrt{l_i+1}\sqrt{\eta_i + l_i + 3}\ \delta_{l_f,l_i+1} \Big) \delta_{\eta_f,\eta_i+1} \tag{5.33}$$

$$\langle \eta_f l_f \| b_1^{(0\,1)} \| \eta_i l_i \rangle = \Big(-\sqrt{l_i}\sqrt{\eta_i + l_i + 1}\ \delta_{l_f,l_i-1} + \sqrt{l_i+1}\sqrt{\eta_i - l_i}\ \delta_{l_f,l_i+1} \Big) \delta_{\eta_f,\eta_i-1}. \tag{5.34}$$

It is important to emphasize that special care must be taken to ensure that the same phase convention is used throughout all calculations. For instance, the computer code implementing the $\mathrm{Sp}(3,\mathbb{R})$ basis construction formula (5.17) relies on the SU(3) coupling-recoupling package [150]. This package uses the phase convention with the radial part of the harmonic oscillator wave functions positive at infinity. In contrast, NCSM wave functions obtained via the MFD code [17], are given with the radial part positive at origin. As a result, NCSM wave functions have to be transformed into the "positive at infinity" phase convention by multiplying each m-scheme state, $|\eta_1 l_1 j_1 m_{j_1}, \ldots, \eta_A l_A j_A m_{j_A}\rangle$, by $(-1)^\phi$, where $\phi = \frac{1}{2}\sum_{i=1}^{A}(\eta_i - l_i)$.

5.2.4 Tests

Each symplectic $\mathrm{Sp}(3,\mathbb{R})$-symmetry adapted state produced by the computer implementation of the symplectic construction formula (5.17) is tested thoroughly in order to verify its symmetry properties with respect to the subgroups of the shell-model symplectic group chain. The orbital angular momentum L, the spin S_σ, the total angular momentum J, and $(\lambda_\omega\, \mu_\omega)$ SU(3) labels, are tested via the Casimir invariants of SO(3), SU(2), and SU(3) subgroups of $\mathrm{Sp}(3,\mathbb{R})$. Each symplectic state, $|\sigma n \rho \omega \kappa (L S_\sigma); J M_J\rangle$, is an eigenstate of these Casimir operators:

$$\begin{aligned}
\hat{L}^2\,|\sigma n \rho \omega \kappa (L S_\sigma); J M_J\rangle &= L(L+1)\,|\sigma n \rho \omega \kappa (L S_\sigma); J M_J\rangle \\
\hat{S}^2\,|\sigma n \rho \omega \kappa (L S_\sigma); J M_J\rangle &= S_\sigma(S_\sigma+1)\,|\sigma n \rho \omega \kappa (L S_\sigma); J M_J\rangle \\
\hat{J}^2\,|\sigma n \rho \omega \kappa (L S_\sigma); J M_J\rangle &= J(J+1)\,|\sigma n \rho \omega \kappa (L S_\sigma); J M_J\rangle \\
\hat{C}_2\,|\sigma n \rho \omega \kappa (L S_\sigma); J M_J\rangle &= C_2(\lambda\,\mu)\,|\sigma n \rho \omega \kappa (L S_\sigma); J M_J\rangle\,.
\end{aligned}$$

The SU(3) second order Casimir invariant operator can be expressed in terms of the symplectic generators $C^{(1\,1)}_{\mathcal{L}M}$ as

$$\hat{C}_2 = \sqrt{2}\left[C^{(1\,1)} \times C^{(1\,1)}\right]^{(0\,0)}_{0\,0}. \tag{5.35}$$

And finally, we have to verify the translational invariance of the symplectic states. This means that the total number of the c.m. excitation quanta must be zero:

$$\hat{N}^{\mathrm{cm}}\,|\sigma n \rho \omega \kappa (L S_\sigma); J M_J\rangle = 0 \tag{5.36}$$

Chapter 6

Evidence for Symplectic Symmetry in Light Nuclei

In this chapter, we examine role of the symplectic $\mathrm{Sp}(3,\mathbb{R})$ symmetry in the ground 0^+_{gs} and the first excited 0^+_2 states of ^{16}O and the ground-state rotational band of ^{12}C. This is achieved through the projection of realistic eigenstates determined in the framework of the *ab initio* NCSM onto $\mathrm{Sp}(3,\mathbb{R})$-symmetric model space.

First we briefly discuss the structure of the lowest-lying states in ^{12}C and ^{16}O as determined by previous theoretical investigations. Next we investigate the role of $\mathrm{Sp}(3,\mathbb{R})$ irreps built over 0p-0h symplectic bandheads. The analysis of the results reveals that the NCSM eigenstates project at approximately the 80% level onto only few 0p-0h spurious center-of-mass free symplectic irreps with a clear dominance of the leading $\mathrm{Sp}(3,\mathbb{R})$ irreps [23]. Comparison of $\mathrm{Sp}(3,\mathbb{R})$ symmetry-adapted and α-cluster wave functions indicates that the restriction of the symplectic model subspace to the dominant 0p-0h irreps is not sufficient to describe highly deformed states with a pronounced α-cluster structure [138, 151, 137, 152]. We therefore augmented the symplectic model space with symplectic irreps built over all $2\hbar\Omega$ 2p-2h and the most deformed $4\hbar\Omega$ 4p-4h $\mathrm{Sp}(3,\mathbb{R})$ bandheads and analyzed their role in a description of the calculated NCSM eigenstates [24]. Our study reveals the important role of the most deformed $2\hbar\Omega$ 2p-2h symplectic irreps for the description of the NCSM eigenstates. The size of the symplectic basis is a mere fraction of the full model space dimension, and hence our proof-of-principle study suggests that a symplectic extension of the NCSM is a viable solution to the m-scheme basis size explosion problem.

6.1 Structure of the Lowest-Lying States of ^{12}C and ^{16}O Nuclei

The investigations of ^{12}C and ^{16}O nuclei structures are relevant for a wide range of physical processes. The latter include parity violating electron scattering from light nuclei [81, 82, 83, 84] where targets like ^{12}C are of particular interest. Accurate microscopic wave functions obtained through the *ab initio* NCSM can also provide

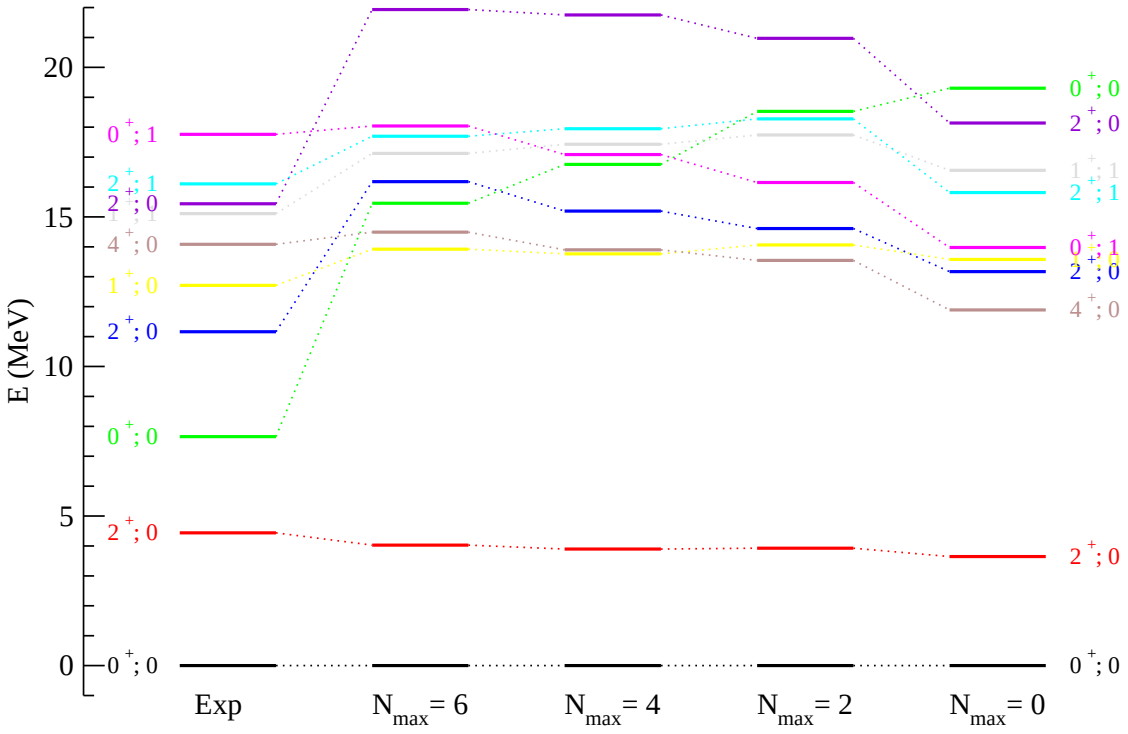

Figure 6.1: Experimental and calculated low-lying spectra of ^{12}C for increasing size of the model space. The NCSM results were obtained using the effective interactions derived from the JISP16 nucleon-nucleon potential with $\hbar\Omega = 15$ MeV.

valuable input for neutrino studies as ^{12}C is an ingredient of liquid scintillator detectors [95] and ^{16}O is the main component of water Čerenkov detectors. Light nuclei with equal numbers of protons and neutrons ($N = Z$) and total particle numbers that are multiples of four ($4n$) display a complex pattern in their low-lying energy spectra with certain states continuing to remain a challenge for *ab initio* techniques. An important example of such a configuration is the first excited 0^+ state in ^{12}C, the Hoyle state, which is essential for a key reaction of stellar nucleosynthesis: the production of ^{12}C nucleus through the triple-α reaction mechanism [153, 154]. Another is the highly deformed first excited 0^+_2 state of ^{16}O.

^{12}C Nucleus

The *ab initio* NCSM calculations of ^{12}C nucleus with the CD-Bonn and JISP16 interactions in the $4\hbar\Omega$ [9, 15] and the $6\hbar\Omega$ [16] model spaces have achieved reasonable convergence of the states dominated by $0\hbar\Omega$ configurations, e.g. the $J=0^+_{gs}$ and the lowest $J=2^+(\equiv 2^+_1)$ and $J=4^+(\equiv 4^+_1)$ states of the ground-state rotational band, as seen in Fig. 6.1. In addition, calculated binding energies and other observables such as ground-state proton root-mean-square (rms) radii and the 2^+_1 quadrupole moment all lie reasonably close to the measured values (see Table 6.1). The electromagnetic

Table 6.1: Comparison of the experimental data of ^{12}C with the results obtained by the NCSM calculation in the $N_{\max} = 6$ model space using the effective interaction derived from the JISP16 with $\hbar\Omega$= 12.5 MeV, and $\hbar\Omega$= 15 MeV. Non-converged states are labeled "N/C".

	Exp	$\hbar\Omega = 12.5$	$\hbar\Omega = 15$
$\lvert E_{\rm gs}\rvert$ [MeV]	92.162	88.211	90.430
r_p [fm]	2.35(2)	2.334	2.183
Q_{2^+} [e fm^2]	+6(3)	5.213	4.478
$E_{\rm x}(0^+0)$ [MeV]	0.0	0.0	0.0
$E_{\rm x}(2^+0)$ [MeV]	4.439	3.790	4.029
$E_{\rm x}(0^+0)$ [MeV]	7.654	N/C	N/C
$E_{\rm x}(2^+0)$ [MeV]	11.160	N/C	N/C
$E_{\rm x}(1^+0)$ [MeV]	12.710	13.807	13.921
$E_{\rm x}(4^+0)$ [MeV]	14.083	13.467	14.490
$E_{\rm x}(1^+1)$ [MeV]	15.110	15.927	17.124
$E_{\rm x}(2^+1)$ [MeV]	16.106	17.893	19.947
B(E2;$2^+0 \rightarrow 0^+0$)	7.59(42)	6.213	4.631
B(M1;$1^+0 \rightarrow 0^+0$)	0.0145(21)	0.005	0.007
B(M1;$1^+1 \rightarrow 0^+0$)	0.951(20)	0.385	0.588
B(E2;$2^+1 \rightarrow 0^+0$)	0.65(13)	0.364	0.393

transition strengths, B(E2;$2^+_1 0 \rightarrow 0^+_{gs} 0$), B(E2;$2^+_1 1 \rightarrow 0^+_{gs} 0$) and B(M1;$1^+_1 1 \rightarrow 0^+_{gs} 0$), are still underestimated, yielding just over 60% of the corresponding experimental strengths. Note that these physical observables were obtained using bare operators. The additional contributions are expected to arise from excluded, high-$\hbar\Omega$ basis states, which produce more complete formation of the exponential tails of the wave functions to which these observables are sensitive.

In contrast, the low-lying α-clustering states, such as the Hoyle state, are not reproduced by the NCSM. The structure of the Hoyle state is crucial for accurate prediction of the triple-α reaction rate [153]. The α-cluster models and the fermionic molecular dynamics model have been more successful in reproducing the properties of this state [155, 156, 157, 158, 130]. However, they have not produced results accurate enough to yield the triple-α reaction rate with sufficient precision [159], and thus the structure of the Hoyle state still represents an ultimate challenge for nuclear structure physics.

The $0\hbar\Omega$ configurations of ^{12}C have four protons and four neutrons distributed over the valence p-shell. Such configurations of valence nucleons give rise to the leading $(0\,4)$ SU(3) irrep describing an oblate deformed nuclear shape. It is the deformation of the nucleus from its spherical shape that induces collective rotations [160]. The Elliott SU(3) model of nuclear rotations describes the states of the ground-state rotational band of ^{12}C solely in terms of the leading $(0\,4)$ SU(3) irrep basis states, and studies performed within the framework of the symplectic shell model reflect

this assumption. Symplectic algebraic approaches with the model space restricted to the single $\mathrm{Sp}(3,\mathbb{R})$ irrep built over the leading $(0\,4)$ bandhead have achieved a good reproduction of the ground-state rotational band energies and B(E2) values using phenomenological interactions [161] or truncated symplectic basis with simplistic (semi-)microscopic interactions [162, 163, 164].

^{16}O Nucleus

In contrast to ^{12}C, where several calculated results are found to reproduce the experimental data quite well, the $6\hbar\Omega$ NCSM calculations for ^{16}O with the JISP16 and CD-Bonn interactions only yield reasonable results for the ground state binding energy [16, 17]. The structure of the ground state of ^{16}O was theoretically explained several decades ago by the independent particle model [165] as being formed by the closed-shell configuration. While this might first appear to be a rather crude approximation, it is confirmed by the NCSM. The closed-shell Slater determinant contribution to the ground state ranges from 40% for $\hbar\Omega = 12$ MeV up to 55% for $\hbar\Omega = 16$ MeV (cf. see Fig. 6.8).

Unlike the ground state, the excited 0^+ states of the double-magic nuclei are usually strongly deformed [166] which can be attributed to a superposition of low-lying, strongly favored multiple-particle-multiple-hole configurations [167, 168, 169]. Perhaps the simplest example is the highly deformed first excited 0^+_2 state of ^{16}O where 4p-4h configurations were recognized early on [168] to be prominent. Later theoretical investigations suggested a dominant 4p-4h character, albeit with some admixture of 0p-0h and 2p-2h configurations [170, 171, 172, 173, 174, 175, 176]. Very large model spaces, well beyond the current computational limits, are needed for an accurate description of low-lying deformed 0^+ states. The current *ab initio* methods such as the $6\hbar\Omega$ NCSM [16, 17] or coupled cluster calculations [12] fail to reproduce the observed excitation energies of the low-lying exited 0^+ states of ^{16}O.

At the same time, it is also well established that the first and the second excited 0^+ states in ^{16}O have a pronounced α-cluster structure [133, 132]. Both states are well described by the microscopic $^{12}\mathrm{C}{+}\alpha$ cluster model [134, 135] whose wave functions were found to overlap at a significant level with the basis states of the leading $4\hbar\Omega$ 4p-4h $[(\lambda_\sigma\,\mu_\sigma) = (8\,4)]$ and $2\hbar\Omega$ 2p-2h $[(\lambda_\sigma\,\mu_\sigma) = (4\,2)]$ $\mathrm{Sp}(3,\mathbb{R})$ irreps [138, 151, 137]. Recently, the coupled-SU(3) algebraic model [177] calculations confirm the significant role of these two leading symplectic irreps [178].

6.2 Dominant Role of 0p-0h Symplectic Irreps

In this section, the role of 0p-0h symplectic $\mathrm{Sp}(3,\mathbb{R})$ irreps in the lowest lying states of ^{16}O and the ground-state rotational band of ^{12}C is considered [23]. The lowest-lying eigenstates of ^{12}C and ^{16}O nuclei were calculated using the *ab initio* NCSM as implemented through the many fermion dynamics (MFD) code [38, 39] with an effective interaction derived from the realistic JISP16 nucleon-nucleon potential [2] for different $\hbar\Omega$ oscillator strengths, and also using the bare JISP16 interaction;

Table 6.2: 0p-0h Sp$(3,\mathbb{R})$ irreps in ^{12}C, $N_\sigma = 24.5$.

$(\lambda_\pi\ \mu_\pi)S_\pi$	$\otimes$	$(\lambda_\nu\ \mu_\nu)S_\nu$	$\rightarrow$	$(\lambda_\sigma\ \mu_\sigma)$	S
$(0\ 2)S_\pi = 0$		$(0\ 2)S_\nu = 0$		$(0\ 4)\ (1\ 2)\ (2\ 0)$	$S_\sigma = 0$
$(0\ 2)S_\pi = 0$		$(1\ 0)S_\nu = 1$		$(0\ 1)\ (1\ 2)$	$S_\sigma = 1$
$(1\ 0)S_\pi = 1$		$(0\ 2)S_\nu = 0$		$(0\ 1)\ (1\ 2)$	$S_\sigma = 1$
$(1\ 0)S_\pi = 1$		$(1\ 0)S_\nu = 1$		$(0\ 1)\ (2\ 0)$	$S_\sigma = 0,\ 1,\ 2$

that is, without taking into account effects of the excluded configurations. In our analysis, we are particularly interested in the $J = 0^+_{gs}$ and the lowest $J = 2^+ (\equiv 2^+_1)$ and $J = 4^+ (\equiv 4^+_1)$ states of the ground-state rotational band of ^{12}C, and also the ground state of ^{16}O, which all appear to be relatively well converged in the $N_{max} = 6$ model space.

6.2.1 Ground-State Rotational Band in ^{12}C Nucleus

For ^{12}C there are 13 distinct SU(3)$\otimes$SU$_S$(2) irreps at the $0\hbar\Omega$ space, listed in Table 6.2, which form the symplectic bandheads with $N_\sigma = 24.5$. For each bandhead we generated Sp$(3,\mathbb{R})$ irrep basis states with the total angular momentum $J = 0, 2$ and 4 up to $6\hbar\Omega$ space and expanded these symplectic states in the m-scheme basis utilizing methods and prescriptions derived in the previous chapter. We then projected the NCSM eigenstates of the ground-state rotational band onto the symplectic model space.

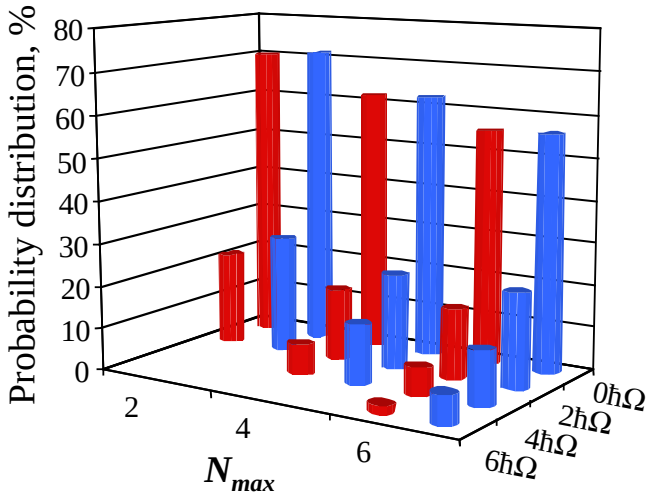

Figure 6.2: NCSM (blue, right) and 0p-0h Sp$(3,\mathbb{R})$ (red, left) probability distribution over $0\hbar\Omega$ to $N_{\max}\ \hbar\Omega$ subspaces for the 0^+_{gs} of ^{12}C for different model spaces, $N_{\max}$, with $\hbar\Omega = 15$MeV.

Table 6.3: Probability distribution of NCSM eigenstates for ^{12}C across the dominant 3 0p-0h Sp$(3,\mathbb{R})$ irreps, $\hbar\Omega$=12 MeV.

		$0\hbar\Omega$	$2\hbar\Omega$	$4\hbar\Omega$	$6\hbar\Omega$	Total
		J=0				
	$(0\,4)S_\sigma = 0$	41.39	19.66	8.73	3.14	72.92
Sp$(3,\mathbb{R})$	$(1\,2)S_\sigma = 1$	2.24	1.49	0.80	0.41	4.94
	$(1\,2)S_\sigma = 1$	2.19	1.46	0.78	0.41	4.84
	Total	45.82	22.61	10.31	3.96	82.70
NCSM		45.90	27.41	15.89	9.03	98.23
		J=2				
	$(0\,4)S_\sigma = 0$	41.20	19.34	8.44	3.06	72.04
Sp$(3,\mathbb{R})$	$(1\,2)S_\sigma = 1$	2.50	1.51	0.77	0.38	5.16
	$(1\,2)S_\sigma = 1$	2.42	1.47	0.75	0.37	5.01
	Total	46.12	22.32	9.96	3.81	82.21
NCSM		46.19	27.10	15.76	9.25	98.30
		J=4				
	$(0\,4)S_\sigma = 0$	44.21	19.23	8.01	2.91	74.36
Sp$(3,\mathbb{R})$	$(1\,2)S_\sigma = 1$	1.69	0.90	0.44	0.21	3.24
	$(1\,2)S_\sigma = 1$	1.68	0.89	0.43	0.21	3.21
	Total	47.59	21.02	8.88	3.33	80.81
NCSM		47.59	25.87	15.24	9.46	98.16

Overlaps

Analysis of overlaps of the symplectic states with the NCSM eigenstates for the 0^+_{gs} and the lowest 2^+ and 4^+ states reveals non-negligible overlaps for only 3 out of the 13 0p-0h Sp$(3,\mathbb{R})$ ($N_\sigma = 24.5$) irreps. Specifically, the leading (most deformed) representation $(\lambda_\sigma\,\mu_\sigma) = (0\,4)$ carrying spin $S_\sigma = 0$ together with the two irreps of identical labels $(\lambda_\sigma\,\mu_\sigma) = (1\,2)$ and spin $S_\sigma = 1$ with different bandhead constructions for protons and neutrons as indicated in Table 6.2. Had we adopted the isospin formalism, we would have obtained two $(1\,2)$ $S_\sigma = 1$ irreps, one with isospin $T = 0$ and the other with $T = 1$. In this case, only one of the two $S_\sigma = 1$ $(1\,2)$ irreps is expected to significantly contribute ($T = 0$), while the other state of definite isospin may only slightly mix because of the presence of the Coulomb interaction.

The overlaps of the most dominant symplectic states with the NCSM eigenstates for the 0^+_{gs}, 2^+_1 and 4^+_1 states in the 0, 2, 4 and $6\hbar\Omega$ subspaces are given for $\hbar\Omega$=12 MeV (Table 6.3) and $\hbar\Omega$=15 MeV (Table 6.4). In order to speed up the calculations, we retained only the largest amplitudes of the NCSM states, those sufficient to account for at least 98% of the norm which is quoted also in the tables. The results show that typically more then 80% of the NCSM eigenstates fall within a subspace spanned by the 3 leading 0p-0h Sp$(3,\mathbb{R})$ irreps. The most deformed irrep $(0\,4)S_\sigma = 0$ is clearly dominant. Its overlap with all three NCSM eigenstates

Table 6.4: Probability distribution of NCSM eigenstates for ^{12}C across the dominant 3 0p-0h Sp$(3,\mathbb{R})$ irreps, $\hbar\Omega$=15 MeV.

		$0\hbar\Omega$	$2\hbar\Omega$	$4\hbar\Omega$	$6\hbar\Omega$	Total
		J=0				
Sp$(3,\mathbb{R})$	$(0\,4)S_\sigma = 0$	46.26	12.58	4.76	1.24	64.84
	$(1\,2)S_\sigma = 1$	4.80	2.02	0.92	0.38	8.12
	$(1\,2)S_\sigma = 1$	4.72	1.99	0.91	0.37	7.99
	Total	55.78	16.59	6.59	1.99	80.95
NCSM		56.18	22.40	12.81	7.00	98.38
		J=2				
Sp$(3,\mathbb{R})$	$(0\,4)S_\sigma = 0$	46.80	12.41	4.55	1.19	64.95
	$(1\,2)S_\sigma = 1$	4.84	1.77	0.78	0.30	7.69
	$(1\,2)S_\sigma = 1$	4.69	1.72	0.76	0.30	7.47
	Total	56.33	15.90	6.09	1.79	80.11
NCSM		56.63	21.79	12.73	7.28	98.43
		J=4				
Sp$(3,\mathbb{R})$	$(0\,4)S_\sigma = 0$	51.45	12.11	4.18	1.04	68.78
	$(1\,2)S_\sigma = 1$	3.04	0.95	0.40	0.15	4.54
	$(1\,2)S_\sigma = 1$	3.01	0.94	0.39	0.15	4.49
	Total	57.50	14.00	4.97	1.34	77.81
NCSM		57.64	20.34	12.59	7.66	98.23

ranges from about 65% for $\hbar\Omega$ = 18 MeV to 75% for $\hbar\Omega$=11 MeV. This reveals the significance of the $(0\,4)S_\sigma = 0$ irrep, which in the framework of the symplectic shell model gives rise to a prominent $J = 0, 2$ and 4 rotational structure and hence suitable for a microscopic description of the ground state rotational band in ^{12}C [161]. Clearly, the restriction of the early symplectic shell model calculations upon the single $(0\,4)$ leading Sp$(3,\mathbb{R})$ irrep turns to be a reasonable approximation. The outcome also demonstrates that the dominance of the three symplectic irreps is consistent throughout the band. The mixing of the two $(1\,2)S_\sigma = 1$ irreps is comparatively much smaller for all the three 0^+_{gs}, 2^+_1 and 4^+_1 states, yet it may affect electric quadrupole transitions from higher-lying $J = 0, 2$ and 4 states toward the ground state band.

Overall, the results show a highly coherent mixing of the three most important Sp$(3,\mathbb{R})$ irreps for all values of $\hbar\Omega$ in spite of Sp$(3,\mathbb{R})$ symmetry breaking. The effective JISP16 interaction apparently mixes in a quite regular way the Sp$(3,\mathbb{R})$ irreps which is referred to as adiabatic coherent mixing of representations [118].

Examination of the role of the model space truncation specified by $N_{\max}$ reveals that the general features of all outcomes are retained as the space is expanded from $2\hbar\Omega$ to $6\hbar\Omega$ (see, e.g., Fig. 6.2 for the 0^+_{gs}). This includes a strong dominance of the most deformed $(0\,4)$ $S_\sigma = 0$ irrep as well as the continued importance of the next

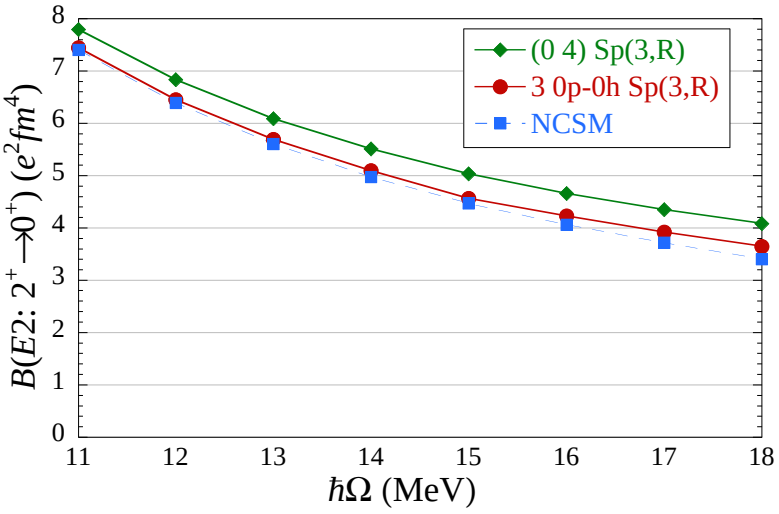

Figure 6.3: NCSM and Sp$(3,\mathbb{R})$ $B(E2:2_1^+ \rightarrow 0_{gs}^+)$ transition rate in e^2fm^4 for ^{12}C as a function of the $\hbar\Omega$ oscillator strength in MeV, N_{max}=6.

most important $(1\,2)$ $S_\sigma = 1$ $0\hbar\Omega$ irreps. In particular, the same three Sp$(3,\mathbb{R})$ irreps dominate for all $N_{\max}$ values with the large overlaps of the NCSM eigenstates with the leading symplectic irreps preserved, albeit distributed outward across higher $\hbar\Omega$ excitations as the number of active shells increases.

Electric Quadrupole Transition Rates

The 0_{gs}^+ and 2_1^+ states, constructed in terms of the three Sp$(3,\mathbb{R})$ irreps with probability amplitudes defined by the overlaps with the ^{12}C NCSM wave functions, were also used to determine B(E2) transition rates. These quantities are typically less accurately reproduced by *ab initio* methods with realistic interactions. The Sp$(3,\mathbb{R})$ $B(E2:2_1^+ \rightarrow 0_{gs}^+)$ values clearly reproduce the NCSM results, namely they slightly increase from 101% to 107% of the corresponding NCSM numbers with increasing $\hbar\Omega$ (Fig. 6.3). Both theoretical estimates for $\hbar\Omega = 11$ MeV agree, at the 2% level, with the measured value of 7.59 e^2fm^4, while they underestimate the experiment for larger oscillator strengths where highly deformed configurations are energetically less favorable. In addition, if only the leading most deformed $(0\ 4)$ Sp$(3,\mathbb{R})$ irrep is considered, that is without the mixing due to both $(1\,2)$ $S_\sigma = 1$ irreps, the $B(E2:2_1^+ \rightarrow 0_{gs}^+)$ values increase only by $5-12\%$. In this regard, note that in addition to its large projection onto the realistic eigenstates, the leading $(0\,4)$ Sp$(3,\mathbb{R})$ irrep is sufficient for a good reproduction of the NCSM B(E2) estimate.

6.2.2 Ground State in ^{16}O Nucleus

A closed-shell nucleus has only one possible 0p-0h Sp$(3,\mathbb{R})$ irrep with a symplectic bandhead coinciding with the single closed-shell Slater determinant. In case of ^{16}O the single Sp$(3,\mathbb{R})$ irrep has $N_\sigma = 34.5$, $(\lambda_\sigma\,\mu_\sigma) = (0\,0)$, and $S_\sigma = 0$ quantum labels.

Table 6.5: Probability distribution of the NCSM ground state in ^{16}O obtained with (a) $\hbar\Omega$=12 MeV and (b) $\hbar\Omega$=15 MeV, respectively, across the 0p-0h Sp$(3,\mathbb{R})$ irrep.

(a)		$\hbar\Omega$=12 Mev				
		$0\hbar\Omega$	$2\hbar\Omega$	$4\hbar\Omega$	$6\hbar\Omega$	Total
Sp$(3,\mathbb{R})$	$(0\,0)S_\sigma = 0$	38.73	23.92	11.89	5.28	79.82
NCSM		38.73	28.78	18.80	12.66	98.97

(b)		$\hbar\Omega$=15 Mev				
		$0\hbar\Omega$	$2\hbar\Omega$	$4\hbar\Omega$	$6\hbar\Omega$	Total
Sp$(3,\mathbb{R})$	$(0\,0)S_\sigma = 0$	50.53	15.87	6.32	2.30	75.02
NCSM		50.53	22.58	14.91	10.81	98.83

As in the ^{12}C case, we generated translationally invariant basis states for this irrep according to formula (5.17) up to $6\hbar\Omega$ subspace.

Consistent with the outcome for ^{12}C, the projection of the ground state onto the symplectic basis reveals a large Sp$(3,\mathbb{R})$-symmetric content in the ground state wave function (Table 6.5). Here, we again retained only the largest amplitudes of the NCSM states, those sufficient to account for at least 98% of the norm. The results show that 75%-80% of the NCSM ground state fall within a subspace spanned by the leading 0p-0h Sp$(3,\mathbb{R})$ irrep $(0\,0)S$=0 and this overlap is increasing with decreasing value of $\hbar\Omega$.

6.2.3 Relevance of Elliott SU(3) Model

As one varies the oscillator strength $\hbar\Omega$ (Fig. 6.4), the overall overlaps increase towards smaller $\hbar\Omega$ HO frequencies and, for example, for the 0^+_{gs} it is 85% for ^{12}C and 80% for ^{16}O in the $N_{max} = 6$ and $\hbar\Omega = 11$MeV case. As expected, Fig. 6.4 also confirms that with increasing harmonic oscillator strength the high $\hbar\Omega$ excitations contribute less, as the lower-lying shell configurations become energetically more favorable.

While the focus here has been on demonstrating the existence of Sp$(3,\mathbb{R})$ symmetry in NCSM results for ^{12}C and ^{16}O, and therefore a possible path forward for extending the NCSM to a Sp-NCSM scheme, the results can also be interpreted as a further strong confirmation of the Elliott SU(3) model since the projection of the NCSM states onto the $0\hbar\Omega$ space [Fig. 6.4, blue (right) bars] is a projection of the NCSM results onto the wave functions of the SU(3) model. For example, for ^{12}C the $0\hbar\Omega$ SU(3) symmetry ranges from just over 40% of the NCSM 0^+_{gs} for $\hbar\Omega = 11$ MeV to nearly 65% for $\hbar\Omega$ =18 MeV [Fig. 6.4, blue (left) bars] with 80%-90% of this symmetry governed by the leading $(0\,4)$ irrep. These numbers are consistent with what has been shown to be a dominance of the leading SU(3) symmetry for SU(3)-based shell-model studies with realistic interactions in $0\hbar\Omega$ model spaces. It

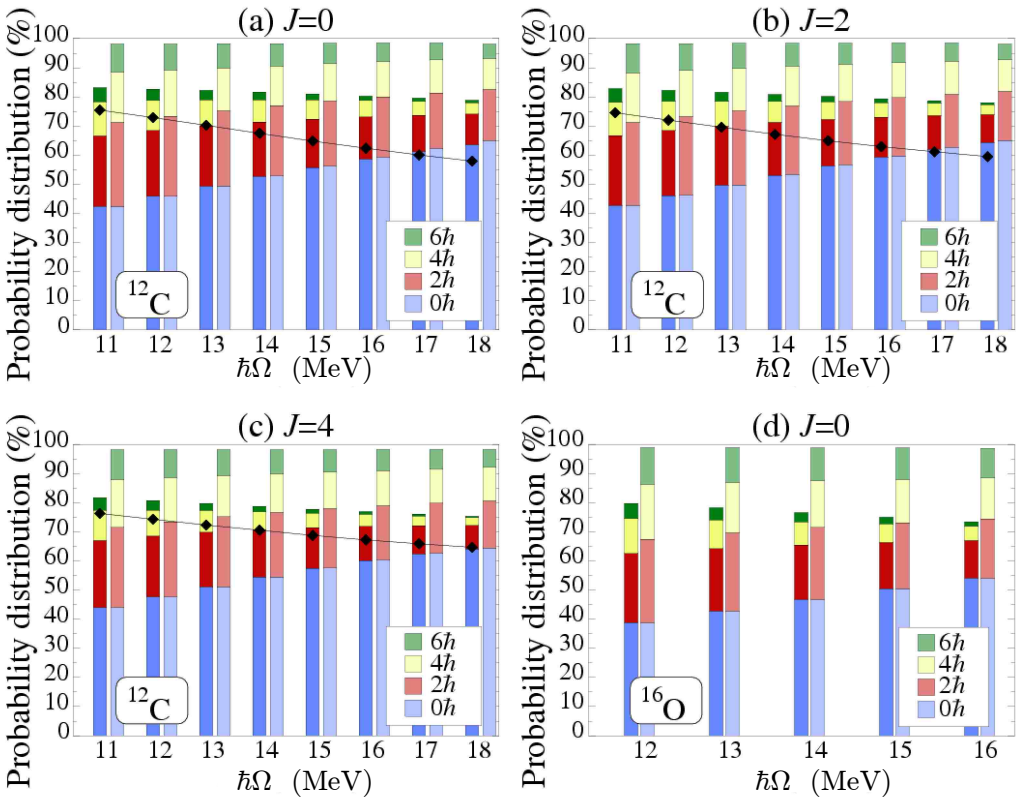

Figure 6.4: Probability distribution for the (a) 0^+_{gs}, (b) 2^+_1 and (c) 4^+_1 states in ^{12}C and (d) 0^+_{gs} in ^{16}O over $0\hbar\Omega$ (blue, lowest) to $6\hbar\Omega$ (green, highest) subspaces for the most dominant 0p-0h $\mathrm{Sp}(3,\mathbb{R})$ irreps case (left) and NCSM (right) together with the (0 4) irrep contribution (black diamonds) in ^{12}C as a function of the $\hbar\Omega$ oscillator strength in MeV for $N_{max} = 6$.

seems the simplest of the Elliott collective states can be regarded as a good first-order approximation in the presence of realistic interactions, whether the latter is restricted to a $0\hbar\Omega$ model space or the richer multi-$\hbar\Omega$ NCSM model spaces.

6.3 Multiple-Particle-Multiple-Hole Symplectic Irreps

The methods described in Section 5.1 were used to construct all translationally invariant $2\hbar\Omega$ 2p-2h $\mathrm{Sp}(3,\mathbb{R})$ bandheads and the most deformed $4\hbar\Omega$ 4p-4h symplectic bandheads in ^{12}C and ^{16}O. The total number of the $2\hbar\Omega$ 2p-2h symplectic bandheads is around 10^3 in the case of ^{12}C, and approximately half of this amount for ^{16}O. However, similarly to the case of 0p-0h symplectic bandheads, only a relatively small fraction of the $2\hbar\Omega$ 2p-2h symplectic bandheads project at the non-negligible level onto the low-lying NCSM wave functions. Specifically, the projection yields

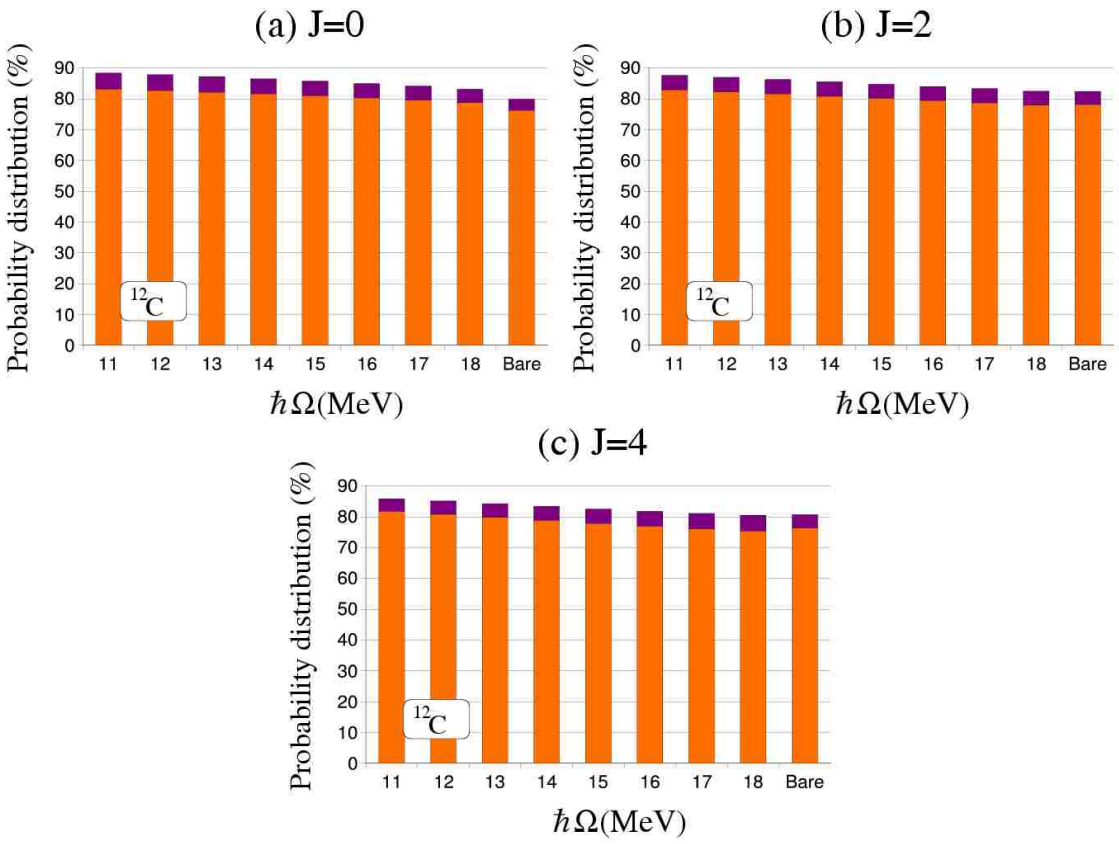

Figure 6.5: Projection of NCSM wave functions for ^{12}C onto the dominant 0p-0h (orange) and $2\hbar\Omega$ 2p-2h (purple) Sp$(3,\mathbb{R})$ irreps for: a) 0^+_{gs}, (b) 2^+_1, and c) 4^+_1 as a function of the $\hbar\Omega$ oscillator strength. Results are also shown for the bare interaction (column on the far right of each figure).

20 most dominant $2\hbar\Omega$ 2p-2h symplectic bandheads. These bandheads are then utilized to generate the corresponding Sp$(3,\mathbb{R})$ translationally invariant irreps up to $N_{\max} = 6$ ($6\hbar\Omega$ model space). The symplectic model space, in addition to the 0p-0h Sp$(3,\mathbb{R})$ irreps, now includes dominant 2p-2h symplectic irreps. The total dimension of the symplectic model space remains a small fraction of the full model space.

6.3.1 Ground-State Rotational Band in ^{12}C Nucleus

In the case of ^{12}C, the expansion of the 0p-0h symplectic model subspace to include the most important $2\hbar\Omega$ 2p-2h Sp$(3,\mathbb{R})$ irreps improves the overlaps between the NCSM eigenstates for the $J = 0, 2$, and 4 states in the ground state rotational band and the Sp$(3,\mathbb{R})$-symmetric basis by about 5% (Fig. 6.5). (Note that for these states the $4\hbar\Omega$ 4p-4h symplectic irreps are found to be negligible.) Overall, approximately 85% of the NCSM eigenstates fall within a subspace spanned by the most significant three 0p-0h and twenty $2\hbar\Omega$ 2p-2h Sp$(3,\mathbb{R})$ irreps. As one varies the $\hbar\Omega$ oscillator

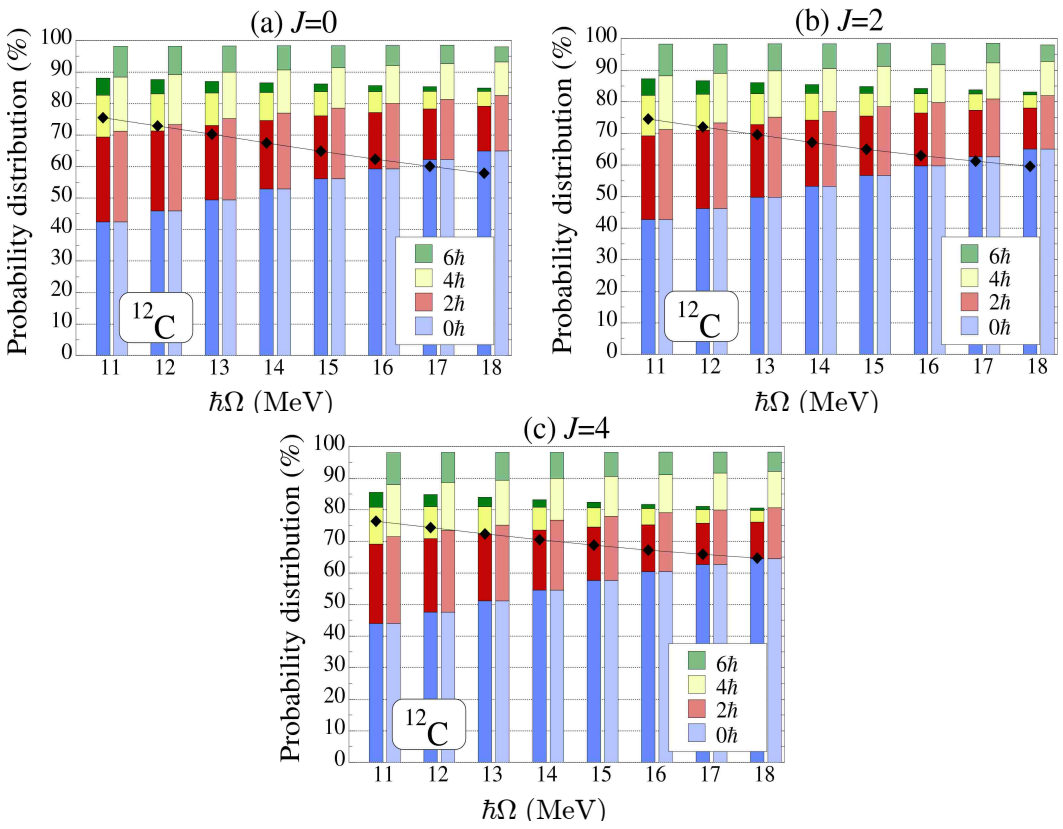

Figure 6.6: Probability distribution for the (a) 0^+_{gs}, (b) 2^+_1 and (c) 4^+_1 states in ^{12}C over $0\hbar\Omega$ (blue, lowest) to $6\hbar\Omega$ (green, highest) subspaces for the most dominant 0p-0h + $2\hbar\Omega$ 2p-2h Sp$(3,\mathbb{R})$ irrep case (left) and NCSM (right) together with the leading (0 4) irrep contribution (black diamonds) as a function of the $\hbar\Omega$ oscillator strength in MeV for $N_{\max} = 6$.

strength, the projection changes slightly reaching close to 90% for $\hbar\Omega = 11$ MeV (Fig. 6.5 and Fig. 6.6).

Among the $2\hbar\Omega$ 2p-2h symplectic irreps, those with bandheads specified by the $(\lambda_\sigma\, \mu_\sigma)$ quantum numbers (2 4) and (1 3) play the most important role, followed by the (6 2) irrep. The significance of the first two $(\lambda_\sigma\, \mu_\sigma)$ sets, in addition to the 0p-0h Sp$(3,\mathbb{R})$ irrep contribution, indicate a propensity of the $2\hbar\Omega$ components in the NCSM ground state band towards oblate deformed shapes. However, the most prolate deformed configuration is also embraced as suggested by projection onto the (6 2) class of the symplectic bandheads. The symplectic excitations above the relevant Sp$(3,\mathbb{R})$ bandheads point to the development of a more complex shape structure as seen, for example, in Fig. 6.7 for the ^{12}C ground state. Among these, the stretched symplectic states appear to be of a special interest as they usually possess larger overlaps with the realistic states under consideration as compared to the other symplectic excitations. The stretched states are those with $\mu_\omega = \mu_\sigma$ and maximum value of λ_ω, namely $\lambda_\sigma + N_n$ for $N_n\hbar\Omega$ excitations above the symplectic

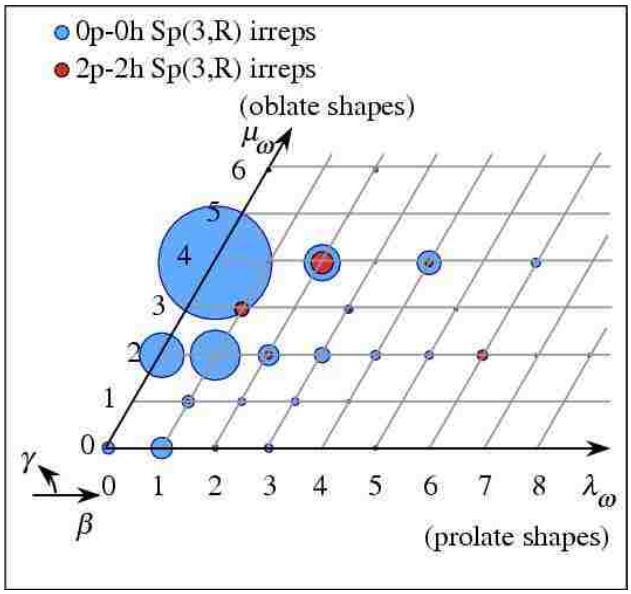

Figure 6.7: Probabilities (specified by the area of the circles) for the symplectic states which make up the most important 0p-0h (blue) and $2\hbar\Omega$ 2p-2h (red) symplectic irreps, within the NCSM ground state in ^{12}C, $\hbar\Omega = 15$ MeV. The $\mathrm{Sp}(3,\mathbb{R})$ states are grouped according to their $(\lambda_\omega\, \mu_\omega)$ SU(3) symmetry, which is mapped onto the $(\beta\, \gamma)$ shape variables of the collective model (see text for further details).

bandhead. These correspond to horizontal (same μ_ω) increments of two λ_ω units in the plane of Fig. 6.7 starting from the bandhead configuration. The dominance of the highly deformed symplectic states within the most important $2\hbar\Omega$ 2p-2h $\mathrm{Sp}(3,\mathbb{R})$ irreps also enhances the corresponding $B(E2 : 2_1^+ \rightarrow 0_{gs}^+)$ values.

6.3.2 Ground State in ^{16}O Nucleus

A much more interesting scenario is observed for the low-lying 0^+ states in ^{16}O. Here, the projection of the NCSM eigenstates onto the symplectic model subspace can also yield insight into the α-cluster structure of the realistic states based on the α+^{12}C cluster model [138, 151, 137, 152]. The latter describes ^{16}O as being made up of α and ^{12}C fragments frozen to the lowest shell-model states with their relative motion carrying arbitrary excitations. The overlaps between the symplectic states and the α+^{12}C cluster model wave functions have been evaluated analytically [137] and it was found that particular symplectic states have a significant overlap with the corresponding cluster model wave functions (see 4.2.5).

As compared to the outcome of the 0p-0h analysis, the inclusion of the $2\hbar\Omega$ 2p-2h $\mathrm{Sp}(3,\mathbb{R})$ irreps constructed over the most significant symplectic bandheads improves the overlaps of the selected symplectic basis with the NCSM eigenstate for the ^{16}O ground state by about 10%. As a result, the ground state in ^{16}O as calculated by NCSM projects at the 85%-90% level onto the $J = 0$ symplectic symmetry-adapted

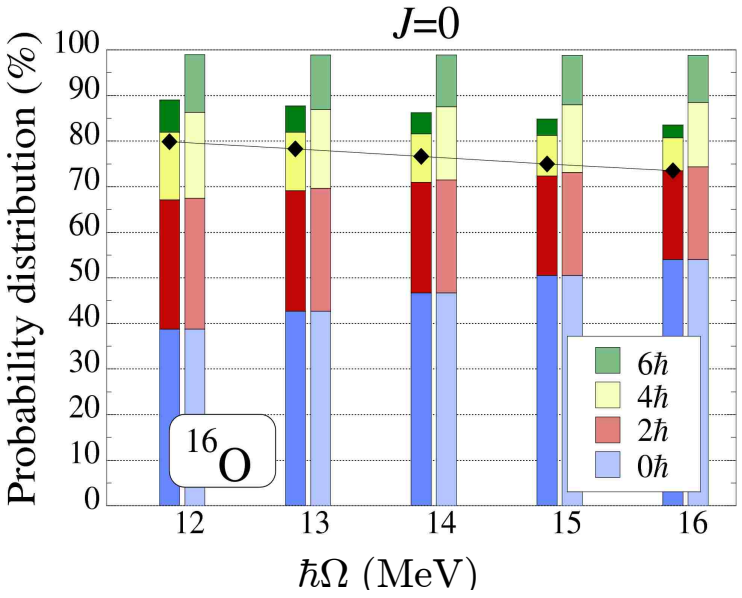

Figure 6.8: Probability distribution for the 0^+_{gs} state in ^{16}O over $0\hbar\Omega$ (blue, lowest) to $6\hbar\Omega$ (green, highest) subspaces for the most dominant 0p-0h + $2\hbar\Omega$ 2p-2h Sp$(3,\mathbb{R})$ irrep case (left) and NCSM (right) together with the leading $(0\,0)$ irrep contribution (black diamonds) as a function of the $\hbar\Omega$ oscillator strength in MeV for $N_{\max} = 6$.

basis (Fig. 6.8 and Fig. 6.10a) with a total dimensionality of only $\approx 0.001\%$ of the NCSM space.

The 0p-0h symplectic model subspace analysis for the ^{16}O ground state reveals the dominance of the $(0\,0)S_\sigma = 0$ symplectic irrep, which is $80-75\%$ of the NCSM realistic wave function for values of the oscillator strength $\hbar\Omega = 12$ MeV to 16 MeV, respectively. The $0\hbar\Omega$ projection of the $(0\,0)S_\sigma = 0$ Sp$(3,\mathbb{R})$ irrep reflects the spherical shape preponderance in the ground state of ^{16}O (Fig. 6.9a), specifically around $40-55\%$ for the same $\hbar\Omega$ range. In addition, a relatively significant mixture of slightly prolate deformed shapes are observed and they are predominantly associated with stretched symplectic excitation states (along the horizontal λ_ω axis in Fig. 6.9a). Among them, the most significant mode with a projection onto the NCSM state of $\sim 13\%$ (for $\hbar\Omega = 16$ MeV) up to $\sim 25\%$ (for $\hbar\Omega = 12$ MeV) is described by the $2\hbar\Omega$ $(2\,0)$ 1p-1h and weaker 2p-2h Sp$(3,\mathbb{R})$-symmetric excitations built over the $(0\,0)S_\sigma = 0$ symplectic bandhead. This $2\hbar\Omega$ $(2\,0)$ symplectic configuration projects at the 65% level [137] on the corresponding α+^{12}C cluster model wave function. Orthogonal to these excitations, the $(2\,0)S_\sigma = 0$ 2p-2h symplectic bandhead constructed at the $2\hbar\Omega$ level are found to be the most dominant among the $2\hbar\Omega$ 2p-2h Sp$(3,\mathbb{R})$ bandheads when compared to the NCSM eigenstates (Table 6.6 and Fig. 6.9a). This means that the appearance $2\hbar\Omega$ 2p-2h Sp$(3,\mathbb{R})$ bandheads in the ground state of ^{16}O is governed in such a way to preserve the shape coherence of all the significant $2\hbar\Omega$ configurations.

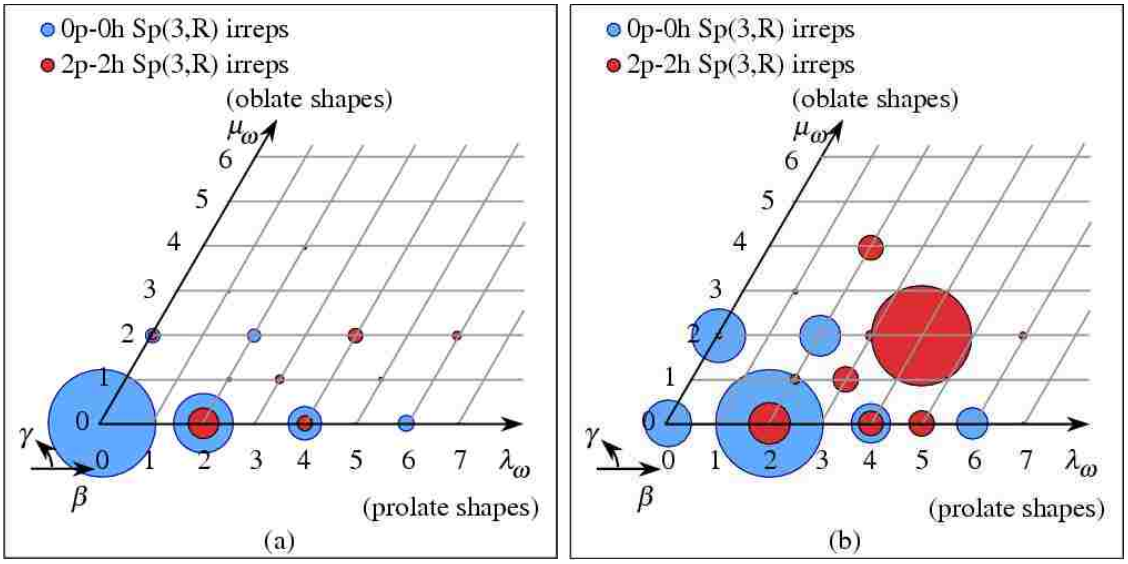

Figure 6.9: Probabilities (specified by the area of the circles) for the symplectic states, which make up the most dominant 0p-0h (blue) and $2\hbar\Omega$ 2p-2h (red) symplectic irreps, within (a) the 0^+ ground state and (b) the first excited 0^+_2 state in ^{16}O calculated by NCSM, $\hbar\Omega = 15$ MeV. The $\mathrm{Sp}(3,\mathbb{R})$ states are grouped according to their $(\lambda_\omega\, \mu_\omega)$ SU(3) symmetry, which is mapped onto the $(\beta\, \gamma)$ shape variables of the collective model.

6.3.3 First Excited 0^+ State in ^{16}O Nucleus

We also analyzed the symplectic structure of the 0^+_2 NCSM eigenstate in ^{16}O, which likewise was calculated using the JISP16 interaction in a $N_{\max} = 6$ space. This state is of a special interest because its microscopic description requires one to take into account highly deformed spatial multiple-particle-multiple-hole configurations. We therefore focused our investigation on determining whether such highly deformed multiple-particle-multiple-hole symplectic irreps are realized within the NCSM eigenstate. It is important to note that this state is not fully converged and the $6\hbar\Omega$ model space is quite restrictive for the development of strong 4p-4h correlations. This is because a very limited range of shells is accessed in the 4p-4h excitations, specifically, the *sd* and the *pf* shells for $N_{\max}$=6 4p-4h configurations. Note that only two particles can reach the *pf* shell under the $N_{\max}$=6 constraint.

The results indicate that the 0^+_2 NCSM eigenstate is dominated by the $2\hbar\Omega$ configurations composing 45% to 55% of the wave function. This is different from what we have observed in the ^{12}C ground state rotational band and the ^{16}O ground state that are mostly governed by $0\hbar\Omega$ configurations with a clear dominance of the 0p-0h $\mathrm{Sp}(3,\mathbb{R})$ irreps. The projection of this NSCM wave function onto the symplectic basis reveals, for the first time, a large contribution of the $2\hbar\Omega$ 2p-2h $\mathrm{Sp}(3,\mathbb{R})$ irreps (see Table 6.6 and Fig. 6.10b). This contribution tends to decrease with increasing $\hbar\Omega$ oscillator strength. It reaches 47% for $\hbar\Omega = 12$ MeV and declines down to 33% for $\hbar\Omega = 16$ MeV, with a clear dominance of the leading,

Table 6.6: Projection of the ground 0^+_{gs} and the first excited (not fully converged) 0^+_2 NCSM states for ^{16}O unto the dominant $2\hbar\Omega$ 2p-2h symplectic bandheads for $\hbar\Omega$=12 MeV.

Number of bandheads	Symplectic bandhead	Probability
	$J = 0^+_{gs}$	
5	$(2\,0)S_\sigma = 0$	2.75
3	$(4\,2)S_\sigma = 0$	0.62
2	$(2\,0)S_\sigma = 2$	0.60
1	$(4\,2)S_\sigma = 2$	0.33
	$J = 0^+_2$	
3	$(4\,2)S_\sigma = 0$	29.17
5	$(2\,0)S_\sigma = 0$	3.37
2	$(5\,0)S_\sigma = 1$	1.18
7	$(3\,1)S_\sigma = 1$	0.96

$(4\,2)$, $2\hbar\Omega$ 2p-2h irrep (Fig. 6.9b). It is important to note that the bandhead of this leading irrep projects at the 100% level onto the α+^{12}C cluster model wave function possessing the same, $(4\,2)$, SU(3) character [137]. The role of the 0p-0h Sp$(3,\mathbb{R})$ irrep within the NCSM eigenstate is also important, increasing from 29% (for $\hbar\Omega = 12$ MeV) up to 45% (for $\hbar\Omega = 16$ MeV). The main contribution to this percentage comes from the $(2\,0)$ configuration, which has significant overlaps with the corresponding α+^{12}C cluster model wave function [137]. This suggests that the cluster structure of the 0^+_2 NCSM eigenstate has already started to emerge in the $6\hbar\Omega$ model space. Overall, the symplectic basis projects at the 80% level onto the first excited 0^+_2 state, which turns to be a superposition of the 0p-0h and $2\hbar\Omega$ 2p-2h symplectic irreps.

In addition to the above, the outcome suggests that the leading most deformed $4\hbar\Omega$ 4p-4h symplectic irrep, $(\lambda_\sigma\,\mu_\sigma) = (8\,4)$, which is identical to the most deformed α+^{12}C cluster model wave function with the relative motion of the clusters carrying eight oscillator quanta [137], contribute rather insignificantly (0.31%-0.16%) to the NCSM first excited 0^+_2 state. Nevertheless, it is important to note that the contribution of this irrep to the ground state is completely negligible ($\approx 10^{-4}$%). The results suggest the need for exploring the Sp-NCSM scheme with model spaces beyond $N_{\max} = 6$ to achieve convergence of such higher-lying collective modes.

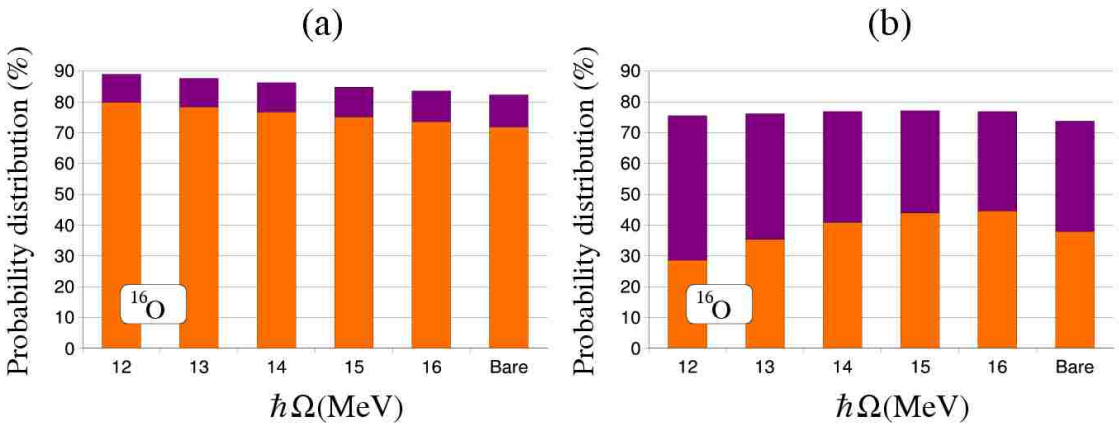

Figure 6.10: Projection of (a) the ground state 0^+_{gs} and (b) the first excited (not fully converged) 0^+_2 NCSM states for ^{16}O as a function of the $\hbar\Omega$ oscillator strength onto the 0p-0h (orange) $\mathrm{Sp}(3,\mathbb{R})$ irrep and the dominant $2\hbar\Omega$ 2p-2h (purple) $\mathrm{Sp}(3,\mathbb{R})$ irreps. Results are also shown for the bare interaction at $\hbar\Omega = 15$ MeV (column on the far right of each figure).

6.4 Symplectic Invariance within the Spin Parts of Realistic Eigenstates

As one varies the oscillator strength $\hbar\Omega$, the overall overlaps slightly increase toward smaller harmonic oscillator frequencies (see e.g. Fig. 6.6 and Fig. 6.8). For example, for ^{12}C and ^{16}O ground states, overlaps are almost 90% in the $\hbar\Omega = 12$ MeV case, and plunge to about 85% for $\hbar\Omega = 16$ Mev. In order to explain this behavior, we examined the spin components of the converged NCSM eigenstates with respect to the same spin carrying $\mathrm{Sp}(3,\mathbb{R})$ irreps.

6.4.1 Spin Decomposition

The NCSM eigenstates are superpositions of different spin components, and hence can be schematically written as,

$$|\mathrm{NCSM}; JM_J\rangle = \sum_{s=0}^{S_{\max}} \alpha_s \, |S = s; JM_J\rangle \, . \tag{6.1}$$

Here, $S_{\max}$ signifies the maximum allowed spin for the given nucleus, e.g. $S_{\max} = 6$ and 8 for ^{12}C and ^{16}O nuclei, respectively, $|S = s; JM_J\rangle$ denotes spin $S = s$ component of the NCSM eigenstate, that is,

$$\hat{S}^2 \, |S = s; JM_J\rangle = s(s+1) \, |S = s; JM_J\rangle \, . \tag{6.2}$$

Here, the coefficient α_s is the probability amplitude, and $\hat{S}^2$ is the total spin-square operator. We can carry out a spin decomposition of the NCSM eigenstates by

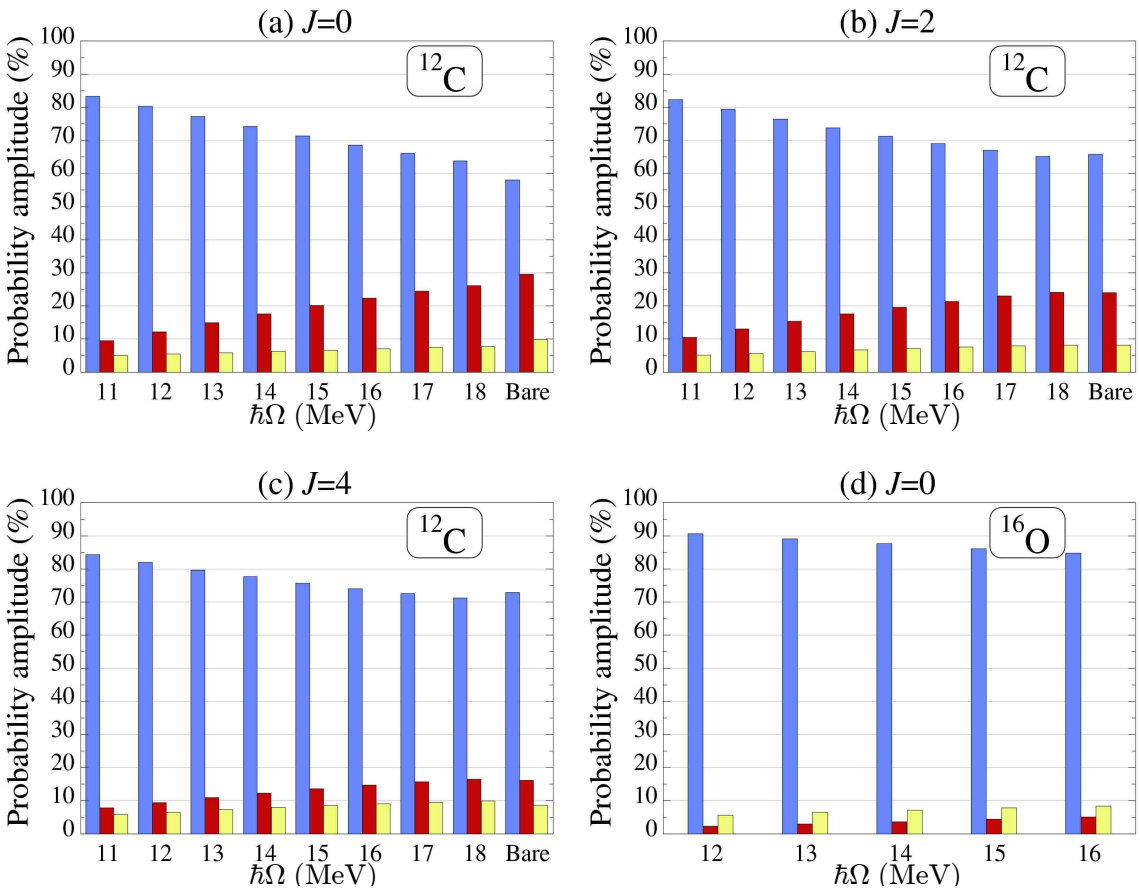

Figure 6.11: Probabilities for the $S = 0$ (blue, left), $S = 1$ (red, middle), and $S = 2$ (yellow, right) components of the NCSM eigenstates for (a) 0^+_{gs}, (b) 2^+_1, and (c) 4^+_1 in ^{12}C and (d) 0^+_{gs} in ^{16}O, $N_{\max} = 6$.

making use of operator $\hat{P}(S_{\min})$ defined as:

$$\hat{P}(S_{\min}) = \prod_{s=S_{\min}}^{S_{\max}} \left(1 - \frac{\hat{S}^2}{s\,(s+1)}\right). \tag{6.3}$$

In the first step, we apply the operator $\hat{P}(S_{\min}{=}1)$ on the given NCSM wave function. As a result, we obtain the $\alpha_0 \,|S = 0; JM_J\rangle$ term which is subsequently subtracted from the original wave function. In the second step, $\hat{P}(S_{\min}{=}2)$ is applied on the modified wave function, yielding, after normalization, the $|S = 1; JM_J\rangle$ component. The probability amplitude α_1 is calculated as $\alpha_1 = \langle \text{NCSM}; JM_J \,|S = 1; JM_J\rangle$, and the term $\alpha_1 \,|S = 1; JM_J\rangle$ is subtracted from the modified wave function. The procedure is repeated with the increasing value of $S_{\min}$ until the complete spin decomposition is achieved for $\hat{P}(S_{\min} = S_{\max} - 1)$.

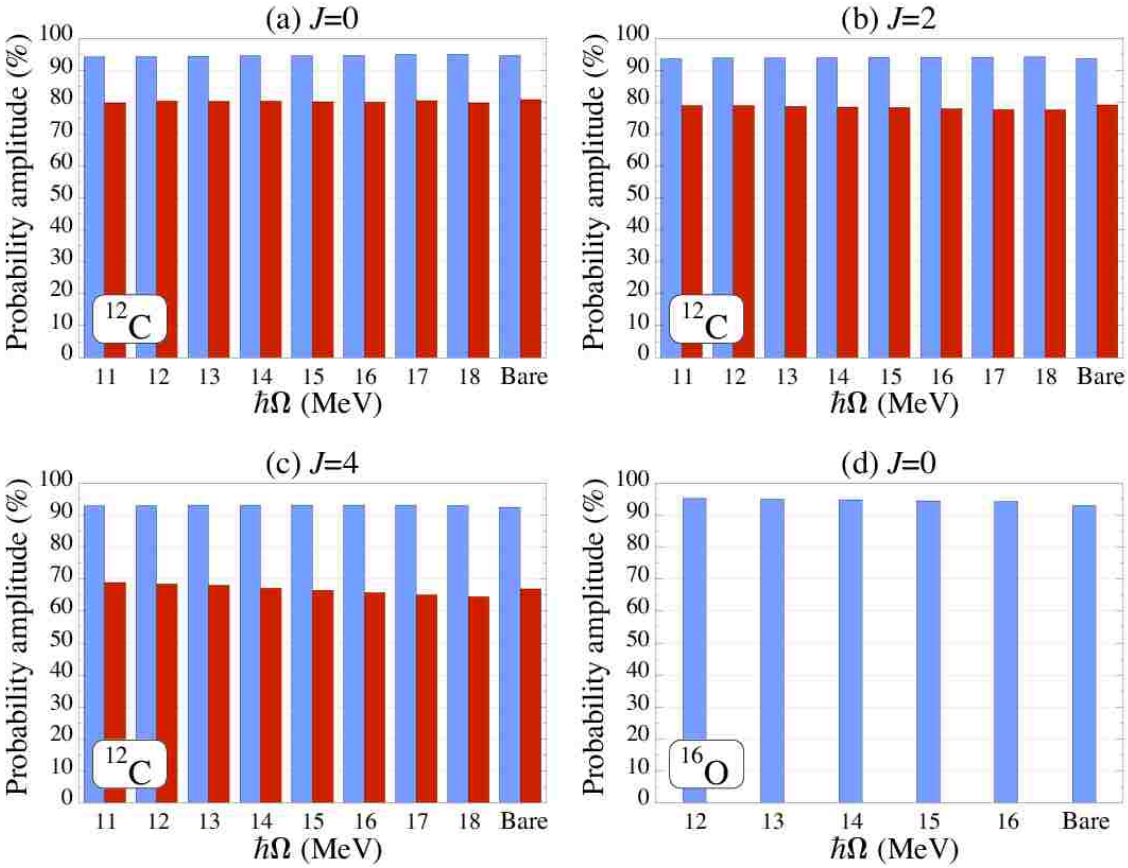

Figure 6.12: Projection of the $S_\sigma = 0$ (blue, left) and $S_\sigma = 1$ (red, right) $\mathrm{Sp}(3,\mathbb{R})$ irreps onto the corresponding significant spin components of the NSCM wave functions for (a) 0^+_{gs}, (b) 2^+_1, and (c) 4^+_1 in ^{12}C and (d) 0^+_{gs} in ^{16}O, for effective interaction for different $\hbar\Omega$ oscillator strengths and bare interaction. (We present only the most significant spin values that account for around 90% of a NCSM wave function).

6.4.2 Analysis of Spin Components

We performed the spin decomposition for the well converged NCSM eigenstates, that is, the ground-state band of ^{12}C and the ground state of ^{16}O. The probability amplitudes of the spin components reveal that the renormalization of the bare interaction through the Lee-Suzuki similarity transformation for different values of $\hbar\Omega$ influences the spin mixing within the NCSM eigenstates (see Fig. 6.11). The $S = 0$ part ($S = 1$ and $S = 2$ parts) of all NCSM eigenstates investigated decreases (increases) towards higher $\hbar\Omega$ frequencies (Fig. 6.11). As the spin $S = 2$ components gain importance, the total projection of the NCSM eigenstates onto the symplectic space declines slightly because the symplectic model space does not include any important, $S_\sigma = 2$ carrying, $\mathrm{Sp}(3,\mathbb{R})$ irreps. In short, no dominant symplectic symmetry content was found within the $S = 2$ components of the investigated NCSM wave functions.

Another striking property is revealed when the spin projections of the converged NCSM eigenstates are examined. Specifically, the spin-zero part of all three NCSM eigenstates for ^{12}C is almost entirely projected (95%) onto only six $S_\sigma = 0$ symplectic irreps, with as much as 90% of the spin-zero components of the NCSM eigenstates accounted for solely by the leading $(0\,4)$ irrep. As for the $S = 1$ part, the overlap with the two $S_\sigma = 1$ $(1\,2)$ symplectic irreps is around 80% for the 0^+_{gs} and 2^+_1 and around 70% for 4^+_1. Clearly, the $S = 1$ part is remarkably well described by merely two Sp$(3,\mathbb{R})$ irreps. In summary, the $S = 0$ and $S = 1$ parts of the NCSM wave functions are very well explained by (only!) three 0p-0h Sp$(3,\mathbb{R})$ irreps. Similar results are obtained for the ground state of ^{16}O. The leading $S_\sigma = 0$ symplectic irrep, $(0\,0)$, projects at the 90% level onto the $S = 0$ component of the 0^+_{gs} eigenstate, and the inclusion of the few most significant 2p-2h Sp$(3,\mathbb{R})$ irreps increases this projection up to 95% (see Fig. 6.12).

Furthermore, as shown in Fig. 6.12, the Sp$(3,\mathbb{R})$ symmetry and hence the geometry of the nucleon system being described is nearly independent of the $\hbar\Omega$ oscillator strength. The symplectic symmetry is present with equal strength in the spin parts of the NCSM wave functions for ^{12}C as well as ^{16}O regardless of whether the bare or the effective interactions are used. This suggests that the Lee-Suzuki transformation, which effectively compensates for the finite space truncation by renormalization of the bare interaction, does not affect the Sp$(3,\mathbb{R})$ symmetry structure of the spatial wave functions. Further, these results suggest that the symplectic structure detected in the present analysis for $6\hbar\Omega$ model space is what would emerge in NSCM evaluations with a sufficiently large model space to justify use of the bare interaction.

6.5 Dimension of Symplectic Model Space

The typical dimension of a symplectic irrep basis in the $N_{max} = 6$ model space is on the order of 10^2 as compared to 10^7 for the full NCSM m-scheme basis space. Note that if one were to include all possible Sp$(3,\mathbb{R})$ irreps with $N\hbar\Omega$ np-nh bandheads ($N \leq N_{max}$), and their basis states up to $N_{\max}\hbar\Omega$ subspace, one would span the entire $N_{\max}\hbar\Omega$ model space. Moreover, the space spanned by a given symplectic irrep, $N_\sigma(\lambda_\sigma\,\mu_\sigma)$, can be decomposed to subspaces of a definite total angular momentum J (see Eq. (5.16)) and can be further reduced to only the subspaces specified by the J values under consideration. In the case of the ground-state band of ^{12}C, these are $J = 0, 2$, and 4, and for the ground state of ^{16}O it is $J = 0$. As the model space, N_{max}, is increased the dimension of the $J = 0, 2$, and 4 symplectic space built on the 13 0p-0h Sp$(3,\mathbb{R})$ irreps grows very slowly compared to the NCSM space dimension (Table 6.7 and Fig. 6.13a). The dominance of only three irreps additionally reduces the dimensionality of the symplectic model space (Table 6.7), which in the $12\hbar\Omega$ model space constitutes only 3.7×10^{-6}% of the NCSM space size. The space reduction is even more dramatic in the case of ^{16}O (Table 6.8 and Fig. 6.13b).

Further reduction in the symplectic model space size can be achieved by considering Sp$(3,\mathbb{R})$ irreps carrying a total spin $S_\sigma \leq 2$. This reduction is based on

Table 6.7: Model space dimensions for different maximum allowed $\hbar\Omega$ excitations, $N_{\max}$, for the NCSM and the 3 most significant 0p-0h Sp$(3,\mathbb{R})$ irreps limited to $J = 0, 2$, and 4 states in ^{12}C. For comparison, the size of the full space of the 3 0p-0h Sp$(3,\mathbb{R})$ irreps (all J values) is shown together with the $J = 0, 2$, and 4 model space dimension of all the 13 0p-0h Sp$(3,\mathbb{R})$ irreps for ^{12}C.

$N_{\max}$	NCSM	3 Sp$(3,\mathbb{R})$ irreps $J = 0, 2, 4$	3 Sp$(3,\mathbb{R})$ irreps all J	13 Sp$(3,\mathbb{R})$ irreps $J = 0, 2, 4$
0	51	13	21	30
2	1.77×10^4	68	127	157
4	1.12×10^6	216	444	495
6	3.26×10^7	514	1098	1169
8	5.94×10^8	1030	2414	2326
10	7.83×10^9	1828	4674	4103
12	8.08×10^{10}	2979	8388	6651

Table 6.8: Model spaces dimension for different maximum allowed $\hbar\Omega$ excitations, N_{max}, for the NCSM and the single 0p-0h Sp$(3,\mathbb{R})$ irrep limited to $J = 0$ states in ^{16}O.

$N_{\max}$	NCSM	$(0\,0)$ Sp$(3,\mathbb{R})$ irrep $J = 0$
0	1	1
2	1.24×10^3	2
4	3.44×10^5	4
6	2.61×10^7	7
8	9.70×10^8	11
10	2.27×10^{10}	16
12	3.83×10^{11}	23

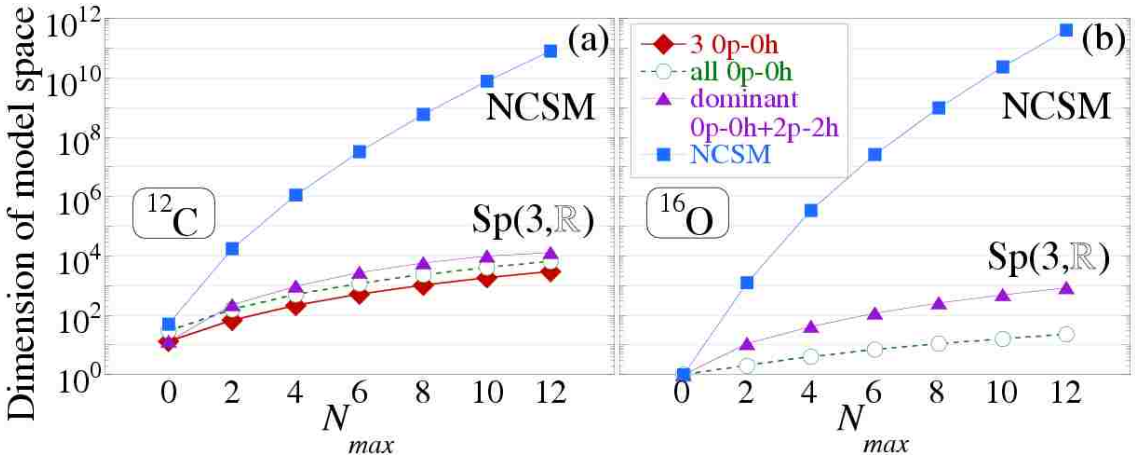

Figure 6.13: NCSM space dimension as a function of the maximum $\hbar\Omega$ excitations, $N_{\max}$, compared to that of the $\mathrm{Sp}(3,\mathbb{R})$ subspace: (a) $J = 0, 2$, and 4 for ^{12}C, and (b) $J = 0$ for ^{16}O.

the fact that the low-lying states in light nuclei do not favor high-spin components as they are shifted upwards in energy by the spin-orbit part of the internucleon interaction [32].

The symplectic model subspace remains a very small fraction of the NCSM basis space, even when the most dominant $2\hbar\Omega$ 2p-2h $\mathrm{Sp}(3,\mathbb{R})$ irreps are included. The reduction is even more dramatic in the case of ^{16}O, where only the $J = 0$ symplectic space can be taken into account for the 0^+ states under consideration (Fig. 6.13b). This means that the space spanned by the set of relevant symplectic basis states is computationally manageable even when high-$\hbar\Omega$ configurations are included.

Chapter 7

Conclusions

The primary goal of our proof-of-principle study was to examine role of the symplectic $\mathrm{Sp}(3,\mathbb{R})$ symmetry in light nuclei as unveiled through the results of *ab initio* NCSM calculations obtained using a modern realistic nucleon-nucleon interaction. Specifically, we examined the symplectic $\mathrm{Sp}(3,\mathbb{R})$ symmetry of the ground-state rotational band of ^{12}C and the ground state of ^{16}O as calculated through the *ab initio* NCSM using the realistic nucleon-nucleon JISP16 potential in the $N_{\max} = 6$ ($6\hbar\Omega$) model space.

To facilitate symmetry identification, we devised and implemented a set of methods for constructing translationally invariant basis states of a general symplectic $\mathrm{Sp}(3,\mathbb{R})$ irrep in a fermion-based spherical harmonic oscillator (m-scheme) basis, the same basis used within the NCSM framework. By utilizing these methods for ^{12}C and ^{16}O nuclei, we expanded all 0p-0h, $2\hbar\Omega$ 2p-2h, and the most deformed $4\hbar\Omega$ 4p-4h translationally invariant symplectic bandheads in the m-scheme basis and subsequently generated corresponding $\mathrm{Sp}(3,\mathbb{R})$ irreps basis states up to the $6\hbar\Omega$ subspace by applying the symplectic construction formula.

We first projected the investigated wave functions onto a symplectic model space composed of all 0p-0h $\mathrm{Sp}(3,\mathbb{R})$ irreps. The analysis of the results reveals that the NCSM eigenstates project at approximately the 80% level onto only a few 0p-0h spurious center-of-mass free symplectic irreps with a clear dominance of the leading $\mathrm{Sp}(3,\mathbb{R})$ irrep. Furthermore, in the case of the ^{12}C ground-state rotational band the three most deformed 0p-0h $\mathrm{Sp}(3,\mathbb{R})$ irreps yield a $B(E2 : 2_1^+ \rightarrow 0_{gs}^+)$ transition rate that closely reproduce the NCSM estimates. These results can be interpreted as a strong confirmation of Elliott SU(3) model since the projection of the NCSM states onto the $0\hbar\Omega$ space is a projection of the NCSM results onto the SU(3) shell model.

As the considered NCSM eigenstates are dominated by the $0\hbar\Omega$ configurations, the role of the 2p-2h $\mathrm{Sp}(3,\mathbb{R})$ irreps is less important. The addition of the symplectic configurations built over a small number of the most deformed $2\hbar\Omega$ 2p-2h bandheads improves the overlaps by about 5% for ^{12}C and 10% for ^{16}O. Furthermore, the dimension of a $\mathrm{Sp}(3,\mathbb{R})$-symmetric space remains a small fraction of the full NCSM space even when the most relevant 2p-2h $\mathrm{Sp}(3,\mathbb{R})$ irreps are included. We also analyzed the structure of highly deformed the first exited 0_2^+ in ^{16}O which is attributed to strongly favored 4p-4h configurations. The NCSM eigenstate for

this state is not converged in the $6\hbar\Omega$ model space and turns out to be a superposition of two dominant, the 0p-0h and the most deformed 2p-2h, symplectic irreps. The most deformed 4p-4h $\mathrm{Sp}(3,\mathbb{R})$ irrep is found to contribute rather insignificantly as the $6\hbar\Omega$ model space is quite restrictive for the development of strong 4p-4h correlations.

The spin decomposition of the converged NCSM wave functions reveals that the symplectic $\mathrm{Sp}(3,\mathbb{R})$ symmetry remains almost invariant with respect to the Lee-Suzuki renormalization procedure. The given set of symplectic irreps is present with equal strength in the spin parts of the NCSM wave functions regardless of whether the bare or the effective interactions are used.

We demonstrated that ^{12}C and ^{16}O NCSM wave functions and electromagnetic transition rates are reproduced remarkably well by the symplectic subspace that is only a small fraction ($\approx 0.001\,\%$) of the full $N_{\max} = 6$ NCSM model space. As $N_{\max}$ increases the symplectic model space amounts to an ever smaller fraction of the NCSM basis space, for instance, a mere $0.000001\,\%$ in the case of $N_{\max} = 12$. This means that a space spanned by a set of translationally invariant symplectic basis states, which correspond to the most relevant collective modes, may be computationally tractable even when high-$\hbar\Omega$ configurations are included. The symplectic $\mathrm{Sp}(3,\mathbb{R})$ symmetry-adapted basis thus bear promise to resolve the scale explosion problem in *ab initio* nuclear structure calculations.

The ultimate goal of the future research will be to augment the conventional m-scheme basis by the physically relevant $\mathrm{Sp}(3,\mathbb{R})$ symmetry-adapted configurations, and to design and implement methods that evaluate realistic nuclear Hamiltonian matrix elements solely in the symplectic basis as well as in the mixed m-scheme and symplectic basis. The dramatic reduction of dimensions for higher-$\hbar\Omega$ spaces and heavier nuclei as compared to the full m-scheme basis will open up a new region of the periodic table, the *sd*-shell up to ^{28}Si nucleus, for investigation with *ab initio* methods and improve the predictive power of the latter.

In summary, we have shown that realistic eigenstates for low-lying states of ^{12}C and ^{16}O nuclei as determined in *ab initio* NCSM calculations with the JISP16 realistic interaction project at a significant level ($\sim 80\,\%$-$90\,\%$) onto a few of the most deformed translationally invariant $\mathrm{Sp}(3,\mathbb{R})$-symmetric basis states, which in addition also closely reproduce $B(E2 : 2_1^+ \rightarrow 0_{gs}^+)$ NCSM estimates. This manifests the dominance of underlying symplectic $\mathrm{Sp}(3,\mathbb{R})$ symmetry in the many-body dynamics of light nuclei. It is important to note that the $\mathrm{Sp}(3,\mathbb{R})$ symmetry is not *a priori* imposed on the realistic JISP16 interaction, and, furthermore, it is found to remain unaltered whether the bare or effective interactions for various harmonic oscillator strengths are used. This indicates the propensity of the internucleon interaction toward preserving the $\mathrm{Sp}(3,\mathbb{R})$ symmetry and suggest that the nuclear many-body system acts as a filter that allows the symplectic symmetry to propagate in a coherent way into the many-body dynamics while reducing the effects of symplectic symmetry breaking terms.

Results of our proof-of-principle study points to the possibility of reaching heavier nuclei and achieving a better convergence for nuclear states of collective nature by expanding the conventional NCSM basis beyond its current limits through

the physically most relevant $\mathrm{Sp}(3,\mathbb{R})$ symmetry-adapted basis states. Particularly, the Sp-NCSM approach has potential to realize experimentally measured $B(E2)$ values without an effective charge, to providing a unified description of phenomena ranging from single-particle effects to clustering correlations and collective rotations, which is currently unfeasible tasks for the m-scheme based NCSM. It is our hope and expectation that the outcomes of this work are sufficiently conclusive to justify and stimulate support for the development of an independent *ab initio* symplectic no-core shell model.

Bibliography

[1] A. M. Shirokov, J. P. Vary, A. I. Mazur, S. A. Zaytsev, and T. A. Weber, Phys. Letts. B **621**, 96 (2005).

[2] A. M. Shirokov, J. P. Vary, A. I. Mazur, and T. A. Weber, Phys. Letts. B **644**, 1 (2007).

[3] V. G. J. Stoks, R. A. M. Klomp, C. P. F. Terheggen, and J. J. de Swart, Phys. Rev. C **49**, 2950 (1994).

[4] R. B. Wiringa, V. G. J. Stoks, and R. Schiavilla, Phys. Rev. C **51**, 38 (1995).

[5] R. Machleidt, F. Sammarruca, and Y. Song, Phys. Rev. C **53**, R1483 (1996).

[6] R. Machleidt, Phys. Rev. C **63**, 024001 (2001).

[7] D. R. Entem and R. Machleidt, Phys. Rev. C **68**, 041001 (2003).

[8] U. van Kolck, Phys. Rev. C **49**, 2932 (1994).

[9] P. Navrátil, J. P. Vary, and B. R. Barrett, Phys. Lett. **84**, 5728 (2000).

[10] S. C. Pieper, K. Varga, and R. B. Wiringa, Phys. Rev. C **66**, 044310 (2002).

[11] S. C. Pieper, Nucl. Phys. A **751**, 516 (2005).

[12] M. Włoch *et al.*, Phys. Rev. Lett. **94**, 212501 (2005).

[13] P. Navrátil and B. R. Barrett, Phys. Rev. C **57**, 562 (1998).

[14] P. Navrátil, G. P. Kamuntavičius, and B. R. Barrett, Phys. Rev. C **61**, 044001 (2000).

[15] P. Navrátil, J. P. Vary, and B. R. Barrett, Phys. Rev. C **62**, 054311 (2000).

[16] J. P. Vary *et al.*, Nucl. Phys. A **746**, 123c (2004).

[17] J. P. Vary, Int. J. Mod. Phys. E **14**, 1 (2005).

[18] P. Navrátil and W. E. Ormand, Phys. Rev. Lett. **88**, 152502 (2003).

[19] G. Rosensteel and D. J. Rowe, Phys. Rev. Lett. **38**, 10 (1977).

[20] G. Rosensteel and D. J. Rowe, Ann. Phys. N.Y. **126**, 343 (1980).

[21] D. J. Rowe, Reports on Progr. in Phys. **48**, 1419 (1985).

[22] T. Dytrych, K. D. Sviratcheva, C. Bahri, J. P. Draayer, and J. P. Vary, Phys. Rev. Lett. **98**, 162503 (2007).

[23] T. Dytrych, K. D. Sviratcheva, C. Bahri, J. P. Draayer, and J. P. Vary, Phys. Rev. C **76**, 014315 (2007).

[24] T. Dytrych, K. D. Sviratcheva, C. Bahri, J. P. Draayer, and J. P. Vary, J. Phys. G: Nucl. Part. Phys. **35**, 095101 (2008).

[25] T. Dytrych, K. D. Sviratcheva, J. P. Draayer, C. Bahri, and J. P. Vary, J. Phys. G: Nucl. Part. Phys. **35**, 123101 (2008).

[26] M. G. Mayer, Phys. Rev. **74**, 235 (1948).

[27] O. Axel, J. H. D. Jensen, and H. E. Suess, Phys. Rev. **75**, 1766 (1949).

[28] S. Weinberg, Phys. Lett. B **251**, 288 (1990).

[29] R. Machleidt and R. Entem, J. Phys. G **31**, S1235 (2005).

[30] R. Machleidt, Nucl. Phys. A **790**, 17c (2007).

[31] P. A. M. Guichon and A. W. Thomas, Phys. Rev. Lett. **93**, 132502 (2004).

[32] A. De-Shalit and I. Talmi, *The Nuclear Shell Theory* (Academic Press, London, 1963).

[33] K. L. G. Heyde, *The Nuclear Shell Model* (Springer-Verlag Berlin Heidelberg, 1990).

[34] E. Caurier, G. Martínez-Pinedo, F. Nowacki, A. Poves, and A. P. Zuker, Rev. Mod. Phys. **77(2)**, 427 (2005).

[35] J. P. Elliott and T. H. R. Skyrme, Proc. Roy. Soc. A **232**, 561 (1955).

[36] R. R. Whitehead, A. Watt, B. J. Cole, and I. Morrison, Adv. Nuc. Phys. **9**, 123 (1977).

[37] E. Caurier and F. Nowacki, Acta Physica Polonica **30**, 705 (1999).

[38] J. P. Vary, The many-fermion-dynamics shell-model code, 1992.

[39] J. P. Vary and D. C. Zheng, ibid, 1994.

[40] J. B. French, E. C. Halbert, J. B. McGrory, and S. S. M. Wong, Adv. Nuc. Phys. **3**, 237 (1969).

[41] C. Lanczos, J. Res. Nat. Bur. Stan. B **45**, 255 (1950).

[42] J. K. Cullum and R. A. Willoughby, *Lanczos algorithms for large symmetric eigenvalue computations* (Birkhäuser, Boston, 1985).

[43] L. Komzsik, *The Lanczos Method* (Society for Industrial Mathematics, Philadelphia, 2003).

[44] M. R. Guarracino, F. Perla, and P. Zanetti, Int. J. Appl. Math. Comput. Sci. **16**, 241 (2006).

[45] C. Forssén, P. Navrátil, and W. E. Ormand, Phys. Rev. C **71**, 2005 (044312).

[46] M. G. Mayer, The shell model, in *Nobel Lectures in Physics 1963-1970*, p. 20, World Scientic Publishing, 1998.

[47] P. Navrátil and W. E. Ormand, Phys. Rev. C **68**, 034305 (2003).

[48] A. Nogga, P. Navrátil, B. R. Barrett, and J. P. Vary, Phys. Rev. C **73**, 064002 (2006).

[49] P. Navrátil, V. G. Gueorguiev, J. P. Vary, W. E. Ormand, and A. Nogga, Phys. Rev. Lett. **99**, 042501 (2007).

[50] V. G. J. Stoks, R. A. M. Klomp, M. C. M. Rentmeester, and J. J. de Swart, Phys. Rev. C **48**, 792 (1993).

[51] W. N. Polyzou and W. Glöckle, Few-Body Syst. **97**, 9 (1990).

[52] R. Machleidt and I. Slaus, J. Phys. G **27**, R69 (2001).

[53] A. Nogga, H. Kamada, and W. Glöckle, Phys. Rev. Lett **85**, 944 (2000).

[54] H. Witała *et al.*, Phys. Rev. C **63**, 24007 (2001).

[55] S. A. Coon and W. Glöckle, Phys. Rev. C **23**, 1790 (1981).

[56] S. M. Coon and H. K. Han, Few-Body Syst. **30**, 131 (2001).

[57] M. R. Robilotta and H. T. Coelho, Nucl. Phys. A **460**, 645 (1986).

[58] S. C. Pieper, V. R. Pandharipande, R. B. Wiringa, and J. Carlson, Phys. Rev. C **64**, 014001 (2001).

[59] J. Carlson, V. R. Pandharipande, and R. B. Wiringa, Nucl. Phys. A **401**, 59 (1983).

[60] I. J. R. Aitchison and A. J. G. Hey, *Gauge Theories in Particle Physics* (Taylor & Francis Group, London, 2003).

[61] P. Doleschall and I. Borbély, Physics Review C **67**, 064005 (2003).

[62] S. Bogner, R. Furnstahl, and R. Perry, Physics Review C **75**, 061001(R) (2007).

[63] S. Glazek and K. Wilson, Physics Review D **48**, 5863 (1993).

[64] F. Wegner, Annalen der Physik (Leipzig) **3**, 77 (1994).

[65] H. Feldmeier, T. Neff, R. Roth, and J. Schnack, Nucl. Phys. A **632**, 61 (1998).

[66] T. Neff and H. Feldmeier, Nucl. Phys. A **713**, 311 (2003).

[67] A. M. Shirokov, A. I. Mazur, S. A. Zaytsev, J. P. Vary, and T. A. Weber, Phys. Rev. C **70**, 044005 (2004).

[68] K. Suzuki and S. Y. Lee, Prog. Theor. Phys. **64**, 2091 (1980).

[69] K. Suzuki, Prog. Theor. Phys. **68**, 246 (1982).

[70] C. P. Viazminsky and J. P. Vary, J. Math. Phys. **42**, 2055 (2001).

[71] K. Suzuki, Prog. Theor. Phys. **68**, 1627 (1982).

[72] K. Suzuki, Prog. Theor. Phys. **68**, 1999 (1982).

[73] O. Mintkevich and N. Barnea, Phys. Rev. C **69**, 2004 (044005).

[74] P. Navrátil and B. R. Barrett, Phys. Rev. C **59**, 1906 (1999).

[75] P. Navrátil and B. R. Barrett, Phys. Rev. C **54**, 2986 (1996).

[76] I. Stetcu, B. R. Barrett, P. Navrátil, and J. P. Vary, Phys. Rev. C **71**, 044325 (2005).

[77] B. R. Barrett, I. Stetcu, P. Navrátil, and J. P. Vary, J. Phys. A **39**, 9983 (2006).

[78] L. D. Faddeev, Sov. Phys. JETP **12**, 1014 (1961).

[79] O. A. Yakubovski, Sov. J. Nucl. Phys. **5**, 937 (1967).

[80] E. Caurier, P. Navrátil, W. E. Ormand, and J. P. Vary, Phys. Rev. C **66**, 024314 (2002).

[81] M. J. Musolf and T. W. Donnelly, Nucl. Phys. A **546**, 509 (1992).

[82] M. J. Musolf *et al.*, Phys. Rep. **239**, 1 (1994).

[83] R. D. Young, R. D. Carlini, A. W. Thomas, and J. Roche, Phys. Rev. Lett **99**, 122003 (2007).

[84] K. A. Aniol *et al.*, Phys. Rev. Lett **96**, 022003 (2006).

[85] W. E. Ormand, Phys. Rev. Lett **82**, 1101 (1999).

[86] D. R. Inglis, Rev. Mod. Phys. **25**, 390 (1953).

[87] E. Baranger and S. Meshkov, Phys. Rev. Lett. **1**, 30 (1958).

[88] B. Jancovici and I. Talmi, Phys. Rev. **95**, 289 (1954).

[89] M. Fayache, L. Zamick, and H. Müther, Phys. Rev. C **60**, 067305 (1999).

[90] S. Aroua *et al.*, Nucl. Phys. A **720**, 71 (2003).

[91] A. Negret *et al.*, Phys. Rev. Lett. **97**, 062502 (2006).

[92] M. Milin *et al.*, Nucl. Phys. A **730**, 285 (2004).

[93] J. Engel, E. Kolbe, K. Langanke, and P. Vogel, Phys. Rev. C **54**, 2740 (1996).

[94] P. Vogel, in *"Physics Beyond the Standard Model": Proceedings of the Fifth International WEIN (Weak and Electromagnetic Interactions in Nuclei) Conference (WEIN98)*, edited by P. Herczeg, C. Hoffman, and H. Klapdor-Kleingrothaus, p. 204, Singapore, 1999, World Scientific, LANL ArXiV: Nucl-Th 9901027.

[95] A. C. Hayes, P. Navrátil, and J. P. Vary, Phys. Rev. Lett. **91**, 012502 (2003).

[96] I. Towner and J. Hardy, J. Phys. G: Nucl. Part. Phys. **29**, 197 (2003).

[97] W. Ormand and B. Brown, Phys. Rev. C **52**, 2455 (1995).

[98] G. Grinyer *et al.*, Phys. Rev. C **76**, 025503 (2007).

[99] M. Mukherjee *et al.*, Phys. Rev. Lett. **93**, 150801 (2004).

[100] D. Seweryniak *et al.*, Phys. Rev. Lett. **94**, 032501 (2005).

[101] P. Navrátil, C. A. Bertulani, and E. Caurier, Phys. Rev. C **73**, 065801 (2006).

[102] K. M. Nollett, S. C. Pieper, R. B. Wiringa, J. Carlson, and G. M. Hale, Phys. Rev. Lett. **99**, 022502 (2007).

[103] N. de Séréville *et al.*, Nucl. Phys. A **791**, 251 (2007).

[104] C. Nesaraja *et al.*, Phys. Rev. C **75**, 055809 (2007).

[105] J. Blackmon, C. Angulo, and A. Shotter, Nucl. Phys. A **777**, 531 (2006).

[106] J. P. Elliott, Proc. Roy. Soc. A **245**, 128 (1958).

[107] J. P. Elliott, Proc. Roy. Soc. A **245**, 562 (1958).

[108] J. P. Elliott and M. Harvey, Proc. Roy. Soc. A **272**, 557 (1963).

[109] H. Ui, Prog. Theor. Phys. **44**, 153 (1970).

[110] L. Weaver and L. C. Bierdenharn, Phys. Lett. B **32**, 326 (1970).

[111] L. Weaver and L. C. Bierdenharn, Nucl. Phys. A **185**, 1 (1972).

[112] J. P. Elliott and C. E. Wilsdon, Proc. Roy. Soc. A **302**, 509 (1968).

[113] M. Harvey, Adv. Nucl. Phys. **1**, 67 (1968).

[114] H. A. Naqvi and J. P. Draayer, Nucl. Phys. A **516**, 351 (1990).

[115] H. A. Naqvi and J. P. Draayer, Nucl. Phys. A **536**, 297 (1992).

[116] C. Bahri, J. Escher, and J. P. Draayer, Nucl. Phys. A **592**, 171 (1995).

[117] J. Escher, C. Bahri, D. Troltenier, and J. P. Draayer, Nucl. Phys. A **633**, 662 (1998).

[118] V. G. Gueorguiev, J. P. Draayer, and C. W. Johnson, Phys. Rev. C **63**, 014318 (2000).

[119] G. Gneuss and W. Greiner, Nucl. Phys. A **171**, 449 (1971).

[120] P. O. Hess, J. Maruhn, and W. Greiner, J. Phys. G **7**, 737 (1981).

[121] W. Greiner and J. Maruhn, *Nuclear Models* (Springer-Verlag Berlin Heidelberg, 1995).

[122] O. Castaños, J. P. Draayer, and Y. Leschber, Z. Phys. A **329**, 33 (1988).

[123] G. Rosensteel, Astrophys. J. **416**, 291 (1993).

[124] C. Bahri and D. J. Rowe, Nucl. Phys. A **662**, 125 (2000).

[125] J. Escher and J. P. Draayer, J. Math. Phys. **39**, 5123 (1998).

[126] G. Rosensteel, Nucl. Phys. A **341**, 397 (1980).

[127] D. J. Rowe, J. Math. Phys. **25**, 2662 (1984).

[128] D. J. Rowe, G. Rosenteel, and R. Carr, J. Math. Phys. A **17**, L399 (1984).

[129] D. J. Rowe, R. L. Blanc, and K. T. Hecht, J. Math. Phys. **29**, 287 (1988).

[130] M. Chernykh, H. Feldmeier, T. Neff, P. von Neumann-Cosel, and A. Richter, Phys. Rev. Lett. **98**, 032501 (2007).

[131] A. Tohsaki, H. Horiuchi, P. Schuck, and G. Röpke, Phys. Rev. Lett. **87**, 192501 (2001).

[132] Y. Fujiwara *et al.*, Prog. Theor. Phys. Suppl. No. **68**, 29 (1980).

[133] K. Wildermuth and Y. C. Tang, *A Unified Theory of the Nucleus* (Academic Press, 1977).

[134] Y. Suzuki, Prog. Theor. Phys. **55**, 1751 (1976).

[135] Y. Suzuki, Prog. Theor. Phys. **56**, 111 (1976).

[136] Y. Suzuki and K. T. Hecht, Nucl. Phys. A **455**, 315 (1986).

[137] Y. Suzuki, Nucl. Phys. A **448**, 395 (1986).

[138] K. T. Hecht, Phys. Rev. C **16**, 2401 (1977).

[139] C. W. Johnson, I. Stetcu, and J. P. Draayer, Phys. Rev. C **66**, 034312 (2002).

[140] V. G. Gueorguiev and J. P. Draayer, Rev. Mex. Fis. **44**, 43 (1998).

[141] V. G. Gueorguiev, *Mixed-symmetry shell-model calculations in nuclear physics*, PhD thesis, LSU, 2003.

[142] J. P. Draayer, Nucl. Phys. **216**, 457 (1973).

[143] B. G. Wybourne, *Classical Groups for Physicists* (J. Wiley and Sons, New York, 1973).

[144] B. J. Verhaar, Nucl. Phys. **21**, 508 (1960).

[145] K. T. Hecht, Nucl. Phys. A **170**, 34 (1971).

[146] J. Escher, *Electron Scattering Studies in the Framework of the Symplectic Shell Model*, PhD thesis, LSU, 1997.

[147] K. T. Hecht, Nucl. Phys. A **62**, 1 (1965).

[148] D. A. Varshalovich, A. N. Moskalev, and V. K. Kersonskii, *Quantum Theory of Angular Momentum* (World Scientic Publishing, 1988).

[149] G. Karniadakis, *Parallel scientific computing in C++ and MPI: a seamless approach to parallel algorithms and their implementation* (Cambridge University Press, 2003).

[150] Y. Akiyama and J. P. Draayer, Comput. Phys. Commun. **5**, 405 (1973).

[151] K. T. Hecht and D. Braunschweig, Nucl. Phys. A **295**, 34 (1978).

[152] Y. Suzuki and S. Hara, Phys. Rev. C **39**, 658 (1989).

[153] F. Hoyle, Astrophys. J. Suppl. Ser. **1**, 121 (1954).

[154] E. E. Salpeter, Astrophys. J. **115**, 326 (1952).

[155] E. Uegaki, S. Okabe, Y. Abe, and H. Tanaka, Prog. Theor. Phys. **57**, 1262 (1977).

[156] Y. Fukushima and M. Kamimura, J. Phys. Soc. Jpn. **44**, 225 (1978).

[157] Y. Funaki, A. Tohsaki, H. Horiuchi, P. Schuck, and G. Röpke, Phys. Rev. C **67**, R051306 (2003).

[158] S. I. Fedotov, O. I. Kartavtsev, V. I. Kochkin, and A. V. Malykh, Phys. Rev. C **70**, 014006 (2004).

[159] F. Herwig, S. M. Austin, and J. C. Lattanzio, Phys. Rev. C **73**, 025802 (2006).

[160] A. Bohr, Phys. Rev. **81**, 134 (1951).

[161] J. Escher and A. Leviatan, Phys. Rev. C **65**, 054309 (2002).

[162] F. Arickx, J. Broeckhove, and E. Deumens, Nucl. Phys. A **318**, 269 (1979).

[163] F. Arickx, J. Broeckhove, and E. Deumens, Nucl. Phys. A **377**, 121 (1982).

[164] S. S. Avancini and E. J. V. de Passos, J. Phys. G **19**, 125 (1993).

[165] K. Brueckner, Phys. Rev. **96**, 508 (1954).

[166] E. I. et al., Phys. Rev. Lett. **87**, 222501 (2001).

[167] G. E. Brown and A. M. Green, Phys. Lett. **15**, 168 (1965).

[168] G. E. Brown and A. M. Green, Nucl. Phys. **75**, 401 (1966).

[169] G. E. Brown and A. M. Green, Nucl. Phys. **93**, 110 (1967).

[170] A. P. Zuker, B. Buck, and J. B. McGrory, Phys. Rev. Lett. **21**, 39 (1968).

[171] G. J. Stephenson and M. K. Banerjee, Phys. Lett. B **24**, 209 (1967).

[172] S. D. Gupta and N. de Takacsy, Phys. Rev. Lett. **22**, 1194 (1964).

[173] E. Boeker, Nucl. Phys. **91**, 27 (1967).

[174] H. Liu and L. Zamick, Phys. Rev. C **29**, 1040 (1984).

[175] D. Auverlot, P. Bonche, H. Flocard, and P. H. Heenen, Phys. Lett. B **149**, 6 (1984).

[176] W. C. Haxton and C. Johnson, Phys. Rev. Lett. **65**, 1325 (1990).

[177] G. Thiamová, D. J. Rowe, and J. L. Wood, Nucl. Phys. A **780**, 112 (2006).

[178] D. J. Rowe, G. Thiamová, and J. L. Wood, Phys. Rev. Lett. **97**, 202501 (2006).

[179] D. J. Rowe, *Practical Group Theory with Applications* (University of Toronto Bookstores, Toronto, 1997).

[180] F. Iachello, *Lie Algebras and Applications* (Springer-Verlag, Heidelberg, 2006).

[181] J. F. Cornwell, *Group Theory in Physics* (Academic Press, Cambridge, 1974).

[182] A. O. Barut and R. Raczka, *Theory of Group Representation and Applications* (World Scientific, 1986).

[183] F. Iachello and A. Arima, *The Interacting Boson Model* (Cambridge University Press, Cambridge, England, 1987).

[184] T. Beuschel, *M1 Strength Distributions in Deformed Nuclei*, PhD thesis, LSU, 1998.

Appendix A

Lie Groups and Lie Algebras: Basic Concepts

In this appendix we present basic definitions and concepts of the theory of Lie groups, Lie algebras, and their representations. Note that our intention is not to provide a comprehensive or mathematically rigorous review, which can be found elsewhere [179, 143, 180, 181, 182], but rather to help the reader become familiar with the application of the group theory in quantum mechanics.

Definition: A *group* G is a set of elements with a binary operation $G \times G \to G$ that satisfies the following four conditions:

1. If $a, b \in G$ then $ab \in G$.
2. The binary operation is associative, $a(bc) = (ab)c$.
3. There exists an element $e \in G$ such that $ea = ae = a$ for every element $a \in G$.
4. For each element $a \in G$ there exist an inverse element $a^{-1} \in G$ such that $aa^{-1} = a^{-1}a = e$.

Groups with a finite number of elements are called *finite groups*. An example of a finite group is the group of permutations of N objects. A group is said to be *discrete* if it has a countable number of elements. An example of a discrete group is the additive group of integers. Groups can also be infinite and *continuous*. Elements of a continuous group can be expressed in terms of r continuous parameters

$$g(\alpha_1, \ldots, \alpha_r) \equiv g(\boldsymbol{\alpha}), \tag{A.1}$$

with the identity element corresponding to the set of null parameters, $e = g(\mathbf{0})$. The most important class of continuous groups is the class of *Lie groups* as it involves some of the most significant groups in physics.

Definition: A Lie group G is a continuous group satisfying continuity requirement for all group operations.

The closure of the group elements requires that the product of any two group elements is an element of the group:

$$g(\boldsymbol{\alpha})g(\boldsymbol{\beta}) = g(\boldsymbol{\gamma}) \equiv g(f(\boldsymbol{\alpha}, \boldsymbol{\beta})). \tag{A.2}$$

The continuity requirement is assured if $f(\boldsymbol{\alpha}, \boldsymbol{\beta})$ is continuously differentiable function of all the parameters $\boldsymbol{\alpha}$ and $\boldsymbol{\beta}$. The associativity requires that

$$f(\boldsymbol{\alpha}, f(\boldsymbol{\beta}, \boldsymbol{\gamma})) = f(f(\boldsymbol{\alpha}, \boldsymbol{\beta}), \boldsymbol{\gamma}), \tag{A.3}$$

and for the identity element $g(\mathbf{0})$ we must have

$$\boldsymbol{\gamma} = f(\boldsymbol{\gamma}, \mathbf{0}) = f(\mathbf{0}, \boldsymbol{\gamma}). \tag{A.4}$$

The existence of the inverse element $g(\boldsymbol{\alpha})^{-1} \equiv g(I(\boldsymbol{\alpha}))$ requires that $I(\boldsymbol{\alpha})$ is continuously differentiable function of parameters $\boldsymbol{\alpha}$.

Lie groups play an important role in quantum mechanics. Unitary transformations of a quantum system such as space translations, rotations, quadrupole deformations, etc., form Lie groups. Linear differential operators acting on an infinite space of square-integrable functions represent just one example of many possible realizations of a Lie group. Other important realizations include linear transformations on a vector space, or a special class of $n \times n$ matrices. For example, the rotation group SO(3) may be regarded as:

- the group of real orthogonal 3×3 matrices with unit determinant,

$$\mathrm{SO}(3) = \left\{ \Omega \in \mathbb{R}^{3\times 3} | \Omega^t \Omega = I_3, \det\Omega = 1 \right\},$$

- a set of linear differential operators of the form

$$\hat{R}(\alpha_1, \alpha_2, \alpha_3) = \mathrm{e}^{i(\alpha_1 \hat{L}_1 + \alpha_2 \hat{L}_2 + \alpha_3 \hat{L}_3)},$$

  where $\hat{L}_i = -i\hbar \left(\hat{\boldsymbol{r}} \times \nabla\right)_i$,

- a set of linear transformations, or equivalently, matrices, on a $(2L+1)$-dimensional Hilbert space spanned by a set of orbital angular momentum eigenstates $\{|lm\rangle,\ \ m = -l, \ldots, +l\}$.

The representation of Lie group elements by matrices is a very powerful technique. To illustrate how the matrix representations arise from a symmetry of a quantum system let us consider the stationary Schrödinger equation

$$H\,|\psi\rangle = E\psi. \tag{A.5}$$

A symmetry of a quantum mechanical system is fundamentally associated with a group G of unitary transformations that leaves the Hamiltonian H invariant,

$$\hat{R}^\dagger H \hat{R} = H, \quad \forall \hat{R} \in G. \tag{A.6}$$

If G is a symmetry of H and $|\psi\rangle$ is an eigenfunction of H with energy E, then $\hat{R}|\psi\rangle$ is also an eigenfunction of H of energy E for all transformations $\hat{R} \in G$. In other words, all transformed solutions $\hat{R}|\psi\rangle$ are degenerate in energy and form a subspace $\mathcal{H}_\psi$ of the Hilbert space $\mathcal{H}$. Let us assume that this subspace has a finite dimension n and let $\{|\psi_1\rangle, |\psi_2\rangle, \ldots, |\psi_n\rangle\}$ be its basis. Because $\hat{R}|\psi_j\rangle \in \mathcal{H}_\psi$, we can expand this state as

$$\hat{R}|\psi_j\rangle = \sum_{k=1}^{n} \langle\psi_k| \hat{R}|\psi_j\rangle |\psi_k\rangle .$$

Thus, each element of the group G can be associated with an $n \times n$ matrix $R_{jk} \equiv \langle\psi_k| \hat{R}|\psi_j\rangle$, or equivalently, a linear operator of a n-dimensional vector space. This map is called a *representation* of G. :

Definition: A representation of a group G is a map T of G into the group of general linear transformations of a vector space (also called the carrier space of the representation) such that

$$T(gg') = T(g)T(g'), \quad \forall g, g' \in G.$$

Definition: A representation $T(G)$ of a group G is *unitary* if

$$T(g^{-1}) = T(g)^\dagger, \quad \forall g \in G.$$

Definition: Let $T(G)$ be a representation of a Lie group G in a Hilbert space $\mathcal{H}$. A subspace $\mathcal{H}_1 \subseteq \mathcal{H}$ is said to be an *invariant* subspace of $\mathcal{H}$ under G if

$$T(g)|\psi\rangle \in \mathcal{H}_1, \quad \forall |\psi\rangle \in \mathcal{H}_1 \text{ and } \forall g \in G. \tag{A.7}$$

Definition: If $\mathcal{H}$ has a proper invariant subspace $\mathcal{H}_1 \subset \mathcal{H}$, $T(G)$ is said to be *reducible representation*. Conversely, if $\mathcal{H}$ has no invariant subspace, $T(G)$ is said to be *irreducible representation* (irrep).

Definition: If a representation $T(G)$ can be transformed by a suitable choice of basis into a block-diagonal form

$$T(g) = \begin{pmatrix} T^{(1)}(g) & 0 & 0 \\ 0 & T^{(2)}(g) & 0 \\ 0 & 0 & \ddots \end{pmatrix},$$

where $T^{(1)}(g)$, $T^{(2)}(g)$, etc., are irreducible representations, we say that $T(G)$ is *fully reducible* representation.

If a representation $T(G)$ is fully reducible, then its carrier space $\mathcal{H}$ can be decomposed into a direct sum of subspaces that are invariant with respect to G.

A generating set of a finite group G is a subset $S \subset G$ such that every element of G can be expressed as the product of finitely many elements of S and their inverses. In contrast to a finite group, it is not possible to define a generating set of a Lie group. Instead, one introduces the concept of infinitesimal generators. Every element $g(\boldsymbol{\alpha})$ of a Lie group that lies in the sufficiently small neighborhood of the identity element $g(\mathbf{0})$ can be expanded by a Taylor expansion

$$g(\boldsymbol{\alpha}) = g(\mathbf{0}) + \sum_{i=1}^{r} \alpha_i X_i + O(\alpha^2), \tag{A.8}$$

where

$$X_i = \left(\frac{\partial g(\boldsymbol{\alpha})}{\partial \alpha_i} \right)_{\boldsymbol{\alpha}=\mathbf{0}}. \tag{A.9}$$

The operators X_i are said to be the *infinitesimal generators* of the group. All elements of a Lie group connected to the identity element can be constructed by means of the infinitesimal group generators as

$$g(\boldsymbol{\beta}) = \exp\left(\sum_{i=1}^{r} \beta_i X_i \right). \tag{A.10}$$

The infinitesimal generators play a fundamental role in quantum mechanics. For instance, the momentum $\hat{\boldsymbol{p}}$ is the infinitesimal generator of the group of space translations; the angular momentum $\hat{\boldsymbol{L}}$ is the infinitesimal generator of the group of rotations SO(3).

It can be shown that the infinitesimal group generators close under commutation,

$$[X_i, X_j] = \sum_{k=1}^{r} C_{ij}^{k} X_r, \tag{A.11}$$

and form an algebraic structure called a Lie algebra.

Definition: A *Lie algebra* over a field $\mathbb{F}$ is a vector space $\mathfrak{g}$ endowed with an operation $[,]{:}\mathfrak{g} \times \mathfrak{g} \to \mathfrak{g}$, called the *Lie bracket*, which satisfies the following conditions:

1. $[aX, bY] = ab\,[X, Y]\,, \quad \forall a, b \in \mathbb{F}$
2. $[X, Y] = -\,[Y, X]$
3. $[X, [Y, Z]] = [[X, Y]\,, Z] + [Y, [X, Z]]$

The fact that any Lie group defines an associated Lie algebra of infinitesimal group generators is of great practical importance. It allows one to reduce the study of an infinite Lie group to the study of a finite vector space of group generators. In particular, the problem of finding irreps of a Lie group thus becomes essentially the same as that of finding irreps of an associated Lie algebra.

Definition: A representation Γ of a Lie algebra $\mathfrak{g}$ is a map of $\mathfrak{g}$ onto the general linear transformations on a vector space V satisfying

$$\Gamma([X,Y]) = [\Gamma(X), \Gamma(Y)]\,, \tag{A.12}$$

where the Lie bracket is defined by commutator.
Definition: Let $\Gamma(\mathfrak{g})$ be a representation of a Lie algebra $\mathfrak{g}$ in a Hilbert space $\mathcal{H}$. A subspace $\mathcal{H}_1 \subseteq \mathcal{H}$ is said to be an *invariant* subspace if

$$\Gamma(X)\,|\psi\rangle \in \mathcal{H}_1, \quad \forall\,|\psi\rangle \in \mathcal{H}_1 \text{ and } \forall X \in \mathfrak{g}. \tag{A.13}$$

Definition: If a representation carrier space has a proper invariant subspace, the representation is said to be reducible. A representation that is not reducible is said to be irreducible.
Definition: An *ideal* is a subalgebra $\mathfrak{h} \subseteq \mathfrak{g}$ satisfying

$$[\mathfrak{g}, \mathfrak{h}] \subseteq \mathfrak{h}. \tag{A.14}$$

If elements of $\mathfrak{h}$ commute, then $\mathfrak{h}$ is said to be an *Abelian ideal*.

Definition: A Lie algebra $\mathfrak{g}$ is *simple* if it contains no ideals other than $\mathfrak{g}$ and $\{0\}$; it is *semi-simple* if it contains no Abelian ideal (other then $\{0\}$).

Example: The $\mathfrak{so}(4)$ Lie algebra is spanned by six elements $\{J_1, J_2, J_3, K_1, K_2, K_3\}$ with commutation relations

$$[J_i, J_j] = \epsilon_{ijk} J_k \quad [K_i, K_j] = \epsilon_{ijk} K_k \quad [K_i, J_j] = 0. \tag{A.15}$$

The triads $\mathfrak{h}_1 = \{J_1, J_2, J_3\}$ and $\mathfrak{h}_2 = \{K_1, K_2, K_3\}$ form proper ideals in $\mathfrak{so}(4)$, and thus the Lie algebra $\mathfrak{so}(4)$ is not simple. The proper ideals $\mathfrak{h}_1$ and $\mathfrak{h}_2$ are non-Abelian, and hence $\mathfrak{so}(4)$ is semi-simple.

Semi-simple Lie algebras constitute an important class of Lie algebras and play a fundamental role in geometry and physics. For instance, the Lie algebras of all the classical Lie groups, including the special linear groups, $\mathrm{SL}(n, \mathbb{R})$, the special unitary group, $\mathrm{SU}(n)$, the special orthogonal groups, $\mathrm{SO}(n)$, and the symplectic groups, $\mathrm{Sp}(n, \mathbb{R})$, are all semi-simple. Some of these groups play an important role in quantum mechanics. For instance, in the context of the nuclear structure physics, the Interacting Boson Model [183], the Elliott SU(3) model, and the Symplectic model utilize irreps of U(6), SU(3) and $\mathrm{Sp}(3, \mathbb{R})$ groups, respectively.

Definition: A subalgebra $\mathfrak{h}$ of a semi-simple algebra $\mathfrak{g}$ is called a *Cartan subalgebra* if $\mathfrak{h}$ is a maximal abelian subalgebra in $\mathfrak{g}$ such that if $[X, \mathfrak{h}] \in \mathfrak{h}$, then $X \in \mathfrak{h}$ as well. The dimension of $\mathfrak{h}$ is called the *rank* of $\mathfrak{g}$.

In quantum mechanics, it is a common approach to classify states by the eigenvalues of a set of mutually commuting operators. Similarly, in seeking the representations of a semi-simple Lie algebra $\mathfrak{g}$ of the rank l, it is useful to start with the Cartan subalgebra $\mathfrak{h} = \{H_1, \ldots, H_l\}$. The operators spanning subalgebra $\mathfrak{h}$ commute,

and hence they can be simultaneously diagonalized. This provides us with sets of eigenvalues $(m_1, m_2, \ldots, m_l)$, also called *weight vectors*, that label basis states of an irrep. All other generators of the semi-simple Lie algebra $\mathfrak{g}$ can be shown to be either raising or lowering operators with respect to $\mathfrak{h}$ so that

$$[H_i, E_\alpha] = \alpha_i E_\alpha, \;\; i = 1, \ldots, l. \tag{A.16}$$

Furthermore, it can be shown that for each semi-simple Lie algebra of rank l, one can construct l invariant operators C_p, called *Casimir operators*, which commute with all elements of the Lie algebra:

$$[C_p, X] = 0 \;\text{ for any } X \in \mathfrak{g}, \;\; p = 1, \ldots, l. \tag{A.17}$$

The operator C_p is called Casimir invariant of order p, and it is built from products of p elements of the Lie algebra $\mathfrak{g}$

$$C_p = \sum_{\alpha_1, \alpha_2, \ldots, \alpha_p} f^{\alpha_1 \alpha_2 \ldots \alpha_p} X_{\alpha_1} X_{\alpha_2} \ldots X_{\alpha_p}. \tag{A.18}$$

Because Casimir invariants commute with all elements of $\mathfrak{h}$, they can be simultaneously diagonalized. Their eigenvalues $c_1, \ldots, c_p$ stay constant for all states spanning a single irrep, while the weight vector varies over particular states of an irrep. Let us label the general eigenfunction of operators $C_1, \ldots, C_l, H_1, \ldots, H_l$ as

$$|(c_1, c_2, \ldots, c_l) m_1, m_2, \ldots, m_l\rangle \,. \tag{A.19}$$

Then

$$H_i \,|(c_1, \ldots, c_l) m_1, m_2, \ldots, m_l\rangle \;=\; m_i \,|(c_1, \ldots, c_l) m_1, \ldots, m_l\rangle \tag{A.20}$$

$$C_i \,|(c_1, \ldots, c_l) m_1, m_2, \ldots, m_l\rangle \;=\; c_i \,|(c_1, \ldots, c_l) m_1, \ldots, m_l\rangle \,, \tag{A.21}$$

and by using the commutation relation (A.16), in conjuction with (A.20), we get

$$H_i E_\alpha \,|(c_1, \ldots, c_l) m_1, \ldots, m_l\rangle = (m_i + \alpha_i) E_\alpha \,|(c_1, \ldots, c_l) m_1, \ldots, m_l\rangle \tag{A.22}$$

This means that

$$E_\alpha \,|(c_1, \ldots, c_l) m_1, \ldots, m_l\rangle \;\sim |(c_1, \ldots, c_l) m_1 + \alpha_1, m_2 + \alpha_2, \ldots, m_l + \alpha_l\rangle \tag{A.23}$$

And hence irreps of semi-simple Lie algebras, and their Lie groups therefore, can be constructed by the application of raising and lowering operators to highest (or lowest) weight states.

Appendix B

Tensor Operators and Wigner-Eckart Theorem

Quantum-mechanical calculations inherently reduce to the evaluation of the matrix elements of interaction terms and other physical observables in some suitable basis. This task can be significantly simplified by the systematic exploitation of the transformation properties of basis states and operators with respect to relevant symmetries of an investigated quantum system. This appendix introduces two essential pillars of this approach, irreducible tensor operators and the Wigner-Eckart theorem.

Let us consider a Lie group G with an unitary fully reducible representation $T(G)$ on a Hilbert space $\mathcal{H}$. The existence of a fully reducible representation implies that $\mathcal{H}$ is decomposable into invariant subspaces associated with irreps of G. Matrix elements of an arbitrary operator $\hat{R} \in T(G)$ between basis states of two different irreps vanish. This means that the effect of $\hat{R}$ acting on a basis state $|\Lambda\lambda\rangle$ of the irrep Λ is to produce a linear combination of basis states spanning this irrep.

$$\hat{R}\,|\Lambda\lambda\rangle = \sum_{\lambda'} \langle\Lambda\lambda'|\,\hat{R}\,|\Lambda\lambda\rangle\,|\Lambda\lambda'\rangle\,, \tag{B.1}$$

Operators acting on a Hilbert space $\mathcal{H}$ also behave in definite ways under symmetry group transformations. In direct analogy with formula (B.1), we can classify operators according to their transformation properties with respect to the symmetry group G.

Definition: A set T^{Λ}_{λ} of $\dim_{\Lambda}$ linearly independent operators form an *irreducible tensor operator* under the group G with a tensorial character Λ if T^{Λ}_{λ} transforms under G as

$$\hat{R}^{\dagger} T^{\Lambda}_{\lambda} \hat{R} = \sum_{\lambda'} \langle\Lambda\lambda'|\,\hat{R}\,|\Lambda\lambda\rangle\, T^{\Lambda}_{\lambda'}. \tag{B.2}$$

Note that $\dim_{\Lambda}$ signifies the dimension of the irrep Λ. The relation (B.2) can be expressed in a more applicable form by means of the infinitesimal generators, $\hat{X}_i$, of the group G as

$$\left[\hat{X}_i, T^{\Lambda}_{\lambda}\right] = \sum_{\lambda'} \langle\Lambda\lambda'|\,\hat{X}_i\,|\Lambda\lambda\rangle\, T^{\Lambda}_{\lambda'}. \tag{B.3}$$

The irreducible tensors can be also coupled to form a new irreducible tensor operator:

$$\left[U^{\Lambda_1} \times V^{\Lambda_2}\right]^{\rho\Lambda}_{\lambda} = \sum_{\lambda_1\lambda_2} \langle \Lambda_1\lambda_1; \Lambda_2\lambda_2 |\, \Lambda\lambda\rangle_\rho U^{\Lambda_1}_{\lambda_1} V^{\Lambda_2}_{\lambda_2}, \tag{B.4}$$

where $\langle \Lambda_1\lambda_1; \Lambda_2\lambda_2|\Lambda\lambda\rangle_\rho$ is a coupling (Clebsch-Gordan) coefficient and the index ρ denotes multiplicity label that is generally needed due to the possibility of multiple occurrences of irrep Λ in the direct product $\Lambda_1 \times \Lambda_2$.

The most important application of irreducible tensor operators, and the theory of group representations generally, is the *Wigner-Eckart theorem*. The Wigner-Eckart theorem states that a matrix element of an irreducible tensor operator T^Λ_λ between basis states of Λ_1 and Λ_2 irreps,

$$\langle \Lambda_1\lambda_1 |\, T^\Lambda_\lambda \,| \Lambda_2\lambda_2\rangle\,, \tag{B.5}$$

factorizes into a geometric part, which carries the labels of the group-subgroup chain under consideration, and a subgroup-independent part called reduced matrix element:

$$\langle \Lambda_1\lambda_1 |\, T^\Lambda_\lambda \,| \Lambda_2\lambda_2\rangle = \sum_\rho \langle \Lambda_2\lambda_2; \Lambda\lambda|\Lambda_1\lambda_1\rangle_\rho \langle \Lambda_1 \| T^\Lambda \| \Lambda_2\rangle_\rho. \tag{B.6}$$

Notice that reduced matrix elements $\langle \Lambda_1 \| T^\Lambda \| \Lambda_2\rangle_\rho$ are independent of quantum numbers λ_1, λ_2, and λ, and thus the Wigner-Eckart theorem reduces computer memory and storage requirements by the factor $\sim \dim_\Lambda \times \dim_{\Lambda_1} \times \dim_{\Lambda_2}$. This is a very important advantage for large scale calculations which are routinely performed in contemporary nuclear structure physics.

If the irrep Λ_1 does not occur in the tensor product $\Lambda_2 \times \Lambda$, or $\lambda_2 + \lambda \neq \lambda_1$, then the coupling coefficient $\langle \Lambda_2\lambda_2; \Lambda\lambda|\Lambda_1\lambda_1\rangle_\rho$ must vanish. The Wigner-Eckart theorem thus implies the existence of selection rules that enable us to immediately identify vanishing matrix elements and thus avoid unnecessary computation.

Appendix C

SU(3) Calculus

In this appendix we briefly summarize those definitions, notation, and formulas of the SU(3) calculus that are utilized throughout this work. For a more comprehensive review see, e.g., Ref. [146, 184].

SU(3) Wigner Coefficients

Two SU(3) irreps $(\lambda_1\,\mu_1)$ and $(\lambda_2\,\mu_2)$ can be coupled to a total SU(3) irrep $(\lambda\,\mu)$ by the unitary transformation:

$$|\rho(\lambda\mu)\alpha\rangle = \sum_{\alpha_1\alpha_2} \langle(\lambda_1\mu_1)\alpha_1;(\lambda_2\mu_2)\alpha_2|\,(\lambda\mu)\alpha\rangle_\rho\,|(\lambda_1\mu_1)\alpha_1\rangle\,|(\lambda_2\mu_2)\alpha_2\rangle\,, \tag{C.1}$$

where $\langle(\lambda_1\,\mu_1)\alpha_1;(\lambda_2\,\mu_2)\alpha_2|\,(\lambda\,\mu)\alpha\rangle_\rho$ is a Wigner SU(3) coupling coefficient. Unlike SO(3) and SU(2) groups, where the coupling of angular momenta j_1 and j_2 to j is unique, an outer multiplicity label ρ is needed to distinguish multiple occurrences of a given total irrep $(\lambda\,\mu)$ in the direct product $(\lambda_1\,\mu_1)\times(\lambda_2\,\mu_2)$. The Wigner SU(3) coefficients form an unitary matrix with real matrix elements, and hence the inverse transformation to the uncoupled basis reads

$$|(\lambda_1\mu_1)\alpha_1\rangle\,|(\lambda_2\mu_2)\alpha_2\rangle = \sum_{\rho(\lambda\mu)\alpha} \langle(\lambda_1\mu_1)\alpha_1;(\lambda_2\mu_2)\alpha_2|\,(\lambda\mu)\alpha\rangle_\rho\,|\rho(\lambda\mu)\alpha\rangle\,. \tag{C.2}$$

In the above formulas, the symbols α represent a set of labels used to distinguish orthonormal basis states within a given SU(3) irrep, $\alpha = \kappa lm$ for the physical SU(3) $\supset$ SO(3) group chain, wheres for the canonical SU(3) $\supset$ SU(2) $\otimes$ U(1) chain $\alpha = \epsilon\Lambda M_\Lambda$.

The orthogonality relations for Wigner SU(3) coefficients are:

$$\sum_{\rho(\lambda\mu)\alpha} \langle(\lambda_1\mu_1)\alpha_1;(\lambda_2\mu_2)\alpha_2|\,(\lambda\mu)\alpha\rangle_\rho\langle(\lambda_1\mu_1)\alpha_1';(\lambda_2\mu_2)\alpha_2'|\,(\lambda\mu)\alpha\rangle_\rho = \delta_{\alpha_1\alpha_1'}\delta_{\alpha_2\alpha_2'}, \tag{C.3}$$

and

$$\sum_{\alpha_1\alpha_2} \langle(\lambda_1\mu_1)\alpha_1;(\lambda_2\mu_2)\alpha_2|\,(\lambda\mu)\alpha\rangle_\rho\langle(\lambda_1\mu_1)\alpha_1;(\lambda_2\mu_2)\alpha_2|\,(\lambda'\mu')\alpha\rangle_{\rho'} = \delta_{\lambda\lambda'}\delta_{\mu\mu'}\delta_{\rho\rho'}. \tag{C.4}$$

For practical purposes it is convenient to factor out the dependence of the SU(3) $\supset$ SO(3) Wigner coupling coefficients on the m label by defining so-called reduced SU(3) coupling coefficients. The relation between the "full" and "reduced" Wigner coefficients is:

$$\begin{aligned}&\langle(\lambda_1\mu_1)\kappa_1 l_1 m_1;(\lambda_2\mu_2)\kappa_2 l_2 m_2|\,(\lambda\mu)\kappa l m\rangle_\rho \\ &\quad= \underbrace{\langle(\lambda_1\mu_1)\kappa_1 l_1;(\lambda_2)\kappa_2 l_2\|(\lambda\mu)\kappa l\rangle_\rho}_{\text{reduced SU(3) coupling coefficient}}\ \ \underbrace{C^{lm}_{l_1 m_1 l_2 m_2}}_{\text{SO(3) coupling coefficient}}.\end{aligned} \tag{C.5}$$

SU(3) Irreducible Tensor Operators and Wigner-Eckart Theorem

The general definition of irreducible tensor operators (B.3) can be specialized for the SU(3) case as

$$\left[C^{(1\,1)}_\alpha, T^{(\lambda\,\mu)}_\beta\right] = \sum_{\beta'} \langle(\lambda\,\mu)\beta'|\,C^{(1\,1)}_\alpha\,|(\lambda\,\mu)\beta\rangle\,T^{(\lambda\,\mu)}_{\beta'}, \tag{C.6}$$

where $C^{(1\,1)}_\alpha$ denotes an infinitesimal generator of SU(3). The SU(3) tensor operators can form a new tensor by coupling:

$$\left[U^{(\lambda_1\mu_1)}\times V^{(\lambda_2\mu_2)}\right]^{\rho(\lambda\,\mu)}_\alpha = \sum_{\alpha_1\alpha_2}\langle(\lambda_1\mu_1)\alpha_1;(\lambda_2\mu_2)\alpha_2|\,(\lambda\mu)\alpha\rangle_\rho U^{(\lambda_1\mu_1)}_{\alpha_1} V^{(\lambda_2\mu_2)}_{\alpha_2}. \tag{C.7}$$

The right hand side of the above formula can be alternatively rewritten in terms of ordinary SO(3) tensors, yielding:

$$\begin{aligned}[U^{(\lambda_1\,\mu_1)}\times V^{(\lambda_2\,\mu_2)}]^{\rho(\lambda\,\mu)}_{\kappa l m} \;=\; &\sum_{\kappa_1 l_1\kappa_2 l_2}\langle(\lambda_1\,\mu_1)\kappa_1 l_1;(\lambda_2\,\mu_2)\kappa_2 l_2\|(\lambda\,\mu)\kappa l\rangle_\rho \\ &\times[U^{(\lambda_1\,\mu_1)}_{\kappa_1 l_1}\times V^{(\lambda_2\,\mu_2)}_{\kappa_2 l_2}]_{lm}.\end{aligned} \tag{C.8}$$

For the SU(3) $\supset$ SO(3) subgroup chain, the Wigner-Eckart theorem takes the following form:

$$\begin{aligned}&\langle(\lambda_1\mu_1)\kappa_1 l_1 m_1|\,T^{(\lambda\mu)}_{\kappa l m}\,|(\lambda_2\mu_2)\kappa_2 l_2 m_2\rangle = \\ &C^{l_1 m_1}_{l_2 m_2 l m}\sum_\rho\langle(\lambda_2\mu_2)\kappa_2 l_2;(\lambda\mu)\kappa l\|(\lambda_1\mu_1)\kappa_1 l_1\rangle_\rho\langle(\lambda_1\mu_1)|||T^{(\lambda\mu)}|||(\lambda_2\mu_2)\rangle_\rho.\end{aligned} \tag{C.9}$$

Notice that the triple barred reduced matrix elements are independent of the SU(3) subgroup chain labels.

Coupling of three SU(3) irreps

Similar to the SU(2) case where a $6J$ coefficient can be written as a sum of Clebsch-Gordan coefficients, the SU(3) U-coefficients can be expressed in terms of SU(3)

Wigner coefficients [64]. For the reduction SU(3) $\supset$ $SO(3)$ this relation between SU(3) Racah and Wigner coefficients is:

$$
\begin{aligned}
&U[(\lambda_1\,\mu_1)(\lambda_2\,\mu_2)(\lambda\,\mu)(\lambda_3\,\mu_3);(\lambda_{12}\,\mu_{12})\rho_{12}\rho_{12,3}(\lambda_{23}\,\mu_{23})\rho_{23}\rho_{1,23}] = \\
&\sum_{\{-\}} U(l_1 l_2 l l_3; l_{12} l_{23})\ \langle(\lambda_1\,\mu_1)\kappa_1 l_1;(\lambda_2\,\mu_2)\kappa_2 l_2\|(\lambda_{12}\,\mu_{12})\kappa_{12} l_{12}\rangle_{\rho_{12}} \\
&\times\langle(\lambda_{12}\,\mu_{12})\kappa_{12} l_{12};(\lambda_3\,\mu_3)\kappa_3 l_3\|(\lambda\,\mu)\kappa l\rangle_{\rho_{12,3}} \\
&\times\langle(\lambda_2\,\mu_2)\kappa_2 l_2;(\lambda_3\,\mu_3)\kappa_3 l_3\|(\lambda_{23}\,\mu_{23})\kappa_{23} l_{23}\rangle_{\rho_{23}} \\
&\times\langle(\lambda_1\,\mu_1)\kappa_1 l_1;(\lambda_{23}\,\mu_{23})\kappa_{23} l_{23}\|(\lambda\,\mu)\kappa l\rangle_{\rho_{1,23}}
\end{aligned}
\tag{C.10}
$$

with the summation going over $\{-\} = \{l_1, l_2, l_3, l_{12}, l_{23}, \kappa_1, \kappa_2, \kappa_3, \kappa_{12}, \kappa_{23}\}$.

Vita

Tomáš Dytrych was born in October 1976, in Jičín, Czech Republic. He attended high school in Jičín, and studied at the Czech Technical University in Prague, where he received his Master of Science degree in computational physics in 2001. From 1997 to 2000 he worked in the Institute of Atmospheric Physics of the Czech Academy of Sciences as a research assistant. Thereafter he was employed as a programmer in MIS AG. He began his studies in the Department of Physics and Astronomy at Louisiana State University in 2002. His doctoral degree is expected to be awarded in December 2008.